Local Møller-Plesset perturbation theory for periodic systems - a study of long-range interactions and convergence

Einar Aurbakken

Thesis submitted for the degree of
Master in Theoretical and physical chemistry
60 credits

Department of Chemistry
Faculty of mathematics and natural sciences

UNIVERSITY OF OSLO

June 2020

Local Møller-Plesset perturbation theory for periodic systems - a study of long-range interactions and convergence

Einar Aurbakken

Local Møller-Plesset perturbation theory for periodic systems - a study of long-range interactions and convergence

http://www.duo.uio.no/

Acknowledgements

I wish to thank my supervisor professor Thomas Bondo Pedersen for guiding me through this project, and always being available for help when needed. I especially want to thank Audun Skau Hansen for his patient efforts in helping me understand both the functioning of the XDEC code and key concepts of the underlying theory. Finally, I wish to thank Dr. Gustav Baardsen for always being available and helpful while he was still working at the Hylleraas center.

Abstract

We study correlation energy in periodic Divide-Expand-Consolidate local second-order Møller-Plesset theory. For the computation of correlation energy, we implement an amplitude solver for non-orthogonal virtual orbitals in periodic systems. We further test the convergence of the correlation energy with an increased number of virtual orbitals when non-orthogonal projected atomic orbitals and virtual Wannier functions are used to span the excitation spaces. For the calculation of long-range correlation energies, we develop and implement a method based on smoothed cubic spline interpolation to automatically determine the significant contributions to the pair correlation energy. Finally, we look at the non-smoothness of potential energy surfaces generated by local correlation methods caused by the cutoffs in the orbital spaces and long-range correlation calculations. In relation to this, we apply the pair cutoff algorithm to the generation of a one-dimensional potential energy surface for LiH.

Contents

Chapter 1

Introduction

Solid matter constitutes the phase of most stuff that we interact with in everyday life. Crystalline solids, or simply crystals, are solids that are characterized by a periodically repeating pattern of atoms at a microscopic level. Crystals constitute an important class of solids, and includes common materials such as salts, rocks, metals and ice. From a chemistry perspective, solid matter is important for example in the field of heterogeneous catalysis, where reaction typically happens after an adsorption of a reactant to the surface of a solid. The theoretical description of the solid matter is therefore of great importance.

It has been known since the 1920s that quantum mechanics is crucial in the physical description and understanding of matter. Due to the conceived completeness of the description of non-relativistic quantum mechanics, the famed physicist Paul Dirac claimed already in 1929 that "The underlying physical laws necessary for the mathematical theory of a large part of physics and the whole of chemistry are thus completely known, and the difficulty is only that the exact application of these laws leads to equations much too complicated to be soluble" [1]. Much effort has since been made in developing methods and approximations that makes it computationally feasible to calculate properties of matter with sufficient accuracy.

For several decades, density functional theory (DFT) has been dominating method for the computation of energies, geometries and other physical and chemical properties of solids. The reason for this dominance has been a favorable trade-off between the accuracy and required computational resources. But the standard formulations of DFT struggles with handling dispersion interactions correctly. In addition, there is no known way to systematically improve the accuracy of DFT calculations.

Today, coupled cluster (CC) theory is generally regarded as the most successful method in calculations on small to medium sized molecular systems. The success stems in part from the systematic improvement in the schemes coupled cluster singles and doubles excitations (CCSD), coupled cluster singles, doubles and perturbative triples excitations (CCSD(T)) coupled cluster singles, doubles and triples excitations (CCSDT) and so on. On systems where a single Slater determinant is a reasonable approximation to the ground state wave func-

tions, the main issue with traditional CC implementations is the steep scaling wall in calculations with increased system size. CC calculations or calculations with other post-Hartree-Fock methods usually follows a canonical Hartree-Fock calculation, in which the methods second-order Møller-Plesset (MP2), CCSD and CCSD(T) and CCSDT formally scales as N^5, N^6, N^7 and N^8 respectively, where N is the number of particles. The scaling walls stems from the delocalized molecular orbitals (MOs), hiding the proper locality of the electron correlation.

Localized molecular orbitals may be obtained by utilizing the degrees of freedom present in the choice of MOs obtained in Hartree-Fock calculations. The resulting sparsity in the two-particle integral matrices, and consequently the sparsity in the excitation amplitude tensor, may then be utilized to obtain post-Hartree-Fock correlation methods that (ideally) scales linearly in the computational cost with the system size.

After the pioneering work of Pulay [2], many attempts at implementations approaching linear scaling has been made for molecular systems. Implementations for periodic systems are fewer, and there are still significant limitations on the systems that can be calculated with high accuracy. The Cryscor program [3] represents a notable implementation for periodic systems. Also, the Cluster-in-Molecule algorithm has been implemented for periodic systems [4]. Rebolini et al. [5] implemented the Divide-Expand-Consolidate (DEC) algorithm for periodic systems under the name extended DEC (XDEC), which is the implementation used in this thesis.

In the DEC algorithm, the system is partitioned into fragments, which are local sets of orbitals for which the MP2 or CC equations are solved independently of each other. The correlation energy can be expressed as a sum of the correlation energy on each fragment, and pairs of fragments.

To achieve linear scaling, the virtual excitation space for the occupied orbitals of each fragment is limited to a subset of spatially close orbitals. Thereafter, the sum over pair energies is truncated. The latter approximation may be justified since the pair energies decay approximately as R^{-6} with distance R, in accordance with the London dispersion force.

Given the two main approximations just mentioned, we are left with two major tasks. The first is to properly select the excitation space for each occupied orbital or subset of orbitals, and the second task is to choose which pairs to calculate such that both the error and computational time is simultaneously minimized.

For the problem with local virtual excitation spaces, it has been shown that that much smaller excitation spaces are needed if projected atomic orbitals (PAOs) are used instead of virtual Wannier functions in the Cryscor implementation [6]. In order to gain further insights, we implement the non-canonical MP2 equations with non-orthogonal virtual orbitals in an implementation of XDEC that retains the translational symmetry of the systems. We further test the convergence of fragment energies with the number of PAOs and virtual Wannier functions in the virtual excitation spaces.

The error caused by pair cutoff can be made insignificant if a very large cutoff distance is chosen, but this comes at the cost of a potentially large increase

in computation time. This is especially problematic in 3D systems where the number of pairs increases cubically with the distance, causing a steep increase in the number of pair calculation with increase in the pair cutoff distance. Rebolini et al. [5] proposed using smoothed spline interpolation to estimate the pair energies, and choose a cutoff based on that. In this thesis, this method is atomized so that a cutoff may be chosen by the program. Furthermore, we expand the method to include sorting of pairs, so as to better estimate the energy of the non-calculated pairs, and to determine what pairs will have significant contributions.

Finally, we investigate the non-smooth behaviour of potential energy surfaces (PESs) generated with local correlation methods, and we apply the automatic pair cutoff determination in the generation of a 1D PES for 3D LiH where the lattice parameter is varied.

Chapter 2

Theoretical Background

In this chapter, the quantum mechanical foundation for the methods studied in this project is laid out. Sections 2.1 to 2.4 is mainly underlying theory, while sections 2.5 to 2.8 will be more specifically about the concepts and methods utilized, developed or implemented in this work.

In section 2.1 the basic principles of quantum theory is presented, while section 2.2 addresses some important principles and concepts for describing many-electron systems. Section 2.3 addresses the electron correlation problem specifically. Definitions of local orbitals which is crucial for the local correlation methods studied in this work is presented in section 2.4, and the local correlation methods, with specific emphasis on the XDEC algorithm is presented and discussed in section 2.5. Aspects of the non-canonical MP2 equations in periodic systems, along with the MP2 equation for non-orthogonal virtual orbitals that are implemented in this work, is presented in section 2.6. Section 2.7 discusses aspects of the pair energy decay, and based on test calculation, the principles of the pair cutoff algorithm developed and implemented in this work is outlined. Finally, in section 2.8, some problematic features of local correlation methods in relation with generating potential energy surfaces are discussed.

2.1 Quantum mechanics

2.1.1 Principles and Dirac notation

We will state the general principles of quantum mechanics, along with a brief introduction to Dirac notation. Except for the Dirac notation, this section will loosely follow Steven Weinbergs *Lectures on Quantum Mechanics* [7]

We begin with the first postulate of quantum mechanics, which states that physical states can be represented by vectors in Hilbert space. We will represent such a state vector by a ket, $|\alpha\rangle$, where whatever inside the ket, in this case α, are simply labels for the state. The inner product of two states $|\alpha\rangle$ and $|\beta\rangle$ is written $\langle\alpha|\beta\rangle$. A Hilbert space is taken to be a inner product space of finite or infinite dimensionality. In the latter case, there must exist an infinite set of linearly independent orthogonal vectors $|i\rangle$ such that for any state vector $|\Psi\rangle$,

the condition $\langle \Psi_N | \Psi_N \rangle \to 0$ for $N \to \infty$ may by satisfied for $|\Psi_N\rangle = |\Psi\rangle - \sum_{i=1}^{N} c_i |i\rangle$. Formally, any vector can then be expressed as a linear combination of orthogonal basis vectors

$$|\Psi\rangle = \sum_i C_i |i\rangle \tag{2.1}$$

where an expression for the coefficient C_i may be obtained by taking the inner product with $|i\rangle$

$$C_i = \frac{\langle i|\Psi\rangle}{\langle i|i\rangle} \tag{2.2}$$

The expansion in equation (2.1) then reads

$$|\Psi\rangle = \sum_i \frac{\langle i|\Psi\rangle}{\langle i|i\rangle} |i\rangle \tag{2.3}$$

We will often assume that the orthogonal basis vectors are normalized to one, meaning that $\langle i|j\rangle = \delta_{i,j}$. In that case, the normalization condition for a state vector is

$$\langle \Psi|\Psi\rangle = \sum_{ij} \langle \Psi|i\rangle \langle \Psi|j\rangle \langle i|j\rangle = \sum_{ij} \langle \Psi|i\rangle \langle \Psi|j\rangle \delta_{i,j} = \sum_i |\langle i|\Psi\rangle|^2 = \sum_i |C_i|^2 = 1 \tag{2.4}$$

The complete set of orthogonal basis vectors may not be denumerable, but rather form a set labeled by some continuous variable ξ. In this case, we may begin by assuming that ξ forms a discrete set such that for a density of ξ values $\rho(\xi)$, $\rho(\xi)d\xi$ is a large number. By normalizing the orthogonal set such that

$$\langle \xi'|\xi\rangle = \rho(\xi)\delta_{\xi',\xi} \tag{2.5}$$

any state vector $|\Psi\rangle$ can be expanded as

$$|\Psi\rangle = \sum_\xi \frac{\langle \xi|\Psi\rangle}{\rho(\xi)} |\xi\rangle \tag{2.6}$$

This is simply the same expansion as in equation (2.3). Assuming that the interval $d\xi$ is so small that $\rho(\xi)$ is constant within the interval, we may replace the sum by an integral according to

$$\sum_\xi f(\xi) \to \int f(\xi)\rho(\xi)d\xi \tag{2.7}$$

This results in the integral expansion of the state vector in terms of the continuous set of basis vectors

$$|\Psi\rangle = \int \langle \xi|\Psi\rangle \, |\xi\rangle \, d\xi \tag{2.8}$$

The inner product of two continuum states is now

$$\langle \Psi|\Psi'\rangle = \int \langle \xi|\Psi\rangle^* \, \langle \xi|\Psi'\rangle \, d\xi \tag{2.9}$$

from which the normalization condition

$$\langle \Psi|\Psi\rangle = \int |\langle \xi|\Psi\rangle|^2 \, d\xi = 1 \tag{2.10}$$

follows. The general statistical interpretation of quantum mechanics holds that the probability that a measurement on a system initially in state $|\Psi\rangle$ will give a result corresponding to state $|\Phi_i\rangle$, is given by

$$P\left(\Psi \to \Phi_i\right) = \frac{|\langle \Phi_i|\Psi\rangle|^2}{\langle \Phi_i|\Phi_i\rangle \, \langle \Psi|\Psi\rangle} \tag{2.11}$$

For normalized vectors, this reduces to

$$P\left(\Psi \to \Phi_i\right) = |\langle \Phi_i|\Psi\rangle|^2 \tag{2.12}$$

For continuum states, the corresponding interpretation is

$$P\left(\Psi \to \Phi_\xi\right) = |\langle \xi|\Psi\rangle|^2 \, d\xi \tag{2.13}$$

Another postulate of quantum mechanics is that observables are represented by Hermitian operators, and that a state has a definite value α for an observable represented by a Hermitian operator A if and only if the state is an eigenstate of A

$$A\,|\Psi\rangle = \alpha\,|\Psi\rangle \tag{2.14}$$

In this context, a *definite value* means that a measurement will yield the same value α every time the measurement is carried out on a system described by the state $|\Psi\rangle$. Hermitian operators are assumed to have a complete set of orthogonal eigenvectors. The expectation value of an observable is defined as the sum of the observable value weighed by the probability of measuring it in accordance with equation (2.12)

$$\langle A\rangle_\Psi = \sum_i \alpha_i \, |\langle i|\Psi\rangle|^2 = \sum_i \langle \Psi|\, A\,|i\rangle \, \langle i|\Psi\rangle = \langle \Psi|\, A\,|\Psi\rangle \tag{2.15}$$

In this expression, we have assumed that $|i\rangle$ are eigenvectors of A. Quantum states are generally time dependent, and when no measurements are performed, the time evolution is determined by the Schrödinger equation

$$i\hbar\frac{d}{dt}|\Psi(t)\rangle = \hat{H}|\Psi(t)\rangle \tag{2.16}$$

where $\hat{H}$ is the Hamiltonian operator, representing the energy of the system.

2.1.2 Wave mechanics

In practice, we often represent quantum states by continuous functions of spatial variables known as wave functions. With the formalism described in the previous chapter, the (spin-0) wave function representation of a state vector $|\Psi\rangle$ may be defined as $\Psi(\boldsymbol{r}) = \langle \boldsymbol{r}|\Psi\rangle$. The wave function is thus the continuous expansion coefficients in the continuous set of eigenkets of the position operator. We will generally assume that quantum states are represented by wave functions, possibly also dependent on a set of spin coordinates.

The Born interpretation of the wave function states that the squared modulus of the wave function gives a probability density for where to find a particle in space. This is a special case of the general statistical interpretation given in equation (2.13), where the positions in space is used as the continuous variable.

The position representation of operators may be obtained by the replacement rules

$$\begin{aligned}\hat{x} &\to x \\ \hat{p} &\to -i\hbar\nabla_x\end{aligned} \tag{2.17}$$

From this, we can construct other operators. For example, the kinetic energy of a particle with mass m is defined as $K = p^2/2m$, so the position representation of the kinetic energy operator is

$$\hat{K} = \frac{\hat{P}^2}{2m} \to -\frac{\hbar^2}{2m}\nabla^2 \tag{2.18}$$

We may then construct the Schrödinger equation in the position representation with a purely position dependent potential as

$$-\frac{\hbar^2}{2m}\nabla^2\psi(\boldsymbol{r},t) + V(\boldsymbol{r})\psi(\boldsymbol{r},t) = i\hbar\frac{\partial}{\partial t}\psi(\boldsymbol{r},t) \tag{2.19}$$

For a time-independent Hamiltonian, this equation separates in space and time coordinates. To see this, we assume a wave function on the form $\psi(\boldsymbol{r},t) = \psi(\boldsymbol{r})\phi(t)$. Putting this into equation (2.19) and dividing by $\psi(\boldsymbol{r})\phi(t)$ gives

$$-\frac{\hbar^2}{2m}\frac{1}{\psi(\boldsymbol{r})}\nabla^2\psi(\boldsymbol{r}) + \frac{1}{\psi(\boldsymbol{r})}V(\boldsymbol{r})\psi(\boldsymbol{r}) = i\hbar\frac{1}{\phi(t)}\frac{\partial}{\partial t}\phi(t) \tag{2.20}$$

Since the two sides of the equation depends on different variables but are (obviously) always equal, they must both equal the same constant. This constant is simply the eigenvalue of the Hamiltonian operator, and is therefore the energy. We then get the two equations

$$-\frac{\hbar^2}{2m}\nabla^2\psi(\boldsymbol{r}) + V(\boldsymbol{r})\psi(\boldsymbol{r}) = E\psi(\boldsymbol{r}) \tag{2.21}$$

$$i\hbar\frac{\partial}{\partial t}\phi(t) = E\phi(t) \tag{2.22}$$

The latter equation have solutions on the form

$$\phi(t) = \exp(iEt/\hbar) \tag{2.23}$$

The former equation is called the time-independent Schrödinger equation, even though it is really just the eigenvalue equation for the Hamiltonian operator.

2.2 The many-particle problem

Exact solutions to the Schrödinger equation are few, and limited only to systems of one, or in special cases, two particles. For systems consisting of many particles, such as molecules, clusters or extended solid, approximations must be imposed. In this section we give a short presentation of the Born-Oppenheimer approximation. Thereafter we look at the independent particle model and Hartree-Fock theory before going through some details for periodic system. We then end with a short discussion of electron correlation. We begin, however, with the Hamiltonian for systems of atoms.

2.2.1 The Pauli principle

Solutions to the many-particle problem must satisfy the Pauli principle, which states that a wave function for a set of identical bosons must be symmetric, while the wave function for identical fermions must be anti-symmetric with respect to interchange of the coordinates of a pair of particles. For a set of N identical particles, this can be formulated mathematically as

$$\begin{aligned} \psi(x_1,...,x_i,...,x_j,...x_N) &= \psi(x_1,...,x_j,...,x_i,...x_N) && \text{Bosons} \\ \psi(x_1,...,x_i,...,x_j,...x_N) &= -\psi(x_1,...,x_j,...,x_i,...x_N) && \text{Fermions} \end{aligned} \tag{2.24}$$

2.2.2 Hamiltonian for systems of atoms

The non-relativistic Hamiltonian for a system of atoms consist of the kinetic energy for the electrons and the nuclei, as well as the potential energy arising from electron-electron repulsion, nucleus-nucleus repulsion and electron-nucleus attraction. The Hamiltonian operator for a system of N electron and M nuclei may be expressed as

$$H = -\frac{1}{2}\sum_{i=1}^{N}\nabla_i^2 - \frac{1}{2}\sum_{A=1}^{M}\frac{\nabla_A^2}{M_j} - \sum_{i=1}^{N}\sum_{A=1}^{M}\frac{Z_A}{r_{iA}} + \sum_{i=1}^{N}\sum_{j>i}^{N}\frac{1}{r_{ij}} + \sum_{A=1}^{M}\sum_{B>A}\frac{Z_A Z_B}{r_{AB}} \tag{2.25}$$

where $r_{ij} = |\boldsymbol{r}_i - \boldsymbol{r}_j|$, M_A is the mass of nucleus A and Z_A is the number of protons in nucleus A.

2.2.3 The Born-Oppenheimer approximation

Due to the large difference in mass, nuclei tends to move much slower than electrons. As a result of this order-of-magnitude difference, we may assume that the system takes a defined electronic structure for each position of the nuclei. We may then solve the electronic Schrödinger equation

$$H_e\Psi_{el}(\boldsymbol{r};\boldsymbol{R}) = E_e\Psi_{el}(\boldsymbol{r};\boldsymbol{R}) \tag{2.26}$$

for each set nuclear positions, where the electronic Hamiltonian H_e contains all the terms in equation (2.25) except for nuclear kinetic energy, and the electron wave function $e\Psi_{el}(\boldsymbol{r};\boldsymbol{R})$ depends only parametrically on the nuclear positions.

The Born-Oppenheimer approximation assumes a partial separation of the Schrödinger equation such that the total wave function may be written as a product of the electron wave function and the nuclear wave function $\phi(\boldsymbol{R})$

$$\Psi(\boldsymbol{r},\boldsymbol{R}) = \Psi_{el}(\boldsymbol{r};\boldsymbol{R})\phi(\boldsymbol{R}) \tag{2.27}$$

and the total Schrödinger equation then becomes

$$\left(T_n + H_e\right)\Psi_{el}(\boldsymbol{r};\boldsymbol{R})\phi(\boldsymbol{R}) = E\Psi_{el}(\boldsymbol{r};\boldsymbol{R})\phi(\boldsymbol{R}) \tag{2.28}$$

where T_n is the nuclear kinetic energy operator. Substituting the result from equation (2.26) gives

$$\left(T_n + E_e\right)\Psi_{el}(\boldsymbol{r};\boldsymbol{R})\phi(\boldsymbol{R}) = E\Psi_{el}(\boldsymbol{r};\boldsymbol{R})\phi(\boldsymbol{R}) \tag{2.29}$$

The complexity of this equation is significantly increased by the fact that T_n also acts on $\Psi_{el}(\boldsymbol{r};\boldsymbol{R})$ due to the parametric dependence on $\boldsymbol{R}$. We can see explicitly how it acts on the Born-Oppenheimer wave function by inserting the explicit form and use the chain rule

$$\begin{aligned} T_n\Psi_{el}(\boldsymbol{r};\boldsymbol{R})\phi(\boldsymbol{R}) &= -\sum_{A=1}^{M}\frac{1}{2M_j}\nabla_A^2\Psi_{el}(\boldsymbol{r};\boldsymbol{R})\phi(\boldsymbol{R}) \\ &= -\sum_{A=1}^{M}\frac{1}{2M_j}\Big[\left(\nabla_A^2\Psi_{el}(\boldsymbol{r};\boldsymbol{R})\right)\phi(\boldsymbol{R}) + \Psi_{el}(\boldsymbol{r};\boldsymbol{R})\nabla_A^2\phi(\boldsymbol{R}) \\ &\qquad + 2\left(\nabla_A\Psi_{el}(\boldsymbol{r};\boldsymbol{R})\right)\nabla_A\phi(\boldsymbol{R})\Big] \end{aligned} \tag{2.30}$$

By putting this back into equation (2.29), multiplying from the left with $\Psi_{el}(\boldsymbol{r};\boldsymbol{R})$ and integrating over the electron coordinates gives

$$\begin{aligned} E\phi(\boldsymbol{R}) &= \langle\Psi_{el}(\boldsymbol{r};\boldsymbol{R})|\,(T_n + E_e)\,|\Psi_{el}(\boldsymbol{r};\boldsymbol{R})\rangle\,\phi(\boldsymbol{R}) \\ &= \langle\Psi_{el}(\boldsymbol{r};\boldsymbol{R})|\,T_n\,|\Psi_{el}(\boldsymbol{r};\boldsymbol{R})\rangle\,\phi(\boldsymbol{R}) + E_e\phi(\boldsymbol{R}) \\ &= -\sum_{A=1}^{M}\frac{1}{2M_j}\Big[\,\langle\Psi_{el}(\boldsymbol{r};\boldsymbol{R})|\,\nabla_A^2\,|\Psi_{el}(\boldsymbol{r};\boldsymbol{R})\rangle\,\phi(\boldsymbol{R}) \\ &\qquad + 2\,\langle\Psi_{el}(\boldsymbol{r};\boldsymbol{R})|\,\nabla_A\,|\Psi_{el}(\boldsymbol{r};\boldsymbol{R})\rangle\,\nabla_A\phi(\boldsymbol{R})\Big] \\ &\qquad + (T_n + E_e)\,\phi(\boldsymbol{R}) \end{aligned} \tag{2.31}$$

The Born-Oppenheimer approximation neglects the first term in the last expression. The resulting equation is then

$$(T_n + E_e(\boldsymbol{R}))\,\phi(\boldsymbol{R}) = E\phi(\boldsymbol{R}) \tag{2.32}$$

which is just a Schrödinger equation for the nuclei where the electronic energy takes the role of the potential energy. We may thus interpret the nuclei as moving on a potential energy surface (PES), and we obtain the PES by solving equation (2.26) for various nuclear positions. In this thesis we shall focus only on solutions to the electronic Schrödinger equation and the resulting PES, and not on properties related to nuclear motion.

2.2.4 The independent particle model

The simplest way of constructing a wave function for N identical fermions that satisfies the Pauli principle is by means of a Slater determinant. A Slater determinant may be written on the form

$$\Psi(x_1, x_2, \ldots, x_N) = \frac{1}{\sqrt{N!}}\begin{vmatrix} \psi_1(x_1) & \psi_2(x_1) & \ldots & \psi_N(x_1) \\ \psi_1(x_2) & \psi_2(x_2) & \ldots & \psi_N(x_2) \\ \vdots & \vdots & \ddots & \vdots \\ \psi_1(x_N) & \psi_2(x_N) & \ldots & \psi_N(x_N) \end{vmatrix} \tag{2.33}$$

where $\psi_i(x_j)$ are single particle wave functions called spin-orbitals, and $x_i = (\boldsymbol{r_i}, \sigma_i)$ are combined spin and spatial coordinates, σ_j being a spin coordinate. Particle-exchange corresponds to interchanging two rows, and since the interchange of two-rows changes the sign of a determinant, the Pauli principle is automatically satisfies. The wave functions also vanishes when two particles have the same coordinate values, creating a so-called Fermi hole. Also, if two particles are put in the same spin-orbital, two columns will be equal, making the wave function vanish in according to Paulis exclusion principle.

This form of a wave function is fine as long as the particles are non-interacting, but we note that the wave function takes a more complicated form if the particles

interacts with each other. In many systems, however, the ground state may be well approximated by a single Slater determinant. In the next section we present the method for obtaining the optimal Slater determinant approximation to the wave function: the Hartree-Fock method.

2.2.5 The variational principle and Hartree-Fock theory

Given an arbitrary normalized wave function $\Psi(x)$ and a complete set of normalized energy eigenfunctions $\{\psi_i\}$ with eigenvalues E_i, the expectation value for the Hamiltonian can be expressed as

$$\begin{aligned}\langle\Psi|\, H\,|\Psi\rangle &= \sum_{ij}\langle\psi_i|\, H\,|\psi_j\rangle = \left(\sum_i C_i^*\,\langle\psi_i|\right)\hat{H}\left(\sum_j C_j\,|\psi_j\rangle\right)\\ &= \sum_{ij} C_j^* C_i E_j\,\langle\psi_i|\psi_j\rangle = \sum_i |C_i|^2\,E_i\end{aligned} \tag{2.34}$$

We assume that the states are labeled such that E_0 is the lowest energy value. Since the functions are normalized in accordance with equation (2.4), we may write

$$E_0 = \sum_i |C_i|^2\,E_0 \leq \sum_i |C_i|^2\,E_i = \langle\Psi|\, H\,|\Psi\rangle \tag{2.35}$$

Thus, the expectation value of the Hamiltonian computed with some trial wave function $\Psi(\boldsymbol{r})$ is always greater than or equal to the exact ground state energy. It is equal if and only if the exact ground state wave function is used. This is called the variational principle. By minimizing the energy of a trial wave function with respect to some parameters, this may be used to obtain approximate wave functions and estimates of the ground state energy.

In the Hartree-Fock method, the energy of a single Slater determinant is variationally minimized with the constraint that the spin-orbitals remain orthonormal. To perform this minimization, we first need an expression for the energy functional of the Slater determinant $\langle\Psi|\, H\,|\Psi\rangle$. We note that the Hamiltonian may be written on the form $\hat{H} = \sum_i h(\boldsymbol{r}_i) + \sum_{i>j} v(r_{ij})$, so that the energy functional may be expressed as

$$E\left[\Psi_{HF}\right] = \sum_i \langle\Psi|\, h(\boldsymbol{r}_i)\,|\Psi\rangle + \sum_{i>j}\langle\Psi|\, v(r_{ij})\,|\Psi\rangle \tag{2.36}$$

By the Slater-Condon rules [8] we have the following relations for Slater determinants

$$\sum_i \langle\Psi|\, h(\boldsymbol{r}_i)\,|\Psi\rangle = \sum_i \langle i|\, h\,|i\rangle \tag{2.37}$$

$$\sum_{i>j}\langle\Psi|\, v(r_{ij})\,|\Psi\rangle = \frac{1}{2}\sum_{ij}\langle ij||ij\rangle \tag{2.38}$$

where we have introduced the notations

$$\langle pq|rs\rangle = \int d\boldsymbol{r}_1 d\boldsymbol{r}_2 \psi_p(\boldsymbol{r}_1)^* \psi_q(\boldsymbol{r}_2)^* r_{ij}^{-1} \psi_r(\boldsymbol{r}_1)\psi_s(\boldsymbol{r}_2) \tag{2.39}$$

and

$$\langle pq||rs\rangle = \langle pq|rs\rangle - \langle pq|sr\rangle \tag{2.40}$$

Inserting this into equation (2.36) gives an energy expression in terms of the spin orbitals

$$E\left[\Psi_{HF}\right] = \sum_i \langle i|\,\hat{h}\,|i\rangle + \frac{1}{2}\sum_{ij}\langle ij||ij\rangle \tag{2.41}$$

Expanding the MOs in equation (2.41) in the atomic orbital (AO) basis yields

$$E\left[\Psi_{HF}\right] = \sum_i \sum_{\mu\nu} C_{\mu i}^* C_{\nu i} \langle \mu|\,\hat{h}\,|\nu\rangle + \frac{1}{2}\sum_{ij}\sum_{\mu\nu\sigma\tau} C_{\mu i}^* C_{\nu j}^* C_{\sigma i} C_{\tau j} \langle \mu\nu||\sigma\tau\rangle \tag{2.42}$$

The extra mathematical constraint that the spin orbitals remain orthonormal, $\langle i|j\rangle = \delta_{i,j}$, may be accounted for by Lagrange multipliers, and the functional L to minimize then becomes

$$L\left[\Psi_{HF}\right] = E[\Psi_{HF}] - \sum_{ij}\left(\lambda_{ji}\sum_{\mu\nu} C_{\mu i}^* C_{\nu j}\langle \mu|\nu\rangle - \delta_{ij}\right) \tag{2.43}$$

We may now create explicit equations to solve by minimizing the energy functional including the Lagrange multiplier condition with respect to the expansion coefficients (using either the coefficients or their complex conjugates yields two independent equations)

$$\frac{\partial}{\partial C_{\mu i}^*}\left[E\left[\Psi_{HF}\right] - \sum_{ij}\lambda_{ji}\sum_{\mu\nu} C_{\mu i}^* C_{\nu j}\langle \mu|\nu\rangle\right] = 0 \tag{2.44}$$

Evaluating the derivatives and inserting the explicit form of the energy functional gives

$$\sum_{\mu\nu} C_{\nu i}\langle \mu|\,\hat{h}\,|\nu\rangle + \sum_j\sum_{\mu\nu\sigma\tau} C_{\nu j}^* C_{\sigma i} C_{\tau j}\langle \mu\nu||\sigma\tau\rangle = \sum_j \lambda_{ji}\sum_{\mu\nu} C_{\nu j}\langle \mu|\nu\rangle \tag{2.45}$$

By switching name on the dummy variables, this may be written on the form

$$\sum_{\nu}\left[\langle\mu|\,\hat{h}\,|\nu\rangle+\sum_{j}\sum_{\sigma\tau}C_{\sigma j}^{*}C_{\tau j}\,\langle\mu\sigma||\nu\tau\rangle\right]C_{\nu i}=\sum_{j}\lambda_{ji}\sum_{\nu}C_{\nu j}\,\langle\mu|\nu\rangle \tag{2.46}$$

Defining the matrix element of the Fock operator in the AO basis as

$$F_{\mu\nu}=\langle\mu|\,\hat{h}\,|\nu\rangle+\sum_{j}\sum_{\sigma\tau}C_{\sigma j}^{*}C_{\tau j}\,\langle\mu\sigma||\nu\tau\rangle \tag{2.47}$$

and elements of the overlap matrix of the AOs

$$S_{\mu\nu}=\langle\mu|\nu\rangle \tag{2.48}$$

equation (2.46) may be written on matrix form as

$$FC=SC\lambda \tag{2.49}$$

This equation has infinitely many solutions, and extra conditions must be imposed in order to obtain an equation with a uniquely defined solution. A unitary transformation of the C-matrix conserves the orthonormality of the MOs. Multiplying the equation from the right by some unitary matrix U and utilize that $U^{\dagger}=U^{-1}$, we get the equation

$$FCU=SCUU^{\dagger}\lambda U \tag{2.50}$$

By defining new matrices $C'\coloneqq CU$ and $\tilde{\lambda}\coloneqq U^{\dagger}\lambda U$, and the Fock matrix in AO basis being invariant to the unitary transformation, we see that this equation is on the same form as equation (2.49). Since λ is a Hermitian matrix, the spectral theorem says that it may be diagonalized by a unitary matrix V such that

$$V^{\dagger}\lambda V=\epsilon \tag{2.51}$$

where epsilon is a diagonal matrix. By setting $U=V$ we obtain the canonical Hartree-Fock equation. This is by far the most common choice of scheme, and gives spin-orbitals that are eigenfunctions of the Fock operator. Since these spin-orbitals are eigenfunctions of an Hamiltonian, they transforms as an irreducible representation of the point group of the system, an are typically delocalized.

We further note that the coefficient matrix C and the Fock matrix in MO basis, λ, in equation (2.47) may be extended to include orbitals not occupied in the HF ground state. We will denote these orbitals *virtual orbitals*. For any i in equation (2.47), the equation is strictly satisfied with a sum only over the virtual orbitals. Given a virtual space that is orthogonal to the occupied space, any contribution λ_{ai} must therefore be zero. The condition that the Fock matrix elements between occupied and virtual orbitals must be zero is the HF

optimization condition. The derivation just given assumed a basis expansion for the MOs at the beginning, and we arrived directly at a matrix equation. A derivation for general MOs without an initial basis expansion is given in reference [9].

The Fock matrix elements in equation (2.47) takes the general form

$$F_{PQ} = \langle P| \hat{h} |Q\rangle + \sum_J \langle PJ||QJ\rangle \tag{2.52}$$

for any two spin orbitals ϕ_P and ϕ_Q.

In this work, we only look at closed-shell systems. In that case, it is often convenient to force pairs of spin-orbitals with opposite spins to take the same spatial form. We will in the following use lowercase letters to signify the index for spatial orbitals, and Greek letters σ, τ and so on to signify the orthonormal spin functions. The spin coordinate will be denoted m, and may take values $\frac{1}{2}$ and $-\frac{1}{2}$ for spin-half particles like electrons. Each spin-orbital is therefore labeled by a pair of indices on the form $p\sigma$. Lets look at the terms in the Fock matrix element expression in equation (2.52) in the formalism. We first note that since the Fock operator is spin-independent, the Fock matrix elements between orbitals of different spin is automatically zero due to the orthogonality of the spin functions. We will show this by assuming that the left index has α-spin and the right β-spin, but the calculation would yield exactly the same result if this were switched. The elements of the core Hamiltonian can be seen to be zero by writing explicitly the integral form

$$\begin{aligned} \langle p\alpha| h(\boldsymbol{r}) |q\beta\rangle &= \int d\boldsymbol{r} dm \phi_p(\boldsymbol{r})^* \alpha(m)^* h(\boldsymbol{r}) \phi_q(\boldsymbol{r}) \beta(m) \\ &= \int dm \alpha(m)^* \beta(m) \int d\boldsymbol{r} \phi_p(\boldsymbol{r})^* h(\boldsymbol{r}) \phi_q(\boldsymbol{r}) = 0 \end{aligned} \tag{2.53}$$

Similarly writing out a term in the sum of two-particle integrals gives

$$
\begin{aligned}
\langle p\alpha, j\alpha || q\beta, j\alpha\rangle &= \int d\boldsymbol{r}_1 d\boldsymbol{r}_2 dm_1 dm_2 \phi_p(\boldsymbol{r}_1)^* \alpha(m_1)^* \phi_j(\boldsymbol{r}_2)^* \alpha(m_2)^* r_{12}^{-1} \\
&\qquad \phi_q(\boldsymbol{r}_1)\beta(m_1)\phi_j(\boldsymbol{r}_2)\alpha(m_2) \\
&\quad - \int d\boldsymbol{r}_1 d\boldsymbol{r}_2 dm_1 dm_2 \phi_p(\boldsymbol{r}_1)^* \alpha(m_1)^* \phi_j(\boldsymbol{r}_2)^* \alpha(m_2)^* r_{12}^{-1} \\
&\qquad \phi_j(\boldsymbol{r}_1)\alpha(m_1)\phi_q(\boldsymbol{r}_2)\beta(m_2) \\
&= \int dm_1 \alpha(m_1)^* \beta(m_1) \int dm_2 \alpha(m_2)^* \alpha(m_2) \\
&\qquad \int d\boldsymbol{r}_1 d\boldsymbol{r}_2 \phi_p(\boldsymbol{r}_1)^* \phi_j(\boldsymbol{r}_2)^* r_{12}^{-1} \phi_q(\boldsymbol{r}_1)\phi_j(\boldsymbol{r}_2) \\
&\quad - \int dm_1 \alpha(m_1)^* \alpha(m_1) \int dm_2 \alpha(m_2)^* \beta(m_2) \\
&\qquad \int d\boldsymbol{r}_1 d\boldsymbol{r}_2 \phi_p(\boldsymbol{r}_1)^* \phi_j(\boldsymbol{r}_2)^* r_{12}^{-1} \phi_j(\boldsymbol{r}_1)\phi_q(\boldsymbol{r}_2) \\
&= 0
\end{aligned}
\tag{2.54}
$$

where the zero value again follows from the orthogonality of the spin functions. The result would also be the same for a spin-orbital label $j\beta$. More interesting are the matrix elements where both spin-orbitals have same spin. The results are the same for α and β spins, so we will assume α spins in the computation. The elements of the core Hamiltonian is easily calculated as follows

$$
\begin{aligned}
\langle p\alpha | \, h \, | q\alpha\rangle &= \int d\boldsymbol{r} dm \phi_p(\boldsymbol{r})^* \alpha(m)^* h(\boldsymbol{r}) \phi_q(\boldsymbol{r}) \alpha(m) \\
&= \int dm \alpha(m)^* \alpha(m) \int d\boldsymbol{r} \phi_p(\boldsymbol{r})^* h(\boldsymbol{r}) \phi_q(\boldsymbol{r}) \\
&= \int d\boldsymbol{r} \phi_p(\boldsymbol{r})^* h(\boldsymbol{r}) \phi_q(\boldsymbol{r}) \\
&= \langle p | \, h \, | q\rangle
\end{aligned}
\tag{2.55}
$$

For the two-particle integrals, we now get two types of contributions: (1) those where the sum-index (J in equation (2.52)) have the same spin as the matrix element indices, and (2) those where the spins of J is different from that in the matrix element indices. Lets calculate the first type of contribution first

$$
\begin{aligned}
\langle p\alpha, j\alpha || q\alpha, j\alpha\rangle &= \int d\boldsymbol{r}_1 d\boldsymbol{r}_2 dm_1 dm_2 \phi_p(\boldsymbol{r}_1)^* \alpha(m_1)^* \phi_j(\boldsymbol{r}_2)^* \alpha(m_2)^* r_{12}^{-1} \\
&\qquad \phi_q(\boldsymbol{r}_1)\alpha(m_1)\phi_j(\boldsymbol{r}_2)\alpha(m_2) \\
&\quad - \int d\boldsymbol{r}_1 d\boldsymbol{r}_2 dm_1 dm_2 \phi_p(\boldsymbol{r}_1)^* \alpha(m_1)^* \phi_j(\boldsymbol{r}_2)^* \alpha(m_2)^* r_{12}^{-1} \\
&\qquad \phi_j(\boldsymbol{r}_1)\alpha(m_1)\phi_q(\boldsymbol{r}_2)\alpha(m_2) \\
&= \int dm_1 \alpha(m_1)^* \alpha(m_1) \int dm_2 \alpha(m_2)^* \alpha(m_2) \\
&\qquad \int d\boldsymbol{r}_1 d\boldsymbol{r}_2 \phi_p(\boldsymbol{r}_1)^* \phi_j(\boldsymbol{r}_2)^* r_{12}^{-1} \phi_q(\boldsymbol{r}_1)\phi_j(\boldsymbol{r}_2) \\
&\quad - \int dm_1 \alpha(m_1)^* \alpha(m_1) \int dm_2 \alpha(m_2)^* \alpha(m_2) \\
&\qquad \int d\boldsymbol{r}_1 d\boldsymbol{r}_2 \phi_p(\boldsymbol{r}_1)^* \phi_j(\boldsymbol{r}_2)^* r_{12}^{-1} \phi_j(\boldsymbol{r}_1)\phi_q(\boldsymbol{r}_2) \\
&= \int d\boldsymbol{r}_1 d\boldsymbol{r}_2 \phi_p(\boldsymbol{r}_1)^* \phi_j(\boldsymbol{r}_2)^* r_{12}^{-1} \phi_q(\boldsymbol{r}_1)\phi_j(\boldsymbol{r}_2) \\
&\quad - \int d\boldsymbol{r}_1 d\boldsymbol{r}_2 \phi_p(\boldsymbol{r}_1)^* \phi_j(\boldsymbol{r}_2)^* r_{12}^{-1} \phi_j(\boldsymbol{r}_1)\phi_q(\boldsymbol{r}_2) \\
&= \langle pj|qj\rangle - \langle pj|jq\rangle
\end{aligned}
\tag{2.56}
$$

For the second contributions, we get

$$
\begin{aligned}
\langle p\alpha, j\beta || q\alpha, j\beta\rangle &= \int d\boldsymbol{r}_1 d\boldsymbol{r}_2 dm_1 dm_2 \phi_p(\boldsymbol{r}_1)^* \alpha(m_1)^* \phi_j(\boldsymbol{r}_2)^* \beta(m_2)^* r_{12}^{-1} \\
&\qquad \phi_q(\boldsymbol{r}_1)\alpha(m_1)\phi_j(\boldsymbol{r}_2)\beta(m_2) \\
&\quad - \int d\boldsymbol{r}_1 d\boldsymbol{r}_2 dm_1 dm_2 \phi_p(\boldsymbol{r}_1)^* \alpha(m_1)^* \phi_j(\boldsymbol{r}_2)^* \beta(m_2)^* r_{12}^{-1} \\
&\qquad \phi_j(\boldsymbol{r}_1)\beta(m_1)\phi_q(\boldsymbol{r}_2)\alpha(m_2) \\
&= \int dm_1 \alpha(m_1)^* \alpha(m_1) \int dm_2 \beta(m_2)^* \beta(m_2) \\
&\qquad \int d\boldsymbol{r}_1 d\boldsymbol{r}_2 \phi_p(\boldsymbol{r}_1)^* \phi_j(\boldsymbol{r}_2)^* r_{12}^{-1} \phi_q(\boldsymbol{r}_1)\phi_j(\boldsymbol{r}_2) \\
&\quad - \int dm_1 \alpha(m_1)^* \beta(m_1) \int dm_2 \beta(m_2)^* \alpha(m_2) \\
&\qquad \int d\boldsymbol{r}_1 d\boldsymbol{r}_2 \phi_p(\boldsymbol{r}_1)^* \phi_j(\boldsymbol{r}_2)^* r_{12}^{-1} \phi_j(\boldsymbol{r}_1)\phi_q(\boldsymbol{r}_2) \\
&= \int d\boldsymbol{r}_1 d\boldsymbol{r}_2 \phi_p(\boldsymbol{r}_1)^* \phi_j(\boldsymbol{r}_2)^* r_{12}^{-1} \phi_q(\boldsymbol{r}_1)\phi_j(\boldsymbol{r}_2) \\
&= \langle pj|qj\rangle
\end{aligned}
\tag{2.57}
$$

We see that the exchange terms vanish in the cases where the spin of the sum index does not match that of the matrix element indices. If we exchange the

sum of J in equation (2.52) with j, and remarks that there are two spin-orbitals for each spatial orbital, we may write the Fock matrix elements in a purely spatial orbital basis as

$$F_{pq} = \langle p| \hat{h} |q\rangle + \sum_j (2 \langle pj|qj\rangle - \langle pj|jq\rangle) \tag{2.58}$$

where we have simply combined the results from equations (2.55), (2.56) and (2.57). Later we will often use the Mulliken notation for the two-particle integrals, which takes the general form

$$g_{pqrs} = (pq|rs) = \int d\boldsymbol{r}_1 d\boldsymbol{r}_2 \phi_p(\boldsymbol{r}_1)^* \phi_q(\boldsymbol{r}_1) r_{12}^{-1} \phi_r(\boldsymbol{r}_2)^* \phi_s(\boldsymbol{r}_2) \tag{2.59}$$

Using this notation, the elements of the Fock matrix can be expressed

$$F_{pq} = h_{pq} - \sum_j (2g_{pqjj} - g_{pjjq}) \tag{2.60}$$

2.2.6 Periodic Boundary Conditions

Crystalline solids are characterized by a periodically repeating pattern of atoms. In the bulk of a macroscopic crystal, the distance to the edges are extremely large seen from a microscopic perspective. Therefore, an infinite three-dimensional lattice of repeating atomic patterns may be used as a model for the crystal. Similarly, a system repeating infinitely in two dimensions may be used as a model for crystalline sheets or surfaces, or in one-dimensions for polymers. We will here assume three dimensions, but the corresponding cases for one and two dimensions may be obtained by only treating the remaining dimensions as non-periodic. The electronic Hamiltonian per unit cell for a periodic system may be expressed as

$$\begin{aligned} H = -\frac{1}{2}\sum_{i=1}^{N} \nabla_i^2 - \sum_n \Bigg(& \sum_{i=1}^{N}\sum_{A=1}^{M} \frac{Z_A}{|\boldsymbol{r}_i - \boldsymbol{r}_A - \boldsymbol{R}_n|} \\ & + \sum_{i=1}^{N}\sum_{j>i}^{N} \frac{1}{|\boldsymbol{r}_i - \boldsymbol{r}_j - \boldsymbol{R}_n|} + \sum_{A=1}^{M}\sum_{B>A} \frac{Z_A Z_B}{|\boldsymbol{r}_A - \boldsymbol{r}_B - \boldsymbol{R}_n|} \Bigg) \end{aligned} \tag{2.61}$$

This Hamiltonian commutes with the lattice translation operator $\hat{T}_{\boldsymbol{R}}$, whose effect is to translate the system according to the general lattice translation vector $\boldsymbol{R}$. This vector is given by $\boldsymbol{R} = n_1\boldsymbol{a}_1 + n_2\boldsymbol{a}_2 + n_3\boldsymbol{a}_3$ where n_i are integers and $\boldsymbol{a}_i$ are lattice vectors. Since all particles are translated into positions physically equivalent to their starting point, the energy of the system must remain the same. Thus, $\left[\hat{T}_{\boldsymbol{R}}, \hat{H}\right] = 0$, and there exists a common set of eigenfunctions of the two operators. According to *Bloch's theorem*, the common set of eigenfunctions

of $\hat{T}_{\boldsymbol{R}}$ and some Hamiltonian for an electron in the lattice can be written on the form

$$\psi_{n\boldsymbol{k}}(\boldsymbol{r}) = \exp(i\boldsymbol{k}\cdot\boldsymbol{r})u_{n\boldsymbol{k}}(\boldsymbol{r}) \tag{2.62}$$

where n is an integer label, $\boldsymbol{k}$ is the crystal momentum and $u_{n\boldsymbol{k}}(\boldsymbol{r}) = u_{n\boldsymbol{k}}(\boldsymbol{r}+\boldsymbol{R})$ is a function with the same periodicity as the crystal. The functions are thus a product of the free particle solution and a periodic function. Due to the discrete translational symmetry (as opposed to the continuous translational symmetry in the case of a free particle), the wave functions also satisfies the periodicity condition in reciprocal space $\psi_{n\boldsymbol{k}}(\boldsymbol{r}) = \psi_{n\boldsymbol{k}+\boldsymbol{K}}(\boldsymbol{r})$, where $\boldsymbol{K}$ is a reciprocal lattice translation vector.

In particular, equation (2.62) gives the form of the eigenfunctions of the Fock operator, and thus the spatial form of the spin-orbitals obtained from canonical Hartree-Fock calculations.

The wave function in equation (2.62) does not in general have the periodicity of the crystal. Rather, the value of wave functions differs by a phase factor between symmetry equivalent points in space. The reason for this is that only the electron density is an observable, and so physically we can only demand that the electron density has same periodicity as the crystal.

In actual calculations, however, we typically enforce so-called Born-von Karman (BvK) boundary conditions, where the wave function is forced to be periodic over a number of unit cells. This set of unit cells is called a Born-von Karman supercell. $\boldsymbol{k}$ then become discrete and only values where $\exp(i\boldsymbol{k}\cdot\boldsymbol{r})$ has the periodicity of the crystal. The approximation introduced by the BvK boundary conditions corresponds to a sort of "folding" of the system where points in space where wave function equality is enforced corresponds the same physical point, rather than merely two symmetry equivalent points. This approximation is improved by increasing the size of the BvK cell, and approaches the correct physical restrictions as the size of the BvK cell approaches infinity.

2.3 Electron correlation

The wave function on the form given in equation (2.33) does not necessarily vanish when two spatial coordinate are equal, since the spin coordinate may differ. The actual wave function of identical charged particles should always go to zero at this point since the Coulomb potential is infinite. The reduced probability of finding another electron in area around any given electron is known as a Coulomb hole, and this effect is neglected in Hartree-Fock theory. The inclusion of electrons closer to each other than in the actual system makes the Hartree-Fock method overestimate the energy, in accordance with the variational principle.

At larger distances, the effect of the Coulomb correlation is more subtle, and are known as London dispersion interactions. A typical somewhat classically motivated explanation is that the instantaneous movement of one electron may create a small dipole such that another electrons may adjust in a manner that is energetically favorable, thus lowering the total energy. Even though these

interaction are typically smaller than the Coulomb hole effect, they may still be significant, and explains for instance the attractive force between helium atoms leading to helium condensation at very low temperatures. We will here present second quantization, a formalism essential for efficient theoretical description of electron correlated methods. We then present some methods for treating electron correlation, with emphasis on Møller-Plesset perturbation theory (MPPT) and CC theory.

2.3.1 Second quantization

In second-quantization, Slater determinants are represented as vectors in Fock space. The basis vectors in Fock space, called occupation number vectors, are chosen so that for a given spin-orbital basis, there is a one-to-one mapping between the Slater determinants and the occupation number vectors.

Lets denote a vector in Fock space as

$$|p_1, p_2, ..., p_N\rangle \coloneqq |\psi_{p_1}, \psi_{p_2}, ..., \psi_{p_N}\rangle \tag{2.63}$$

such that a Slater determinant with combined spin-space coordinates is defined as

$$\langle x_1, x_2, ..., x_N | p_1, p_2, ..., p_N\rangle = \frac{1}{\sqrt{N!}} \begin{vmatrix} \psi_1(x_1) & \psi_2(x_1) & \dots & \psi_N(x_1) \\ \psi_1(x_2) & \psi_2(x_2) & \dots & \psi_N(x_2) \\ \vdots & \vdots & \ddots & \vdots \\ \psi_1(x_N) & \psi_2(x_N) & \dots & \psi_N(x_N) \end{vmatrix} \tag{2.64}$$

Now we define the creation and annihilation operators $a^\dagger_{p_i}$ and a_{p_i} with the properties

$$a^\dagger_q |p_1, p_2, ..., p_N\rangle = |q, p_1, p_2, ..., p_N\rangle \tag{2.65}$$

and

$$a^\dagger_q |p_1, p_2, ..., q, ..., p_N\rangle = |p_1, p_2, ..., p_N\rangle \tag{2.66}$$

We assume that the annihilation operator first permute the relevant spin-orbital to the first index, and then destroys it. The sign in equation (2.66) is therefore positive for an even number of spin-orbitals to the left of q, and negative otherwise. Also, $a^\dagger_q |p_1, p_2, ..., p_N\rangle = 0$ if $q \in \{p_1, p_2, ..., p_N\}$ since this would correspond to creating two equal columns in the Slater determinant. Correspondingly, we will assign to the annihilation operator the property that $a_q |p_1, p_2, ..., p_N\rangle = 0$ if $q \notin \{p_1, p_2, ..., p_N\}$.

The creation and annihilation operators satisfies the following relations

$$\begin{aligned} \{a_p^\dagger, a_q^\dagger\} &= 0 \\ \{a_p, a_q\} &= 0 \\ \{a_p^\dagger, a_q\} &= \delta_{p,q} \end{aligned} \tag{2.67}$$

where $\hat{B}$ as $\{A, B\} = \hat{A}\hat{B} + \hat{B}\hat{A}$ is the anti-commutator of two operators $\hat{A}$ and $\hat{B}$. The first relation is obvious since applying $\{a_p^\dagger, a_q^\dagger\} = 0$ switches the order of the two first columns in the determinant relative to applying $\{a_q^\dagger, a_p^\dagger\} = 0$, which changes the sign of the determinant. Therefore, $a_q^\dagger a_p^\dagger = -a_p^\dagger a_q^\dagger \rightarrow a_q^\dagger a_p^\dagger + a_p^\dagger a_q^\dagger = 0$.

For the second relation, we assume that p is to the left of q. Then, applying a_p first will change the number of states to the left of q by one, by the defining property of the annihilation operator in equation (2.66), $a_q a_p$ must have opposite sign of $a_p a_q$. By the symmetry of the anti-commutator, this must be true also if q is to the left of p.

The final relation is true for $p \neq q$ for essentially the same reasons as argued for the two first relations. In the case $p = q$, one of the terms in the anti-commutator will annihilate the state: $a_p^\dagger a_p$ if p is unoccupied in the state and $a_p a_p^\dagger$ if p is occupied in the state. The term that does not annihilate the state will return the same state since we either first remove p and then put it back, or put in p and then remove it. The sign factor cancels when the two operators are used successively.

Operators in second quantization The form of the operators in second quantization are achieved be making sure expectation values are the same as in first quantization. Expectation values must be the same since first and second quantization formalism ought to describe the same physics, and any measurable value must therefore be the same. We will here simply state how to construct operators in second quantization. We will care only about to types of operators: one-particle operators and two-particle operators. The one particle operators may be expressed in a spin-orbital basis as

$$\hat{f} = \sum_{PQ} f_{PQ} a_P^\dagger a_Q \tag{2.68}$$

where

$$f_{PQ} = \int d\boldsymbol{x} \phi_P^*(\boldsymbol{x}) f(\boldsymbol{x}) \phi_Q(\boldsymbol{x}) \tag{2.69}$$

Two-particle operators take the general form

$$\hat{f} = \frac{1}{2} \sum_{PQRS} g_{PQRS} a_P^\dagger a_R^\dagger a_S a_Q \tag{2.70}$$

with the two-particle integrals defined as

$$g_{PQRS} = \int d\boldsymbol{x}_1 d\boldsymbol{x}_2 \phi_P^*(\boldsymbol{x}_1)\phi_R^*(\boldsymbol{x}_2)g(\boldsymbol{x}_1,\boldsymbol{x}_2)\phi_Q(\boldsymbol{x}_1)\phi_S(\boldsymbol{x}_2) \tag{2.71}$$

The electronic Hamiltonian in second quantization may be expressed as a sum of a constant term, a one-particle operator and a two-particle operator as

$$\hat{H} = \sum_{PQ} h_{PQ} a_P^\dagger a_Q + \frac{1}{2}\sum_{PQRS} g_{PQRS} a_P^\dagger a_R^\dagger a_S a_Q + h_{nuc} \tag{2.72}$$

The explicit form of the second quantized spin-free operators in a spatial orbital basis can be obtained by integrating out the spin coordinates in the same way as was done for the Fock matrix elements. We will state the general form only for spin-independent operators since operators on this form will be used later. The one-particle spin-free operator in spatial orbital basis takes the general form

$$\hat{f} = \sum_{pq} f_{pq} E_{pq} \tag{2.73}$$

where the lowercase indices refer to spatial orbitals and the *singlet excitation operator* is defined as

$$E_{pq} = a_{p\alpha}^\dagger a_{q\alpha} + a_{p\beta}^\dagger a_{q\beta} \tag{2.74}$$

Similarly, the two-particle operators in spatial orbital basis may be written

$$\hat{g} = \frac{1}{2}\sum_{pqrs} g_{pqrs} e_{pqrs} \tag{2.75}$$

where the *two-particle excitation operator* is defined as

$$e_{pqrs} = \sum_{\sigma\tau} a_{p\sigma}^\dagger a_{r\tau}^\dagger a_{s\tau} a_{q\sigma} = EpqErs - \delta_{qr} E_{ps} \tag{2.76}$$

The one-electron and two-electron integrals f_{pq} and g_{pqrs} are defined as in equations (2.69) and (2.71), but with purely spatial orbitals and integral variables. The electronic Hamiltonian can be constructed in a spatial orbital basis by exchanging the operators in spin-orbital basis in equation (2.72) with the operators in spatial orbital basis given in equations (2.73) and (2.75).

2.3.2 Configuration Interaction

Due to the completeness of Slates determinants in the space of anti-symmetric functions, it is possible to write the exact ground state wave function as a linear combination of Slater determinants. The most straight forward way of treating electron correlation is therefore a linear parameterization in the basis of Slater determinants. This method is called configuration interaction (CI), and typically follows a HF calculation from which the Slater determinants are obtained. Using second quantization formalism, the state may be expressed as

$$|CI\rangle = \left(C_0 + \sum_{IA} \hat{X}_I^A + \sum_{I>J,A>B} \hat{X}_{IJ}^{AB} + \dots \right) |HF\rangle \tag{2.77}$$

where weighed excitation operators are defined as

$$\hat{X}_{IJ\dots}^{AB\dots} = C_{IJ\dots}^{AB\dots} a_A^\dagger a_B^\dagger \dots a_I a_J \dots \tag{2.78}$$

The problem is thus reduced to finding the coefficients. Minimizing the energy variationally gives a set of secular equations

$$HC = ESC \tag{2.79}$$

and the CI wave function is found by diagonalizing H. However, the number of possible Slater determinants scales exponentially with the system size. Some simplification is achieved by including only those Slater determinants with correct spin and space symmetries, but full CI is still computationally infeasible for anything but very small systems.

The computational effort may be massively reduced by truncating the sum in equation (2.77) so that it excludes Slater determinants with an excitation order higher than some threshold. Truncated CI however, suffers from slow convergence in the errors as higher excitation levels are included. In addition, it is not size-extensive, meaning that properties computed with the method does not scale correctly with system size, even when the system is extended with non-interacting subsystems. The issue with size-extensivity makes truncated CI not only computationally problematic, but also physically dubious.

2.3.3 Coupled Cluster Theory

In this section, we will give a review of coupled cluster theory with special focus on CCSD. In the coupled cluster method, the state is written on the form

$$|\Psi_{CC}\rangle = \exp\left(\hat{T}\right) |\Psi_0\rangle \tag{2.80}$$

where Ψ_0 is the Hartree-Fock ground state. The exponential of the operator is defined by

$$\exp\left(\hat{T}\right) = \sum_{m=0}^{\infty} \frac{\hat{T}^m}{m!} \tag{2.81}$$

The cluster operator $\hat{T}$ may be written on the form

$$\hat{T} = \sum_{n}^{N} \hat{T}_n \tag{2.82}$$

where $\hat{T}_n$ is a n-particle excitation operator on the form

$$\hat{T}_n = \left(\frac{1}{n!}\right)^2 \sum_{\substack{i_1,i_2,\ldots,i_n \\ a_1,a_2\ldots,a_n}} t_{i_1 i_2 \ldots i_n}^{a_1 a_2 \ldots a_n} a_{a_1}^\dagger a_{a_2}^\dagger \ldots a_{a_n}^\dagger a_{i_n} \ldots a_{i_2} a_{i_1} \tag{2.83}$$

Given a set of Hartree-Fock wave functions, the CC wave function is fully determined by the excitation amplitudes $t_{i_1 i_2 \ldots i_n}^{a_1 a_2 \ldots a_n}$. The goal in CC calculations is therefore to determine the excitation amplitudes. In practical calculations, the sum in equation (2.82) is truncated, giving rise to various truncated CC schemes. For example, excluding terms where $n > 2$ gives CCSD, excluding $n > 3$ gives CCSDT and excluding $n > 4$ gives CCSDTQ, where S,D,T and Q refers to single, double, triple and quadruple cluster operators.

To find a set of equations that may be solved, the Schrödinger equation with the CC wave function ansatz is first multiplied from the left with $\exp\left(-\hat{T}\right)$, and then projected down on the set of Hartree-Fock states, giving rise to an energy equation and a set of amplitude equations

$$\langle \Phi_0 | \exp\left(-\hat{T}\right) \hat{H} \exp\left(\hat{T}\right) | \Phi_0 \rangle = E \tag{2.84}$$

$$\left\langle \Phi_I^A \right| \exp\left(-\hat{T}\right) \hat{H} \exp\left(\hat{T}\right) | \Phi_0 \rangle = 0 \tag{2.85}$$

where $\left|\Phi_I^A\right\rangle$ refers to the determinants with excitation orders corresponding to the cluster excitation operators included in the scheme. The energy in equation (2.84) is not in general the exact expectation value of the Hamiltonian with the CC state, and the CC method is not variational. An exception occurs, however, if the highest order excitation operator matches the number of electrons. In this case, the CC method is exact.

The inclusion of the left-multiplication of $\exp\left(-\hat{T}\right)$ before mapping lets us utilize the Baker–Campbell–Hausdorff (BCH) expansion

$$\exp\left(-\hat{A}\right)\hat{B}\exp\left(\hat{A}\right) = \hat{B} + \left[\hat{B},\hat{A}\right] + \frac{1}{2!}\left[\left[\hat{B},\hat{A}\right],\hat{A}\right] + \frac{1}{3!}\left[\left[\left[\hat{B},\hat{A}\right],\hat{A}\right]\hat{A},\right] + \ldots \tag{2.86}$$

Lets begin, however, with the energy expression in equation (2.84). We first note that since the excitation operators acts de-excitations on a bra, the following simplification holds

$$\langle \Phi_0 | \exp\left(-\hat{T}\right) = \langle \Phi_0 | \tag{2.87}$$

This is true since all de-excitations from virtual orbitals will destroy the bra-state and leave only the constant term from the sum in equation (2.81). Further simplifications can be made by noting that all terms with triple-excitation operators and higher order excitation operators vanish from the orthogonality of Slater-determinants since the Hamiltonian is a two-particle operator, only capable of maximum a double de-excitation. Furthermore, contributions from single-excitation operators vanish due to the Brilluoin theorem (assuming optimized HF ground state). By employing these simplifications, the energy expression reads

$$E = \langle \Phi_0 | \hat{H} \left(1 + \hat{T}_2 + \frac{1}{2}\hat{T}_1^2\right) | \Phi_0 \rangle = E_0 + \langle \Phi_0 | \hat{H} \left(\hat{T}_2 + \frac{1}{2}\hat{T}_1^2\right) | \Phi_0 \rangle \tag{2.88}$$

Subtracting the Hartree-Fock ground state energy, E_0 from the equation gives an expression for the CC correlation energy

$$E_{CC,corr} = \langle \Phi_0 | \hat{H} \left(\hat{T}_2 + \frac{1}{2}\hat{T}_1^2\right) | \Phi_0 \rangle \tag{2.89}$$

Closed-Shell equations For the explicit form of the equations we look only at closed-shell calculations. Furthermore, for the amplitude we reduce the problem to that of MP2. Assuming a spin-0 reference determinant, we only want spin-conserving excitations. The one and two-electron parts of the cluster operator in equation (2.83) then takes the form

$$\hat{T}_1 = \sum_{ia} t_i^a \hat{E}_i^a \tag{2.90}$$

$$\hat{T}_2 = \frac{1}{2} \sum_{iajb} t_{ij}^{ab} \hat{E}_i^a \hat{E}_j^b \tag{2.91}$$

where the spin-singlet excitation operators $\hat{E}_i^a = a_{a\alpha}^\dagger a_{i\alpha} + a_{a\beta}^\dagger a_{i\beta}$ and the lower-case indices refers to purely spatial orbitals.

Since the cluster operators acting on a bra destroys the state, equation 2.89 may just as well be expressed in terms of commutators as

$$E_{CC,corr} = \langle \Phi_0 | \left[\hat{H}, \hat{T}_2\right] + \frac{1}{2} \left[\left[\hat{H}, \hat{T}_1\right], \hat{T}_1\right] | \Phi_0 \rangle \tag{2.92}$$

Writing out the excitation operators in accordance with equations (2.90) and (2.91) gives

$$E_{CC,corr} = \frac{1}{2}\sum_{iajb}(t_{ij}^{ab} + t_i^a t_j^b)\left\langle\Phi_0\right| \left[\hat{H}, E_{aj}E_{bj}\right] + \left[\left[\hat{H}, E_{ai}\right], E_{bj}\right] \left|\Phi_0\right\rangle \quad (2.93)$$

Furthermore, the expression

$$\left\langle\Phi_0\right| \left[\hat{H}, E_{aj}E_{bj}\right] \left|\Phi_0\right\rangle = \left\langle\Phi_0\right| \left[\left[\hat{H}, E_{ai}\right], E_{bj}\right] \left|\Phi_0\right\rangle \quad (2.94)$$

since the only difference between the commutator on the left and right side of the equation involves excitation operator to the left, which destroys the state. Utilizing this relation, equation (2.93) may be rewritten as

$$E_{CC,corr} = \sum_{iajb}(t_{ij}^{ab} + t_i^a t_j^b)\left\langle\Phi_0\right| \left[\left[\hat{H}, E_{ai}\right], E_{bj}\right] \left|\Phi_0\right\rangle \quad (2.95)$$

By explicitly evaluating the commutators (shown in appendix A), the correlation energy may be expressed as

$$E_{corr} = \sum_{ijab}\left(t_{ij}^{ab} + t_i^a t_j^b\right)\left(2g_{iajb} - g_{ibja}\right) \quad (2.96)$$

In CCD and MP2 the terms including single amplitudes are gone.

$$E_{corr} = \sum_{ijab} t_{ij}^{ab}\left(2g_{iajb} - g_{ibja}\right) \quad (2.97)$$

The amplitudes in this work are obtained with second-order Møller-Plesset theory, as shown in the next section.

We finally mention some features of CC calculations. A great benefit of CC is that CCD, CCSD, CCSDT and so on constitute a series of systematically improving approximations to the solutions of the Schrödinger equation. The improvements are more systematic and faster than for CI. The method is also size-extensive for truncated schemes.

2.3.4 Møller-Plesset perturbation theory

In time-independent Rayleigh-Schrödinger perturbation theory it is assumed that the time-independent Schrödinger equation is solved for some Hamiltonian H^0 that is in some sense not too different from the Hamiltonian H of the system we want to solve for. The difference between the solved system and the target system is then treated as a perturbation with a corresponding Hamiltonian H' such that $H = H^0 + H'$. Given a solved Schrödinger equation

$$H^0\psi_n^0 = E_n^0\psi_n^0 \tag{2.98}$$

an attempt of the exact wave function and energy is expanded in some parameter λ as

$$\psi_n = \psi_n^0 + \lambda\psi_n^1 + \lambda^2\psi_n^2 \dots \tag{2.99}$$

and

$$E_n = E_n^0 + \lambda E_n^1 \lambda^2 E_n^2 \dots \tag{2.100}$$

Putting this into the time-independent Schrödinger equation gives

$$\begin{aligned} &H^0\psi_n^0 + \lambda\left(H^0\psi_n^1 + H'\psi_n^0\right) + \lambda^2\left(H^0\psi_n^2 + H'\psi_n^1\right) + \dots \\ &= E_n^0\psi_n^0 + \lambda\left(E_n^0\psi_n^1 + E_n^1\psi_n^0\right) + \lambda^2\left(E_n^0\psi_n^2 + E_n^1\psi_n^1 + E_n^2\psi_n^0\right) + \dots \end{aligned} \tag{2.101}$$

Equating terms of equal order gives equations of zeroth, first and second order, and so on

$$H^0\psi_n^0 - E_n^0\psi_n^0 = 0 \tag{2.102}$$

$$H^0\psi_n^1 + H'\psi_n^0 - E_n^0\psi_n^1 - E_n^1\psi_n^0 = 0 \tag{2.103}$$

$$H^0\psi_n^2 + H'\psi_n^1 - E_n^0\psi_n^2 - E_n^1\psi_n^1 - E_n^2\psi_n^0 = 0 \tag{2.104}$$

The non-canonical MP2 amplitude equations Møller-Plesset perturbation theory is an application of Rayleigh-Schrödinger perturbation theory where we assume the solved system is that described by the Fock Hamiltonian, such that the exact Hamiltonian is given by

$$H = H^0 + \mathcal{V} \tag{2.105}$$

where $\mathcal{V}$ is referred to as the fluctuation potential. Equation (2.97) (given closed-shell system and orbital basis) may be derived from equation (2.104) with the amplitudes derived from equation (2.103). In the case where canonical HF orbitals is used, the Fock matrix is diagonal and a closed-form solution may be

obtained for the amplitudes, such that also second-order energy may be written on a closed-form. For non-canonical HF orbitals, this is not possible and the MP2 equations must be solved iteratively. In principle, $\{\psi_n^0\}$ is a complete set, and we may write psi_0^1 as a linear combination of the unperturbed functions. Putting this into equation (2.103) gives

$$\sum_m \left(H^0 - E_0^0\right) c_m \psi_m^0 + (\mathcal{V} - E_0^1)\psi_0^0 = 0 \tag{2.106}$$

for the ground state. Only second-order amplitudes of second order in excitation contributes, so we may replace

$$c_n \to t_{ij}^{ab} \tag{2.107}$$

and

$$\psi_n^0 \to \left|\Psi_{ij}^{ab}\right\rangle \tag{2.108}$$

Multiplying from the left with $\left\langle\Psi_{ij}^{ab}\right|$ and writing out the full summation then gives

$$\begin{aligned}
&\sum_{k\neq i} \left\langle\Psi_{ij}^{ab}\right| H^0 \left|\Psi_{kj}^{ab}\right\rangle t_{kj}^{ab} + \sum_{k\neq j} \left\langle\Psi_{ij}^{ab}\right| H^0 \left|\Psi_{ik}^{ab}\right\rangle t_{ik}^{ab} \\
&+ \sum_{c\neq a} \left\langle\Psi_{ij}^{ab}\right| H^0 \left|\Psi_{ij}^{cb}\right\rangle t_{ij}^{cb} + \sum_{c\neq b} \left\langle\Psi_{ij}^{ab}\right| H^0 \left|\Psi_{ij}^{ac}\right\rangle t_{ij}^{ac} \\
&+ \left(\left\langle\Psi_{ij}^{ab}\right| H^0 \left|\Psi_{ij}^{ab}\right\rangle - E_0^0\right) t_{ij}^{ab} + \left\langle\Psi_{ij}^{ab}\right| V \left|\Psi_0^0\right\rangle = 0
\end{aligned} \tag{2.109}$$

E_0^0 is the sum of the occupied diagonal Fock matrix elements, and using the Slater-Condon rules on all the other terms, the explicit form of the MP2 amplitude equations may be expressed as

$$\begin{aligned}
&- \sum_{k\neq i} \langle i|\, f\, |k\rangle\, t_{kj}^{ab} - \sum_{k\neq j} \langle j|\, f\, |k\rangle\, t_{ik}^{ab} \\
&+ \sum_{c\neq a} \langle a|\, f\, |c\rangle\, t_{ij}^{cb} + \sum_{c\neq b} \langle b|\, f\, |c\rangle\, t_{ij}^{ac} \\
&+ \left(\langle a|\, f\, |a\rangle + \langle b|\, f\, |b\rangle - \langle i|\, f\, |i\rangle - \langle j|\, f\, |j\rangle\right) t_{ij}^{ab} + (ia|jb) = 0
\end{aligned} \tag{2.110}$$

Finally, this expression may be made nicer by including the diagonal Fock matrix elements in the sums and replacing $\langle p|\, f\, |q\rangle \to f_{pq}$, which gives

$$\sum_k f_{ik} t_{kj}^{ab} + \sum_k f_{jk} t_{ik}^{ab} + \sum_c f_{ac} t_{ij}^{cb} + \sum_c f_{bc} t_{ij}^{ac} + (ia|jb) = 0 \tag{2.111}$$

The left hand side of this equation is itself a component of the residual tensor R_{ij}^{ab}. Using this notation, the amplitude equations simply reads

$$R_{ij}^{ab} = 0 \tag{2.112}$$

A downside with MPPT is that it sometimes struggles with convergence problems, especially for higher orders. Also, it does not have systematic improvements as the order is increased in the same way as CC schemes. All the terms in equation (2.111) also appears in the CCSD doubles amplitude equations, and in this work we treat MP2 as lowest order of the CC schemes.

2.4 Local orbitals

Local orbitals are crucial for local correlation methods, and the locality may greatly affect the possibility of performing small enough cutoffs on orbital spaces and pair calculations to make the local correlation methods computationally feasible. In this section we present some methods for obtaining local orbitals and measuring orbital locality. We then present Wannier functions, which are local orbitals for periodic systems.

2.4.1 Definitions of local orbitals

As there are infinitely many choices for sets of occupied HF orbitals and different ways of measuring orbital locality and spreads, a local HF MO is not uniquely defined. In practice, a canonical HF calculation is usually first carried out, and the HF MOs are then subsequently localized by a unitary transformation of the orbitals that optimizes a localization functional. We will mention three localization schemes here: Boys, Pipek-Mezey and Edmiston-Ruedenberg.

The localization functional may be a sum of central moments, or powers of central moments. Generally, such a localization functional may be expressed as

$$\xi_m^n = \sum_p \langle p| \left(\hat{\boldsymbol{r}} - \langle p| \hat{\boldsymbol{r}} |p\rangle\right)^m |p\rangle^n \tag{2.113}$$

Most commonly, both m and n are set to 1, which gives the Boys (sometimes Foster-Boys) localization functional. However, increasing the value of m typically gives orbitals with smaller tail spread. Furthermore, higher values for n tends to punish outlier orbitals and give set of orbitals with more even distribution of orbital spreads. [10]

In the Pipek-Mezey functional [11] the sum of squared population charges (originally Mulliken charges) is maximized. Generally, this may be expressed as

$$\xi = \sum_{p=1}^{N} \sum_{A} \left(\sum_{\mu \in A} \langle p | \hat{P}_\mu | p \rangle \right) \tag{2.114}$$

where p is an orbital index (of either a set of occupied or virtual orbitals), A is an atom, μ an atomic orbital and $\hat{P}_\mu$ a projector, for instance for Mulliken or Löwdin population.

Finally, the Edmiston-Ruedenberg functional is a self-repulsion integral given by

$$\xi = \sum_{p} \langle pp | r_{12}^{-1} | pp \rangle \tag{2.115}$$

that is maximized to give local orbitals.

As a measurement of the locality of an orbital, we use the second-central moment

$$\sigma^2 = \langle p | \left(\hat{\boldsymbol{r}} - \langle p | \hat{\boldsymbol{r}} | p \rangle \right)^2 | p \rangle \tag{2.116}$$

and we denote

$$\sigma = \left(\langle p | \left(\hat{\boldsymbol{r}} - \langle p | \hat{\boldsymbol{r}} | p \rangle \right)^2 | p \rangle \right)^{1/2} \tag{2.117}$$

the orbital spread. We note, however, that this is a definition, and that the measured locality is not uniquely defined.

2.4.2 Wannier functions

Wannier functions are real-space formulations of wave functions in systems with periodic boundary conditions, and takes essentially the role of local MOs in systems of periodic boundary conditions. Here, we shall use them in the context of local correlation methods, but they have also been used to study bond structures and polarization. [12], [13] Given a set of Bloch functions defined in equation (2.62), Wannier functions are generated by a Fourier transform according to

$$\psi_{\boldsymbol{R}n}(\boldsymbol{r}) = \frac{V}{(2\pi)^3} \int_{BZ} \psi_{n\boldsymbol{k}}(\boldsymbol{r}) \exp(-i\boldsymbol{k} \cdot \boldsymbol{R}) d\boldsymbol{k} \tag{2.118}$$

$$= \frac{V}{(2\pi)^3} \int_{BZ} u_{n\boldsymbol{k}}(\boldsymbol{r}) \exp(i\boldsymbol{k} \cdot (\boldsymbol{r} - \boldsymbol{R})) d\boldsymbol{k} \tag{2.119}$$

where the integration is over the Brillouin zone and $\boldsymbol{R}$ is a unit cell coordinate. Since the Bloch functions $u_{n\boldsymbol{k}(\boldsymbol{r})}$ have the same periodicity as the crystal, the two Wannier functions with the same label n in two different unit cells $\boldsymbol{R}$ and

$\boldsymbol{R'}$ are related by a simple translation according to $\psi_{\boldsymbol{R'}n}(\boldsymbol{r}) = \psi_{\boldsymbol{R}n}(\boldsymbol{r} - (\boldsymbol{R'} - \boldsymbol{R})) = \psi_{\boldsymbol{0}n}(\boldsymbol{r} - \boldsymbol{R'})$. All Wannier functions may therefore be generator by simple translations from a set of Wannier functions in a reference cell. For a position $\boldsymbol{r'}$ such that $|\boldsymbol{r} - \boldsymbol{R}|$ is a large number, the exponential factor will vary quickly as we integrate along $\boldsymbol{k}$. This corresponds to a rapid rotation around the unit circle in the complex plane. Since $u_{n\boldsymbol{k}}$ is a smooth function of $\boldsymbol{k}$, any contribution to the integral will quickly be canceled by neighboring contributions where the exponential factor has a value corresponding to the opposite side of the unit circle. The magnitude of the value of the Wannier function will therefore be small. Thus, Wannier functions are in some sense local, having significant values only close to the unit cell they are associated with.

In fact there are more degrees of freedom available for localization. Similarly to the unitary transformation of spin-orbital in molecular systems as shown in equation (2.50), we now the possibility of unitary transformations at each $\boldsymbol{k}$ point, according to

$$\psi_{\boldsymbol{R}n}(\boldsymbol{r}) = \frac{V}{(2\pi)^3} \int_{BZ} \sum_m U^{\boldsymbol{k}}_{mn} \psi_{n\boldsymbol{k}}(\boldsymbol{r}) \exp(-i\boldsymbol{k} \cdot \boldsymbol{R}) d\boldsymbol{k} \tag{2.120}$$

This form of unitary transformations may further improve on the locality of Wannier functions.

With BvK boundary conditions, the Wannier functions are generated by a sum

$$\psi_{\boldsymbol{R}n}(\boldsymbol{r}) = \frac{1}{\sqrt{N}} \sum_{\boldsymbol{k}} \psi_{n\boldsymbol{k}}(\boldsymbol{r}) \exp(-i\boldsymbol{k} \cdot \boldsymbol{R}) \tag{2.121}$$

where N is the number of primitive unit cells in the BvK cell. Let $\boldsymbol{B}$ be a vector whose components are integer numbers of the side lengths of the BvK cell. Since the Bloch wave functions satisfies the translational symmetry condition $\psi_{n\boldsymbol{k}}(\boldsymbol{r}) = \psi_{n\boldsymbol{k}}(\boldsymbol{r} - \boldsymbol{B})$, this must now also be true for Wannier functions: $\psi_{n\boldsymbol{R}}(\boldsymbol{r}) = \psi_{n\boldsymbol{R}}(\boldsymbol{r} - \boldsymbol{B})$. The Wannier functions are thus local only within the BvK cell, and may similarly be normalized within the BvK cell.

Finally, we note that the Wannier functions are translationally orthogonal. This can be shown from the orthogonality of the Block functions (who must be orthogonal at k-values of different energies since they are eigenfunctions of some

Hamiltonian operator) by

$$\begin{aligned}\langle\psi_{n\boldsymbol{R}}|\psi_{n\boldsymbol{R}'}\rangle &= \int_{BvK}\psi_{n\boldsymbol{R}}(\boldsymbol{r})^*\psi_{n\boldsymbol{R}'}(\boldsymbol{r})d\boldsymbol{r}\\ &= \frac{1}{N}\sum_{\boldsymbol{k}\boldsymbol{k}'}\int_{BvK}\exp(i\boldsymbol{k}\cdot\boldsymbol{R})\psi_{n\boldsymbol{k}}(\boldsymbol{r})\exp(-i\boldsymbol{k}'\cdot\boldsymbol{R}')\psi_{n\boldsymbol{k}'}(\boldsymbol{r})d\boldsymbol{r}\\ &= \frac{1}{N}\sum_{\boldsymbol{k}\boldsymbol{k}'}\int_{BvK}\exp(i\boldsymbol{k}\cdot\boldsymbol{R})\exp(-i\boldsymbol{k}'\cdot\boldsymbol{R}')\delta_{\boldsymbol{k}.\boldsymbol{k}'}\\ &= \frac{1}{N}\sum_{\boldsymbol{k}}\int_{BvK}\exp(i\boldsymbol{k}\cdot(\boldsymbol{R}-\boldsymbol{R}')) = \delta_{\boldsymbol{R},\boldsymbol{R}'}\end{aligned} \tag{2.122}$$

This is a rather strict orthogonality requirement not present in normal molecular calculations, and may affect the localizability significantly. In particular, long tails with complicated nodal structure may be enforced on the orbitals in order to satisfy the orthogonality condition.

2.5 Local Correlation Methods

Local correlation methods seek to achieve reduced scaling by exploiting the locality of electron correlation, the ultimate goal being methods that scales linearly in the computational resources with increased system size.

The DEC algorithm, as to be described in the forthcoming section, belongs to a class of methods that split the system into smaller parts for which the amplitude equations are solved individually.

2.5.1 The DEC algorithm

In the original DEC algorithm [14], the correlation energy expression is partitioned by which atoms the occupied orbitals in the two-particle integrals are associated with. The correlation energy expression in equation (2.96) may then conveniently be reformulated as

$$E_{corr} = \sum_P E_P + \sum_{P>Q}\Delta E_{PQ} \tag{2.123}$$

where the atomic fragment energies E_P and pair fragment energies are defined as

$$E_P = \sum_{ij\in P}\sum_{ab}\left(t_{ij}^{ab} + t_i^a t_j^b\right)\left(2g_{iajb} - g_{ibja}\right) \tag{2.124}$$

$$\Delta E_{PQ} = \sum_{ij\in P\cup Q}\sum_{ab}\left(t_{ij}^{ab} + t_i^a t_j^b\right)\left(2g_{iajb} - g_{ibja}\right) - E_P - E_Q \tag{2.125}$$

In the DEC algorithm, the atomic fragment energy of atom P in equation (2.124) is computed using only those occupied orbitals that, by some means, are associated with atom P. An occupied orbital may be associated with an atom that is closest to its center of charge, but also other criteria, like Mulliken charges may be used. The virtual space is limited to orbitals that are spatially close, and is expanded until the fragment energy converges within a threshold. The space of occupied and virtual orbitals used to calculate a fragment energy is denoted the energy orbital space (EOS). The amplitude equations in equation 2.111) are solved for each atomic fragment, and space for which the amplitudes are solved for a fragment i called the amplitude orbital space (AOS). Compared to the EOS, an extra buffer regions is included for the orbitals in the AOS.

For the pair energies ΔE_{PQ} in equation (2.125), the union of the orbital of fragment P and Q is employed. With the extra truncation in the virtual spaces, the fragment energies and pair fragments energies may be expressed as

$$E_P = \sum_{ij \in P} \sum_{ab \in [P]} \left(t_{ij}^{ab} + t_i^a t_j^b\right) \left(2g_{iajb} - g_{ibja}\right) \tag{2.126}$$

$$\Delta E_{PQ} = \sum_{ij \in P \cup Q} \sum_{ab \in [P] \cup [Q]} \left(t_{ij}^{ab} + t_i^a t_j^b\right) \left(2g_{iajb} - g_{ibja}\right) - E_P - E_Q \tag{2.127}$$

where $[P]$ denotes the virtual EOS of atom P. Both the virtual space of the atomic fragments, and the occupied and virtual buffer regions are expanded until the energy change is smaller than some threshold called the *fragment optimization threshold* (FOT). The central idea is that the total error in the correlation energy should be determined solely by the FOT.

2.5.2 Extended DEC

The Extended DEC (XDEC) algorithm [5] is an extension of the DEC algorithm to systems with periodic boundary conditions. Formally, the difference from the original DEC algorithm lies mainly in a redefinition of the local MOs. In addition, an alteration of the equations are necessary, so that they capture the physical aspects of the periodic system. This may be done either by solving for a big chunk of the system as a cluster, or by reformulating the energy and amplitude equation to a periodic form (see section 2.5.3). For the local occupied MOs, the Wannier functions defined by equation (2.121) are used. For virtual orbitals, either Wannier functions or PAOs defined in equations (2.149).

The correlation energy is calculated for a reference unit cell. The energy expression may now be formulated as

$$E_{corr} = \sum_P E_{P\mathbf{0}} + \sum_{P<Q} \Delta E_{P\mathbf{0},Q\mathbf{0}} + \sum_{PQ} \sum_{\boldsymbol{L} \neq \mathbf{0}} \Delta E_{P\mathbf{0},Q\boldsymbol{L}} \tag{2.128}$$

where $\boldsymbol{L}$ is a lattice coordinate and $\mathbf{0}$ is taken to be the reference cell for which the correlation energy is calculated. The amplitudes are found by solving equation (2.137) for each fragment.

As for pair fragments, the amplitude equations are solved in the union of the fragment spaces. Buffer amplitudes are used only for the occupied indices, since virtual buffer amplitudes seem have little effect.

2.5.3 Two versions of the XDEC code

There exist two implementations of XDEC. The work with interpolating pair energies were originally done with the original implementation as described in reference [5], and later implemented in the new implementation of XDEC. A description of the characteristics of the two implementations is therefore justified. In this section, the key differences between the two XDEC implementations are laid out.

In the original implementation, the equations are solved essentially as for a cluster, and the symmetries in the two-particle matrix

$$g(\mathbf{0}p, (\mathbf{Q}-\mathbf{P})\,q, (\mathbf{R}-\mathbf{P})\,r, (\mathbf{S}-\mathbf{P})\,s) = g(\mathbf{P}p, \mathbf{Q}q, \mathbf{R}r, \mathbf{S}s), \tag{2.129}$$

are not utilized. In addition, the Wannier functions are fitted on a subset of the original set of AOs. This subset is denoted an orbital extent. Density fitting is done on a fragment level.

In the newly developed XDEC code, the symmetries in 2.129 are utilized such that one lattice index may be removed. In addition, the density fitting is done periodically, instead of on a fragment level. In the process of finding the coefficients of the density fitting, the Coulomb matrix in the basis of the auxiliary basis must be inverted. However, this becomes a scaling wall due to the slow convergence of the matrix elements with increasing distance. The fitting is therefore done with an attenuated Coulomb operator [15] defined as

$$\frac{\mathrm{erfc}(\omega r)}{r} = \frac{1}{r} - \frac{\mathrm{erf}(\omega r)}{r} \tag{2.130}$$

If the attenuation parameter ω is chosen to be zero, the Coulomb operator is retained. For positive non-zero values, the effect of the error function is to undermine the long-distance values. This introduces another parameter that affects the accuracy of the calculation. If this parameter is chosen sufficiently small, however, the errors may be made negligible at the expense of increase in computation time and memory.

Another difference is in the fragmentation. In the original implementation, atomic fragments where always used. In the new version, the fragmentation is more flexible, but the standard scheme is based on proximity between the orbitals, and the orbitals are not assigned to atoms.

2.5.4 A detail about the orbital spaces for pair fragments

Due to the relevance for the cutoff algorithm, we will mention a detail about the AOSs that are used for pairs in the new XDEC program.

The amplitudes for the pairs are supposed to be solved in a AOS that the union of the AOS of each of the fragments. That is, an AOS ω_{PQ} for the pair P, Q is defined by $\omega_{PQ} = \underline{P}_{\mathbf{0}} \cup \underline{Q}_{\boldsymbol{N}} \cup [P_{\mathbf{0}}] \cup [Q_{\boldsymbol{N}}]$, buffer amplitudes are included in $\underline{P}_{\mathbf{0}}$ and $\underline{Q}_{\boldsymbol{N}}$.

In the new XDEC program, the first occupied indices for the amplitude tensors are only stored for the reference cell. This may be resolved by replacing the relevant missing excitations from $\underline{Q}_{\boldsymbol{N}}$ to $P_{\mathbf{0}}$ with excitations from $\underline{Q}_{\mathbf{0}}$ to $P_{-\boldsymbol{N}}$. In the implementation this forces the overlapping buffer amplitudes of $[\hat{P}]$ and $[\hat{P}]$ to be equal. With the imposed cutoffs in the orbital spaces in the DEC algorithm, however, these amplitudes should be allowed to differ somewhat. This issue leads to a loss of translational symmetry of the pairs in the sense that $\Delta E_{\mathbf{0}P,\boldsymbol{N}Q} \neq \Delta E_{-\boldsymbol{N}P,\mathbf{0}Q}$.

As a solution, the new XDEC program solves the amplitude equations in the orbital space defined by $\omega_{PQ} = \omega_{PQ,-\boldsymbol{N}} \cup \omega_{PQ,\mathbf{0}} \cup \omega_{PQ,\boldsymbol{N}}$, where $\omega_{PQ,\boldsymbol{N}} = \underline{P}_{\boldsymbol{N}} \cup \underline{Q}_{\boldsymbol{N}} \cup [P_{\boldsymbol{N}}] \cup [Q_{\boldsymbol{N}}]$

When solving the amplitude equations for in this space, the amplitudes for computing $\Delta E_{\mathbf{0}P,\boldsymbol{N}Q}$, $\Delta E_{\mathbf{0}Q,\boldsymbol{N}P}$, $\Delta E_{\mathbf{0}P,\boldsymbol{N}P}$ and $\Delta E_{\mathbf{0}Q,\boldsymbol{N}Q}$ are obtained simultaneously. At this point, it is therefore computationally cheap to calculate the energy for all four pairs simultaneously.

2.5.5 General fragments

The fragmentation of the occupied and virtual orbital spaces are possible due to the gradual decoupling of any two amplitudes when their indices refer to sets of orbitals that are separated by an increasing distance. The fragmentation is therefore simply a splitting of the system up in subsystems where we assume that the amplitudes in each subsystem are essentially non-coupled to amplitudes in the other subsystems. The buffer amplitudes are introduced since the sets of amplitudes are not completely decoupled. From this perspective, however, the atomic fragmentation is just an example of how the fragmentation may be done automatically, and we will here briefly mention some other methods of fragmentation that can be useful in periodic systems.

A key feature of a fragment is that the set of occupied orbitals, and consequently the virtual orbitals, is local in the sense that all the orbitals decay to zero at points in space sufficiently far away from any occupied orbital in the fragment.

An alternative approach to generating fragments used in the new XDEC code is to start with one initial occupied orbital, and include in the fragment all occupied orbitals closer than a given distance. This is repeated for the orbitals that has yet to be included in a fragment until all occupied orbitals have been assigned to a fragment.

It is also possible to make one fragment for each occupied MO.

The previously described fragmentation schemes make sense in molecular systems and periodic systems with large unit cells since they all generate local fragments. These schemes have also been used in periodic systems with small unit cells. In these systems, however, it may make sense to include all the occupied orbitals in the unit cell in on fragment, since this set of orbitals is already

local. This will, depending on the size of the unit cell, create larger fragments. On the other hand, it may dramatically reduce the number of pair calculations.

2.5.6 Another example of a fragmentation based method

The various local correlation methods varies in how the equations are sliced up, how the virtual space is represented, or other approximation made, like extent fitting or attenuated fitting. The way of slicing up the energy equation in the DEC algorithm as shown in equation (2.123) and in periodic form in equation (2.128) is just an example of how the equation may be split up. In the CiM algorithm [16], [4], which is another notable fragmentation method, the energy expression is written as

$$E_{corr} = \sum_i \Delta E_i \tag{2.131}$$

where ΔE_i is defined as

$$\Delta E_i = \sum_{jab} (ia|jb)\, t_{ij}^{ab} \tag{2.132}$$

Given that atomic fragmentation is used, the DEC algorithm divides the correlation energies into the interactions on each atom, and the interactions between atoms. The CiM algorithm on the other hand, splits up the energy into the contribution from a occupied orbital and the interaction of this occupied orbital. This contribution for each occupied MO is summed up.

2.6 MP2 equations in periodic systems

In this work we will look at the effect of using PAOs as virtual orbitals. The PAOs are non-orthogonal to each other, and non-orthogonal virtual orbitals cannot be directly used in the MP2 amplitude equations presented previously. There are mainly two ways to deal with the non-orthogonality. Either, the orbitals must be orthogonalized, for instance made pseudo-canonical, or the non-orthogonality must be accounted for in the equations. Here, we take the latter approach. First however, the structure of block Toeplitz matrices is presented.

2.6.1 Block Toeplitz matrices

Block Toeplitz matrices are important for the theoretical description of periodic systems, and will be presented in this section.

A Toeplitz matrix is a matrix where all elements along any given chosen diagonal

is equal. An infinite Toeplitz matrix can be written on the form

$$A = \begin{bmatrix} \ddots & \vdots & \vdots & \vdots & \vdots & \vdots & \iddots \\ \dots & a_0 & a_1 & a_2 & a_3 & a_4 & \dots \\ \dots & a_{-1} & a_0 & a_1 & a_2 & a_3 & \dots \\ \dots & a_{-2} & a_{-1} & a_0 & a_1 & a_2 & \dots \\ \dots & a_{-3} & a_{-2} & a_{-1} & a_0 & a_1 & \dots \\ \dots & a_{-4} & a_{-3} & a_{-2} & a_{-1} & a_0 & \dots \\ \iddots & \vdots & \vdots & \vdots & \vdots & \vdots & \ddots \end{bmatrix} \tag{2.133}$$

In a Block Toeplitz matrix, the elements a_i are themselves matrices referred to as blocks. The block Toeplitz matrices occurs naturally in the description of 1D periodic systems since matrices like the periodic overlap matrix $S_{\boldsymbol{I}i,\boldsymbol{J}j}$ or the periodic Fock matrix $F_{\boldsymbol{I}i,\boldsymbol{J}j}$ may by organized such that the cell index refers to blocks while the orbital indices refers to single matrix elements within each block. In 2D and 3D systems, such properties can be written on a block Toeplitz form by an appropriate flattening of the lattice indices. Figure 2.1 shows an idealized illustration of the typical block Toeplitz structure of periodic matrices, where the color signifies the magnitude of the elements in each block. It is assumed that the blocks are ordered such that the distance between cells increases with increased distance between the blocks and the main diagonal.

Since the periodic systems are assumed to be infinite, the Toeplitz matrices are also in principle infinitely large. In most cases, the magnitude of the elements decreases with distance from the diagonal, and from an implementation point of view, only block with elements larger than a given tolerance needs to be stored. It is also apparent that only one row or one column of blocks defines the whole matrix, and only one row or one column needs to be stored.

The periodic matrices have the translational symmetry

$$a_{\boldsymbol{I}i,\boldsymbol{J}j} = a_{(\boldsymbol{I}-\boldsymbol{R})i,(\boldsymbol{J}-\boldsymbol{R})j} \tag{2.134}$$

which can be used to reduce the dimensionality in the following manner

$$a_{\boldsymbol{I}i,\boldsymbol{J}j} = a_{\boldsymbol{0}i,(\boldsymbol{J}-\boldsymbol{I})j} =: a_{ij}^{\boldsymbol{J}-\boldsymbol{I}} \tag{2.135}$$

This is the form in which the Toeplitz matrices are stored in the XDEC program.

2.6.2 MP2 equations in periodic systems

We may extend the energy and amplitude equations given in equations (2.97) and (2.111) to periodic systems by including sums over lattice indices $\boldsymbol{L}$. The closed-shell CC correlation energy expression for the reference cell then reads

$$E_{corr,MP2} = \sum_{i\boldsymbol{A}a\boldsymbol{J}j\boldsymbol{B}b} \left(2t_{\boldsymbol{0}i,\boldsymbol{J}j}^{\boldsymbol{A}a,\boldsymbol{B}b} g_{\boldsymbol{0}i,\boldsymbol{J}j}^{\boldsymbol{A}a,\boldsymbol{B}b} - t_{\boldsymbol{0}i,\boldsymbol{J}j}^{\boldsymbol{A}a,\boldsymbol{B}b} g_{\boldsymbol{0}i,\boldsymbol{J}j}^{\boldsymbol{B}b,\boldsymbol{A}a} \right) \tag{2.136}$$

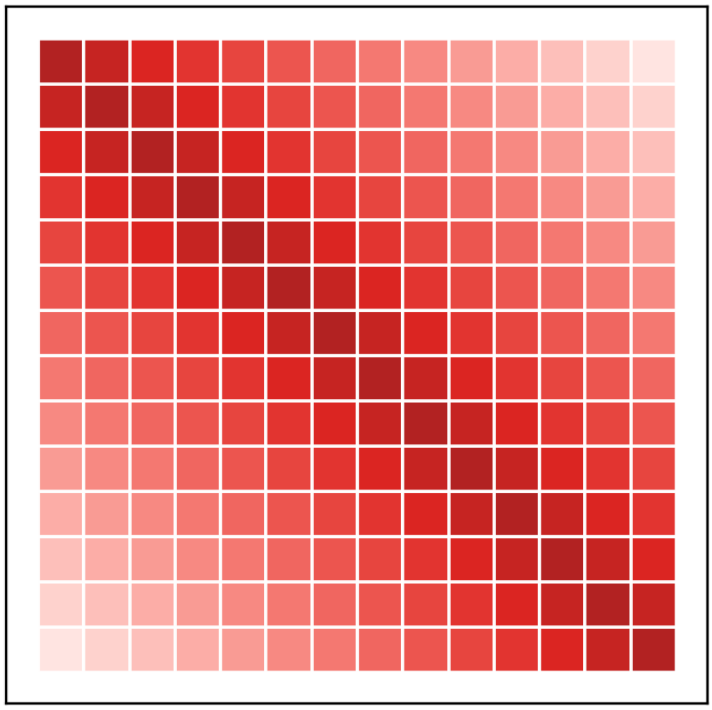

Figure 2.1: An idealized illustration of the typical structure of a block Toeplitz matrix of a periodic system. Each block represent a matrix for some property between two lattice cells. The blocks are assumed to be ordered such that the distance between cells increases with the distance from the diagonal blocks of the matrix.

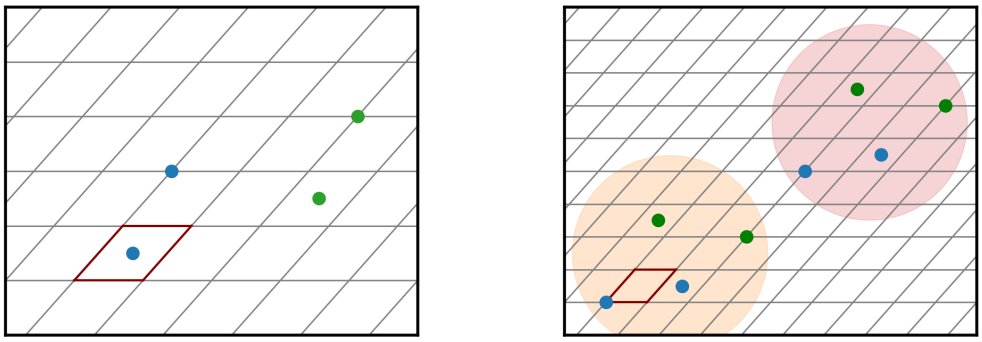

Figure 2.2: Visual illustration of the translational symmetry of the Toeplitz matrices and amplitude tensors in a periodic lattice. Sets of two or four orbitals always have a symmetry equivalent set relative to the reference cell, which is marked with red lines.

The periodic non-canonical MP2 amplitude equations can similarly be formulated as

$$0 = (\boldsymbol{I}i, \boldsymbol{A}a|\boldsymbol{J}j, \boldsymbol{B}b) + \sum_{\boldsymbol{C}c} t^{\boldsymbol{C}c,\boldsymbol{B}b}_{\boldsymbol{I}i,\boldsymbol{J}j} f_{\boldsymbol{A}a,\boldsymbol{C}c} + \sum_{\boldsymbol{C}c} t^{\boldsymbol{A}a,\boldsymbol{C}c}_{\boldsymbol{I}i\boldsymbol{J}j} f_{\boldsymbol{B}b,\boldsymbol{C}c} \tag{2.137}$$

$$- \sum_{\boldsymbol{K}k} t^{\boldsymbol{A}a,\boldsymbol{B}b}_{\boldsymbol{K}k,\boldsymbol{J}j} f_{\boldsymbol{K}k,\boldsymbol{I}i} - \sum_{\boldsymbol{K}k} t^{\boldsymbol{A}a,\boldsymbol{B}b}_{\boldsymbol{I}i,\boldsymbol{K}k} f_{\boldsymbol{K}k,\boldsymbol{J}j}. \tag{2.138}$$

We note that for any lattice translation vector $\boldsymbol{R}$, we have the following translational symmetries in the tensors with two and four cell vector indices:

$$S_{\boldsymbol{I}i,\boldsymbol{J}j} = S_{(\boldsymbol{I}-\boldsymbol{R})i,(\boldsymbol{J}-\boldsymbol{R})j} \tag{2.139}$$

$$t^{\boldsymbol{A}a,\boldsymbol{B}b}_{\boldsymbol{I}i,\boldsymbol{J}j} = t^{(\boldsymbol{A}-\boldsymbol{R})a,(\boldsymbol{B}-\boldsymbol{R})b}_{(\boldsymbol{I}-\boldsymbol{R})i,(\boldsymbol{J}-\boldsymbol{R})j} \tag{2.140}$$

The overlap matrix and amplitude tensors are used as examples here, but the same symmetries are true for any tensor on the with translational symmetry. We may use this symmetry to reduce the dimensionality of the tensors. In equations (2.139) and (2.140) for example, we may translate the tensors by the vector I to obtain

$$S_{\boldsymbol{I}i,\boldsymbol{J}j} = S_{\boldsymbol{0}i,(\boldsymbol{J}-\boldsymbol{I})j} =: S^{\boldsymbol{J}-\boldsymbol{I}}_{ij} \tag{2.141}$$

$$t^{\boldsymbol{A}a,\boldsymbol{B}b}_{\boldsymbol{I}i,\boldsymbol{J}j} = t^{(\boldsymbol{A}-\boldsymbol{I})a,(\boldsymbol{B}-\boldsymbol{I})b}_{\boldsymbol{0}i,(\boldsymbol{J}-\boldsymbol{I})j} \tag{2.142}$$

This is the form in which the tensors are stored in the XDEC program. Using this form of the tensors, we only need the residuals of the form $R^{\boldsymbol{A}a,\boldsymbol{B}b}_{\boldsymbol{0}i,\boldsymbol{J}j}$, and the amplitude equations given in equation 2.137 may be reformulated as

$$0 = (\boldsymbol{0}i, \boldsymbol{A}a|\boldsymbol{J}j, \boldsymbol{B}b) + \sum_{\boldsymbol{C}c} t^{\boldsymbol{C}c,\boldsymbol{B}b}_{\boldsymbol{0}i,\boldsymbol{J}j} f^{\boldsymbol{C}-\boldsymbol{A}}_{ac} + \sum_{\boldsymbol{C}c} t^{\boldsymbol{A}a,\boldsymbol{C}c}_{\boldsymbol{0}i,\boldsymbol{J}j} f^{\boldsymbol{C}-\boldsymbol{B}}_{bc} \tag{2.143}$$

$$- \sum_{\boldsymbol{K}k} t^{(\boldsymbol{A}-\boldsymbol{K})a,(\boldsymbol{B}-\boldsymbol{K})b}_{\boldsymbol{0}k,(\boldsymbol{J}-\boldsymbol{K})j} f^{-\boldsymbol{K}}_{ki} - \sum_{\boldsymbol{K}k} t^{\boldsymbol{A}a,\boldsymbol{B}b}_{\boldsymbol{0}i,\boldsymbol{K}k} f^{\boldsymbol{J}-\boldsymbol{K}}_{kj}. \tag{2.144}$$

From an implementation point of view, the term of the form

$$\sum_{\boldsymbol{K}k} t^{(\boldsymbol{A}-\boldsymbol{K})a,(\boldsymbol{B}-\boldsymbol{K})b}_{\boldsymbol{0}k,(\boldsymbol{J}-\boldsymbol{K})j} f^{-\boldsymbol{K}}_{ki} \tag{2.145}$$

is the most challenging. By utilizing the symmetry

$$t^{\boldsymbol{A}a,\boldsymbol{B}b}_{\boldsymbol{K}k,\boldsymbol{J}j} = t^{\boldsymbol{B}b,\boldsymbol{A}a}_{\boldsymbol{J}j,\boldsymbol{K}k} \tag{2.146}$$

and then translate the tensor by J such that

$$t^{\boldsymbol{B}b,\boldsymbol{A}a}_{\boldsymbol{J}j,\boldsymbol{K}k} = t^{(\boldsymbol{B}-\boldsymbol{J})b,(\boldsymbol{A}-\boldsymbol{J})a}_{\boldsymbol{0}j,(\boldsymbol{K}-\boldsymbol{J})k} \tag{2.147}$$

the contraction in equation (2.145) may alternatively be expressed as

$$\sum_{\boldsymbol{K}k} t^{(\boldsymbol{A}-\boldsymbol{J})a,(\boldsymbol{B}-\boldsymbol{J})b}_{\boldsymbol{0}j,(\boldsymbol{K}-\boldsymbol{J})k} f^{-\boldsymbol{K}}_{ki} \tag{2.148}$$

This form has the apparent advantage of only summing over one index in the amplitude tensor, but the difference in implementation is of minor importance.

2.6.3 Projected Atomic Orbitals

The occupied and virtual orbital spaces are vector spaces, and in principle any set of functions that span either the occupied or virtual spaces can be used as a basis. To span the virtual space, we may use PAOs instead of virtual Wannier functions. A PAO is generated from an AO by projecting out the portion of the AO in the occupied space

$$\left|\phi^{PAO}_{\mu}\right\rangle = \sum_{i} (1 - |i\rangle \langle i|) |\mu\rangle \tag{2.149}$$

The PAOs are orthogonal to the occupied space, as can be seen by

$$\left\langle j \middle| \phi^{PAO}_{\mu} \right\rangle = \langle j| \left(\sum_{i} (1 - |i\rangle \langle i|) |\mu\rangle \right) = \langle j|\mu\rangle - \sum_{i} \langle j|i\rangle \langle i|\mu\rangle \tag{2.150}$$

$$= \sum_{i} \delta_{ji} \langle i|\mu\rangle = \langle j|\mu\rangle - \langle j|\mu\rangle = 0 \tag{2.151}$$

We can generate as many PAOs as there are AOs, and the PAOs therefore constitute a non-orthogonal and linearly depend basis set for the virtual space. This must be taken into account when the equations of some correlation method are solved, either by orthogonalization and elimination of linearly dependency, or by altering the equations. The latter approached has been implemented in XDEC and is described for non-canonical MP2 in the next section.

2.6.4 MP2 equations with non-orthogonal virtual basis functions

The non-orthogonal MP2 amplitude equations with non-orthogonal virtual basis functions for a periodic system are [17]

$$\Omega_{MP2}(t) = (\mathbf{0}i\boldsymbol{A}a|\boldsymbol{J}j\boldsymbol{B}b) + A^{\boldsymbol{A}a,\boldsymbol{B}b}_{\mathbf{0}i,\boldsymbol{J}j}(t) + B^{\boldsymbol{A}a,\boldsymbol{B}b}_{\mathbf{0}i,\boldsymbol{J}j}(t) = 0 \tag{2.152}$$

where the terms $A^{\boldsymbol{A}a,\boldsymbol{B}b}_{\mathbf{0}i,\boldsymbol{J}j}(t)$ and $B^{\boldsymbol{A}a,\boldsymbol{B}b}_{\mathbf{0}i,\boldsymbol{J}j}(t)$ are defined as

$$A^{\boldsymbol{A}a,\boldsymbol{B}b}_{\mathbf{0}i,\boldsymbol{J}j} = \sum_{\boldsymbol{C}\boldsymbol{D}}\sum_{cd} f^{\boldsymbol{C}-\boldsymbol{A}}_{ac} t^{\boldsymbol{C}c,\boldsymbol{D}d}_{\mathbf{0}i,\boldsymbol{J}j} S^{\boldsymbol{B}-\boldsymbol{D}}_{db} + \sum_{\boldsymbol{C}\boldsymbol{D}}\sum_{cd} S^{\boldsymbol{C}-\boldsymbol{A}}_{ac} t^{\boldsymbol{C}c,\boldsymbol{D}d}_{\mathbf{0}i,\boldsymbol{J}j} f^{\boldsymbol{B}-\boldsymbol{D}}_{db} \tag{2.153}$$

$$B^{\boldsymbol{A}a,\boldsymbol{B}b}_{\mathbf{0}i,\boldsymbol{J}j} = -\sum_{\boldsymbol{C}\boldsymbol{D}}\sum_{cd} S^{\boldsymbol{C}-\boldsymbol{A}}_{ac} \beta'^{\boldsymbol{C}c,\boldsymbol{D}d}_{\mathbf{0}i,\boldsymbol{J}j} S^{\boldsymbol{B}-\boldsymbol{D}}_{db} - \sum_{\boldsymbol{C}\boldsymbol{D}}\sum_{cd} S^{\boldsymbol{C}-\boldsymbol{A}}_{ac} \beta''^{\boldsymbol{C}c,\boldsymbol{D}d}_{\mathbf{0}i,\boldsymbol{J}j} S^{\boldsymbol{B}-\boldsymbol{D}}_{db} \tag{2.154}$$

where $\beta'^{\boldsymbol{C}c,\boldsymbol{D}d}_{\mathbf{0}i,\boldsymbol{J}j}$ and $\beta''^{\boldsymbol{C}c,\boldsymbol{D}d}_{\mathbf{0}i,\boldsymbol{J}j}$ are given by

$$\beta'^{\boldsymbol{C}c,\boldsymbol{D}d}_{\mathbf{0}i,\boldsymbol{J}j} = \sum_{\boldsymbol{K}k} f^{\boldsymbol{J}-\boldsymbol{K}}_{jk} t^{\boldsymbol{C}c,\boldsymbol{D}d}_{\mathbf{0}i,\boldsymbol{K}k} \tag{2.155}$$

$$\beta''^{\boldsymbol{C}c,\boldsymbol{D}d}_{\mathbf{0}i,\boldsymbol{J}j} = \sum_{\boldsymbol{K}k} f^{\boldsymbol{K}}_{ik} t^{\boldsymbol{C}-\boldsymbol{K}c,\boldsymbol{D}-\boldsymbol{K}d}_{\mathbf{0}k,\boldsymbol{J}-\boldsymbol{K}j} \tag{2.156}$$

The equations may alternatively be formulated using the transformed amplitudes [18]

$$\bar{t}^{\boldsymbol{A}a,\boldsymbol{B}b}_{\boldsymbol{I}i,\boldsymbol{J}j} = \sum_{\boldsymbol{C}c\boldsymbol{D}d} S^{\boldsymbol{C}-\boldsymbol{A}}_{ac} t^{\boldsymbol{C}c,\boldsymbol{D}d}_{\boldsymbol{I}i,\boldsymbol{J}j} S^{\boldsymbol{B}-\boldsymbol{D}}_{db} \tag{2.157}$$

where the term $B^{\boldsymbol{A}a,\boldsymbol{B}b}_{\mathbf{0}i,\boldsymbol{J}j}$ now may be expressed as

$$B^{\boldsymbol{A}a,\boldsymbol{B}b}_{\mathbf{0}i,\boldsymbol{J}j} = -\sum_{\boldsymbol{K}k} f^{\boldsymbol{K}-\boldsymbol{I}}_{ik} \bar{t}^{\boldsymbol{A}-\boldsymbol{K}a,\boldsymbol{B}-\boldsymbol{K}b}_{\mathbf{0}k,\boldsymbol{J}-\boldsymbol{K}j} - \sum_{\boldsymbol{K}k} \bar{t}^{\boldsymbol{A}a,\boldsymbol{B}b}_{\mathbf{0}i,\boldsymbol{K}k} f^{\boldsymbol{J}-\boldsymbol{K}}_{kj} \tag{2.158}$$

2.7 Pair energy decay and cutoff

2.7.1 Decay of the pair energy with local orbitals

As equation (2.96) shows, the correlation energy in CC and MP2 calculations are essentially determined by integrals of the form

$$g_{iajb} = (ia|jb) = \int d\boldsymbol{r}_1 d\boldsymbol{r}_2 \phi_i(\boldsymbol{r}_1)^* \phi_a(\boldsymbol{r}_1) r_{12}^{-1} \phi_j(\boldsymbol{r}_2)^* \phi_b(\boldsymbol{r}_2) \tag{2.159}$$

were we may interpret the function products as density distributions, $\rho_{ia}(\boldsymbol{r}) = \phi_i(\boldsymbol{r})^* \phi_a(\boldsymbol{r})$. Each of the orbitals involved in the integral are in some sense spatially localized, and these density distributions will consequently vanish if the center of ϕ_i is far enough away from the center of ϕ_a. As a result, the integral in equation (2.159) will be zero. We may therefore limit the excitation space of an occupied orbital to include only virtual orbitals that are spatially close.

The integral also vanished if the two density distributions ρ_{ia} and ρ_{jb} are sufficiently separated, in which case the product $\rho_{ia}(\boldsymbol{r}_1)\rho_{jb}(\boldsymbol{r}_2)$ only will have significant values when r_{12}^{-1} is very small. By a multipole expansions, the integrals may be shown to decay with distance as r^{-3} when the distance separation is sufficiently large. [19], [20]

The resulting pair energies decay as r^{-6} as its essentially a product of the two-particle integral and an amplitude determined predominantly by the two-particle integral. As mentioned before, we may therefore impose a cutoff for computation of the correlation energy for pairs of occupied orbitals, or fragments in the DEC algorithm.

2.7.2 Test systems

In this section, some test systems that will be used in the following sections are presented. The model systems are simple, but has certain interesting features, and they reflect what until recently have been computationally feasible to calculate in the XDEC codes.

The computationally simplest system we will use is the 1D ethylene system illustrated in figure 2.3. This system is not physically stable under normal condition, but serves as computationally cheap system that still has the ability to illustrate important features of the pair energy behavior.

We also use two 2D ethylene systems created from the 1D ethylene system by adding another axis with periodicity. In one of the systems, which we will refer to as *flat 2D ethylene*, the second axis is perpendicular to the periodic axis in 1D ethylene, but in the molecular plane. This is illustrated in figure 2.5. In the other system, the second periodic axis is perpendicular to the periodic axis in 1D ethylene and perpendicular to the molecular plane. This system, which we refer to as *stacked 2D ethylene*, is illustrated in figure 2.4. The ethylene systems are especially interesting due to the strongly directional covalent bonds within the ethylene molecules, which may cause significant angle dependencies in the pair energies.

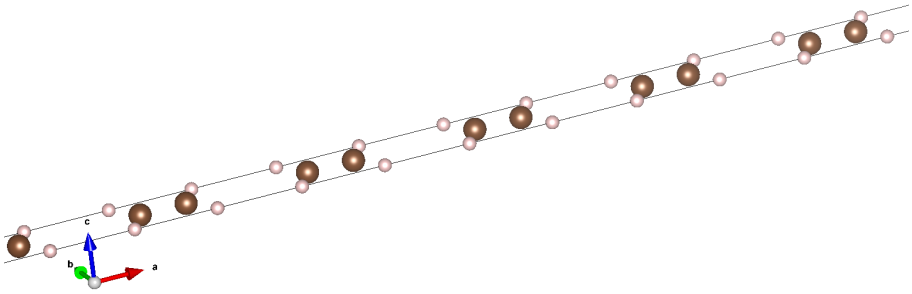

Figure 2.3: Visualization of the 1D ethylene test system.

Finally we use a 3D LiH system with a rock salt structure. The primitive unit cell is shown in figure 2.6. The LiH system is interesting since the amount of pair computation is particularly problematic in 3D systems. Moreover, it is a realistic system.

2.7.3 Pair cutoff and the magnitude of pair energies

One main difference between molecular systems and periodic systems is the lack of edges on the periodic system. As a consequence, there is always in principle infinitely many pairs, and a pair cutoff is necessary for the possibility of doing calculation even on systems with few atoms in the reference cell. The biggest problem appears in 3D systems, where the number of pairs scales cubically with the cutoff distance. Figure 2.7 shows a plot of the number of pairs as a function of the cutoff distance in LiH 3D. The number of pairs quickly becomes large, massively increasing the computation time. Choosing a large cutoff to be on the safe side on the accuracy may therefore make the computation infeasible.

Even though the decay of pair energies at long distances goes as r^{-6}, there may be a large difference in energy for different pairs at any given distance. This is clearly seen in for instance figure 2.8, where pair correlation energy is shown as a function of pair distance in the 3D LiH system. It is worth mentioning here that due to the symmetry of the system, there are several (potentially many) pairs for each point in figure 2.8. If a purely distance-based cutoff is imposed, the cutoff will be done as illustrated at the top in figure 2.9, but in this case we compute many pairs that does not contribute significantly to the energy, and leave out many pairs that contribute a lot more.

Because of this, we ideally want to do a horizontal cutoff as illustrated in the middle of figure 2.9 instead. In addition, we want an estimate of the correlation energy that is not regained as result of leaving out the pairs in the red area. The main issue is of course that in a calculation situation, those pairs are not calculated and we therefore do not know their exact values.

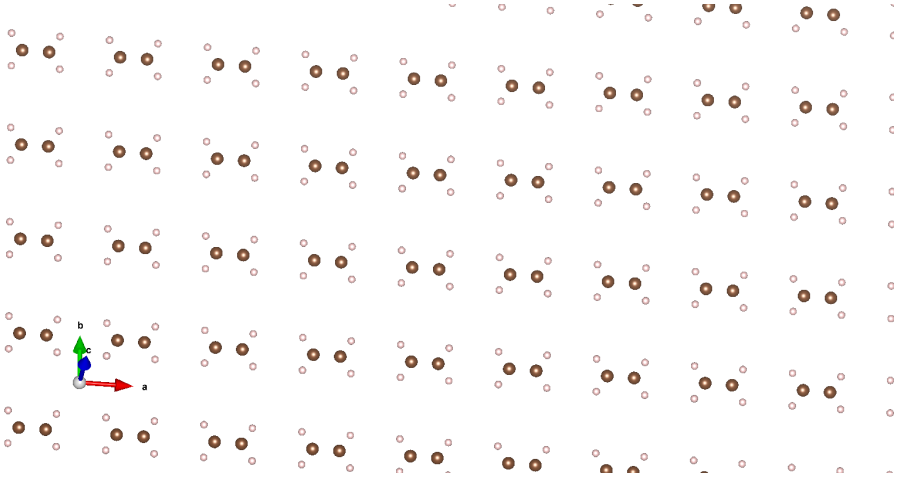

Figure 2.4: Visualization of the flat 2D ethylene test system.

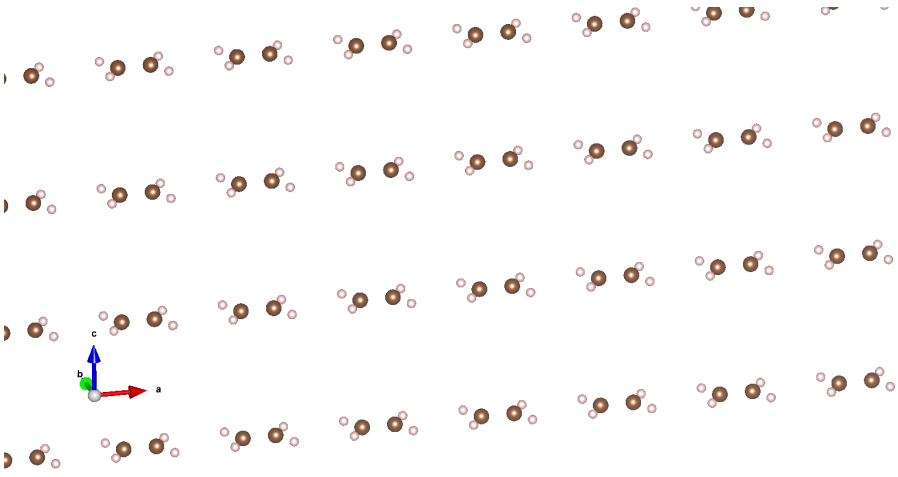

Figure 2.5: Visualization of the stacked 2D ethylene test system.

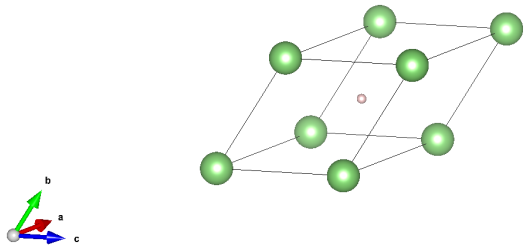

Figure 2.6: Visualization of the primitive unit cell of the 3D LiH test system.

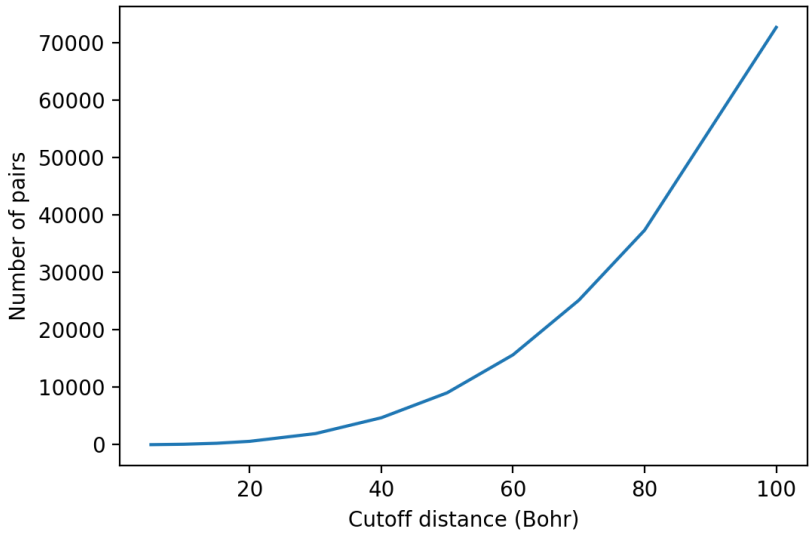

Figure 2.7: Number of pairs as function of cutoff distance in 3D LiH with a lattice parameter for the primitive unit cell of 2.8874 Å.

Another feature of periodic systems that distinguishes them from molecular systems is that pairs repeat regularly at various distances and angles. It may therefore be fruitful to look for patterns in the behaviour of similar pairs as a function of distances and angles.

The approach we take to try to mimic the horizontal type of cutoff is to attempt to sort the pairs into groups based on characteristics of the involved fragments known before the computation, and then interpolate on each of the groups such that a pair cutoff can be given for each group separately. The details of how this is done in the implementation is described in section 3.2.4, but as an example, figure 2.10 shows that the pairs in LiH can be sorted by atomic type when atomic fragments are used. With respect to the interpolation, we cannot just start calculating from the smallest distance for each group, but instead we need some pairs at relatively large distances and intermediate distances.

The main idea behind the cutoff algorithm presented here is to initially compute some of the pairs at both short, intermediate and large pair distance for each group to get an outline of the pair energy behaviour as function of distance, and then interpolate on the pairs. We use smoothed cubic spline for this matter. The interpolation curves are used to estimate the pair energy of the pairs that are not yet computed within some sufficiently large interpolation domain. We use these estimated energies to both estimate the remaining pair energy, and from that a cutoff, and to determine which pair to calculate at any time. This situation including some illustrative spline curves is shown in figure at the bottom of 2.9. Since we always compute the pair with the largest estimated energy and can estimate the energy of the pairs not yet computed, we get a method reminiscent of the ideal horizontal cutoff scenario described above.

A similar trend of that seen for LiH in figure 2.10 is seen in the similar plot for 2d ethylene in figure 2.12. In this case, however, the C atoms are divided into C4 and C5 with dramatically different pair energies. The reason for this is that the C5 fragment has be given both the C-C bond orbitals. Furthermore, there is a significant spread in the C-C pair energies at a given distance. As seen in figure 2.11, most of this may be explained by angle dependencies. This angle dependency stems from the large deviation from spherical symmetry in the C-C bond orbitals. For a given distance, the energy therefore depends on the nature of the fragments involved, along the relative angles between them.

We may therefore attempt to write the pair energy for a given distance as a function of the set of orbitals defined by the fragment, and a set of angles.

$$E_{AB}\left(\phi_A, \theta_A, \alpha_A, \phi_B, \theta_B, \alpha_B; r_{AB}\right) \tag{2.160}$$

where ϕ_A and θ_A are the azimuthal and polar angles of fragment A on the interfragment axis between fragment A and B. That this angle is relative to the $A - B$ axis is assumed implicitly, and not included in the notation. The direction of the fragment must be defined somehow, for instance by the direction of largest spread of the least local orbital. α_A is a rotational angle around the axis along the direction of the fragment.

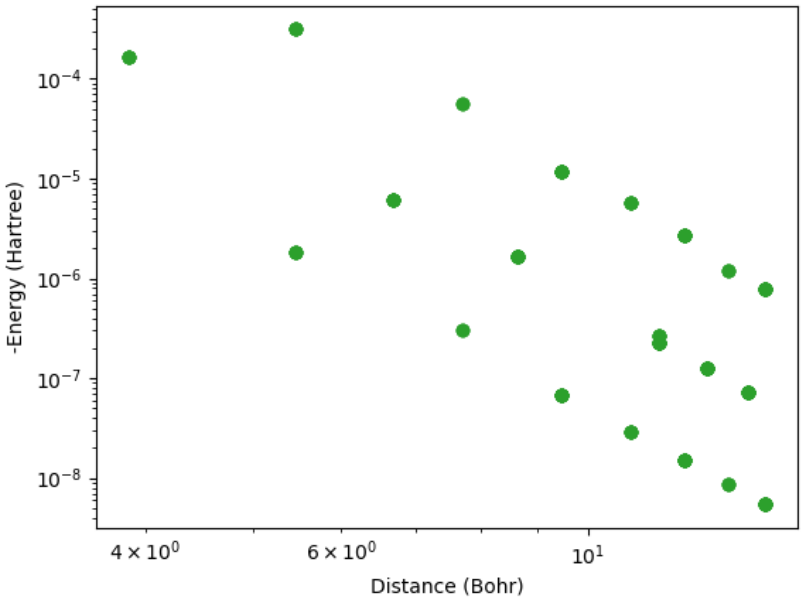

Figure 2.8: Pair-fragment energies for 3D LiH as function of distance. The MP2 calculations were done using the original XDEC code with FOT = 10^{-3} Hartree, extent tolerance = 10^{-3} and a pair cutoff distance of 25 Bohr. Logarithmic scale is used on both axes.

With this notation, the plot in figure 2.11 shows the angles θ_A and θ_B, which are always equal in this case due to the symmetry of the system. The other angles are constant, and as such, this case represents a quite simple case. The more general case in three dimensions is significantly more complicated, and may have to be simplified in order to be practically useful.

2.7.4 Pair energies and orbital spread

We see a strong relationship between the pair energies and the orbital spreads (equation (2.117)) of the occupied orbitals. The general trend is that a larger orbital spread gives a larger pair energy at a given distance. As an example, the occupied orbital on Hydrogen in figure 2.10 has an orbital spread of 1.917 while the orbital spread of the occupied orbital on Li is 0.671. The H-H pairs energies are correspondingly about two orders of magnitude greater than the Li-Li pair energies at any fixed distance. Similarly, the binding orbitals in the Carbon fragments in figure 3.1 has an orbital spread of 1.806 compared to that of 1.517 for the occupied orbitals on the Hydrogen atoms. The C-C energies are correspondingly larger than the H-H energies for a given distance.

We may also use orbital spreads to study the angular dependencies of a pair. The expression for the second central moment in equation (2.116) can be reformulated as

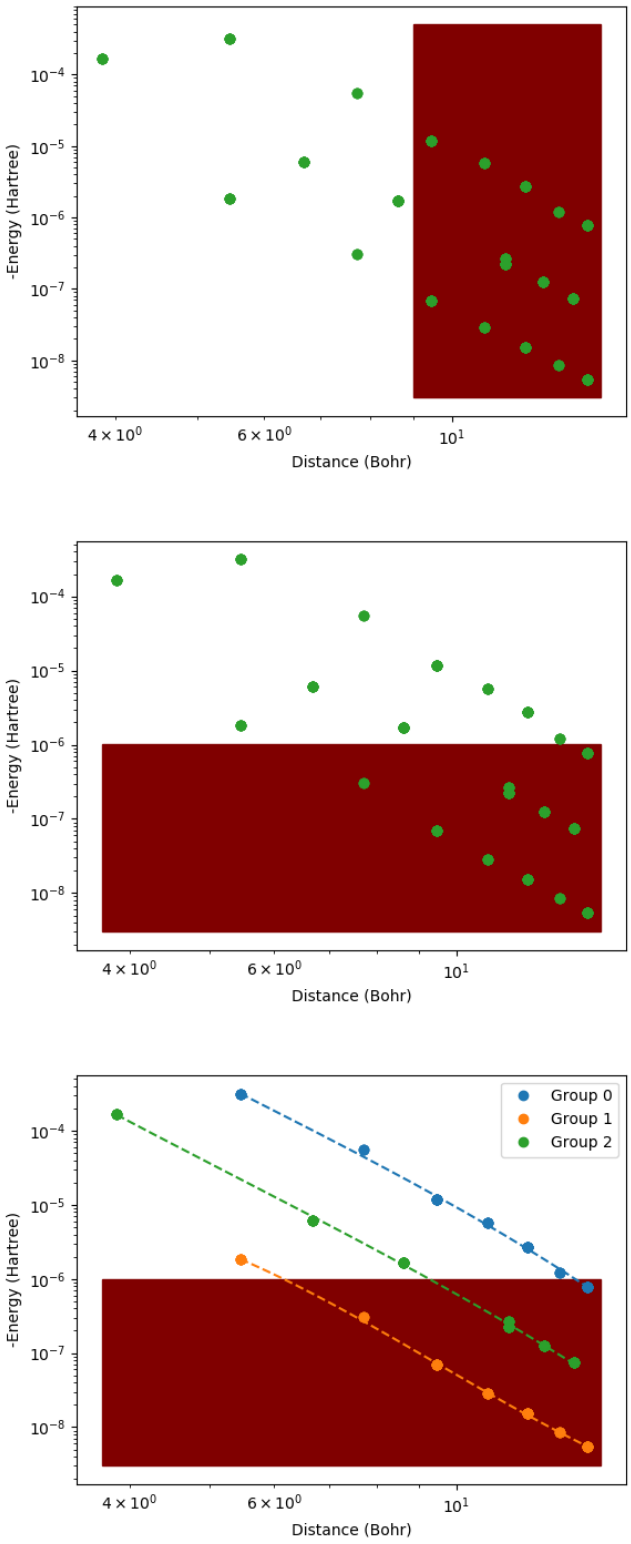

Figure 2.9: Illustration of a distance based vertical cutoff at 10 Bohr (top), an ideal horizontal cutoff (middle) and an interpolation based horizontal cutoff (bottom) of pair energies in 3D LiH. The pairs in the red area (and pairs at larger distances in the vertical cutoff or lower energies in the horizontal cutoff) would be left out of the calculation.

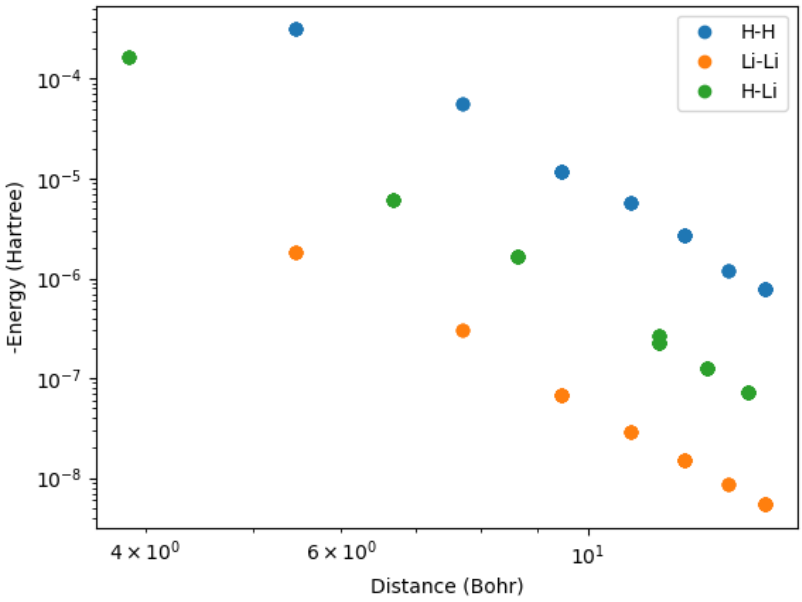

Figure 2.10: Pair-fragment energy for 3D LiH as function of interfragment distance where the pairs are sorted by the atoms involved in the pairs.

$$\sigma^2 = \sigma_x^2 + \sigma_y^2 + \sigma_z^2 \tag{2.161}$$

where

$$\sigma_x^2 = \langle p| \left(\hat{x} - \langle p| \hat{x} |p\rangle\right)^2 |p\rangle \tag{2.162}$$

and σ_x is the spread along the x-axis. The spread along the y-axis and z-axis is defined in the same way. The Cartesian axes are arbitrarily defined, and the computation of orbital spread can be projected onto any axis defined by a unit vector $\boldsymbol{e}$ as

$$\sigma^2 = \langle p| \left(\hat{\boldsymbol{r}} \cdot \boldsymbol{e} - \langle p| \hat{\boldsymbol{r}} \cdot \boldsymbol{e} |p\rangle\right)^2 |p\rangle \tag{2.163}$$

This will generally require computation of matrix elements of products of $\hat{x}$, $\hat{y}$ and $\hat{z}$.

For orbitals with significant angular dependency as seen in figure 2.11, we have seen a correlation between the pair energy and the orbital spread along the interfragment axis. As a simple example, the orbital spread in of the C-C

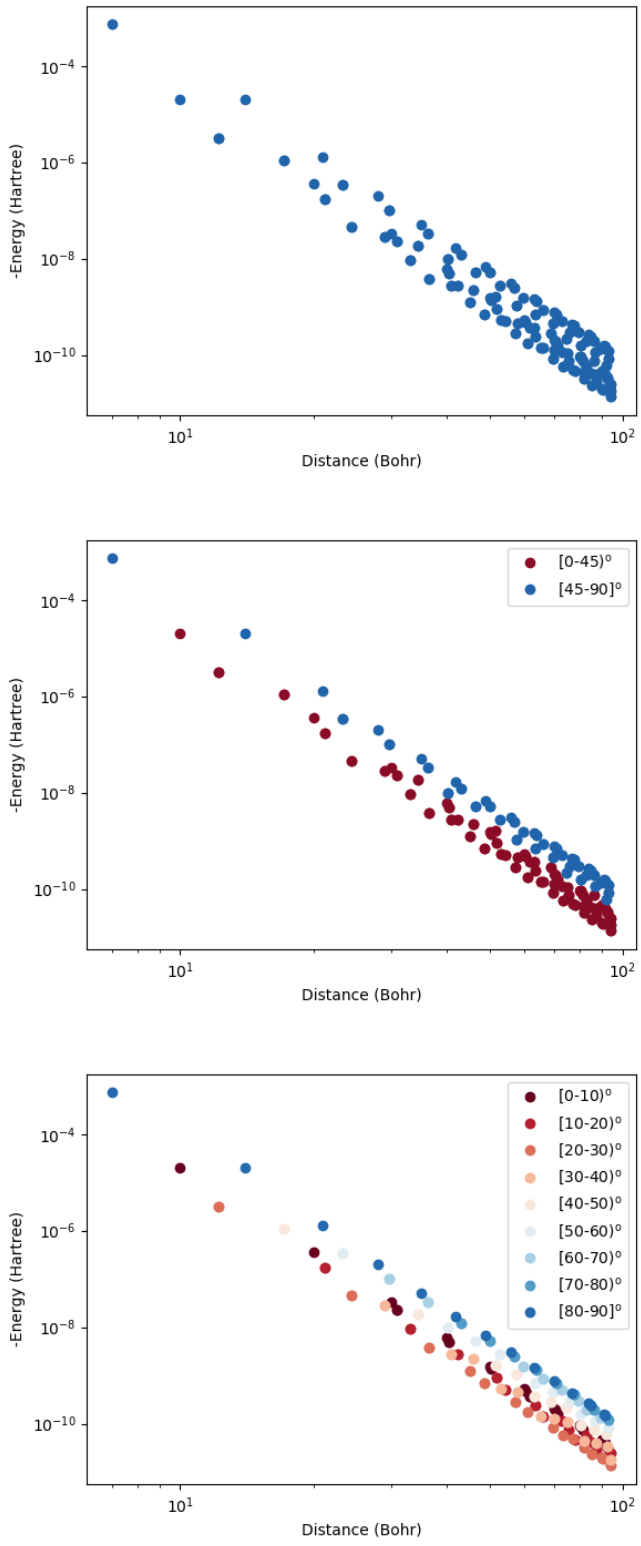

Figure 2.11: Energy vs distance plot for the C5-C5 pairs in flat 2D ethylene. Left: no additional sorting, middle: sorted into two groups distinguished by an angle smaller or greater that $2\pi/8$ from the polymer direction, right: sorted into nine groups, each with a range of 10^o angles from 0^o to 90^o from the polymer direction.

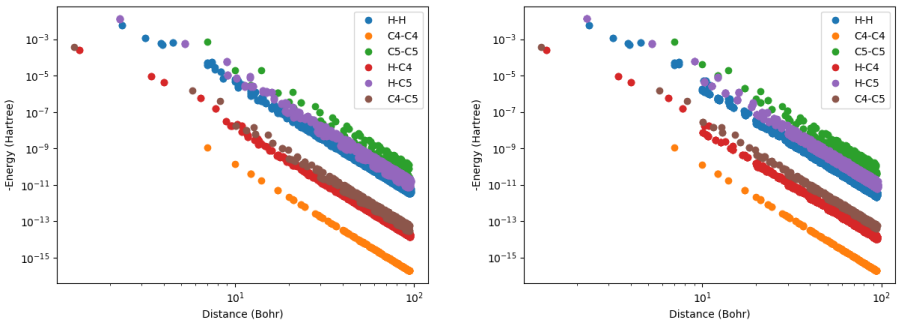

Figure 2.12: Energy versus distance plot for flat 2D ethylene (left) and stacked 2D ethylene (right). The MP2 calculations were done using the original XDEC code with FOT = 10^{-3} Hartree, extent tolerance = 10^{-3} and a pair cutoff distance of 100 Bohr. Logarithmic scale is used on both axes.

bond orbitals in figure 2.11 are 1.184 in the x-direction (0°) and 0.831 in the y-direction (90°).

As another interesting example, we may look at the H-H pairs in the flat and stacked 2D ethylene systems with pair energies plotted in figure 2.12. Figure 2.13 shows only the H-H pairs for these system with pairs exactly along the x-axis and y-axis highlighted. The x-axis is along the polymer axis, while the y-axis in both instances is in the direction that is perpendicular to the x-axis and has periodicity.

In the stacked 2D ethylene system shown at the bottom in figure 2.13, the orbital spread is greatest in the polymer direction where it is 0.867 compared to 0.806 perpendicular to the polymer, and the pair energies generally lies a bit higher in the polymer direction at a given distance. For the flat 2D ethylene system the situation is reversed. Here, the orbital spread is greater perpendicular to the polymer direction with 0.951 compared to 0.868 along the polymer. Correspondingly, we see to the top in figure 2.13 that the energies along the polymer direction generally lies lower than those perpendicular to the polymer direction.

2.7.5 Integrals in the Born-von Karman realm

As previously mentioned, when BvK boundary conditions are imposed on the system, Wannier functions become periodic, and integrals over $\mathbf{R}^3$ involving Wannier functions will in general diverge. Integrals may instead be limited to the BvK supercell, interpreting anything that leaves the BvK cell on one side as re-entering the BvK cell on the opposite side. An illustration of this condition is shown in figure 2.14. This is usually fine as long as we are dealing with integrals close to the reference cell. For pair calculations, however, this is problematic since the pair energy contributions will be periodic, and the total pair energy will therefore diverge. There are mainly two ways of resolving this problem.

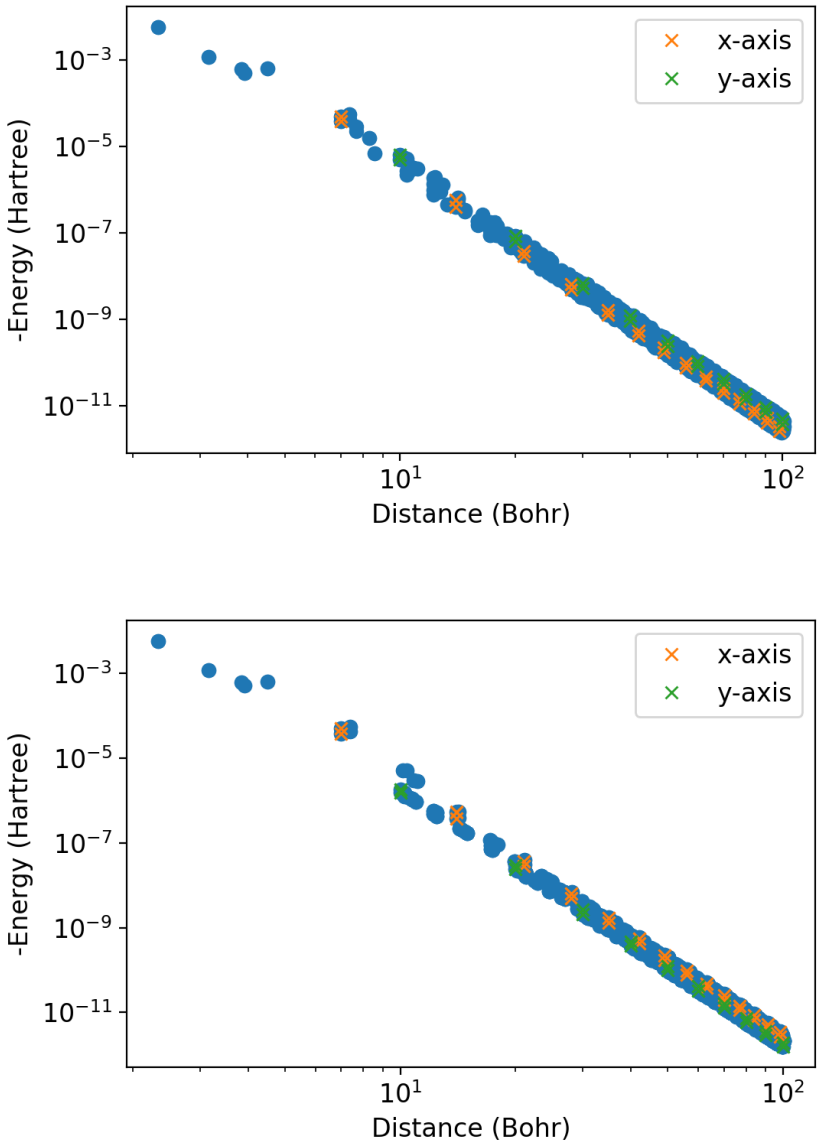

Figure 2.13: Energy vs distance plot for the H-H pairs in flat 2D ethylene (top) and stacked 2D ethylene (bottom). The pairs exactly along the x-axis and y-axis are highlighted.

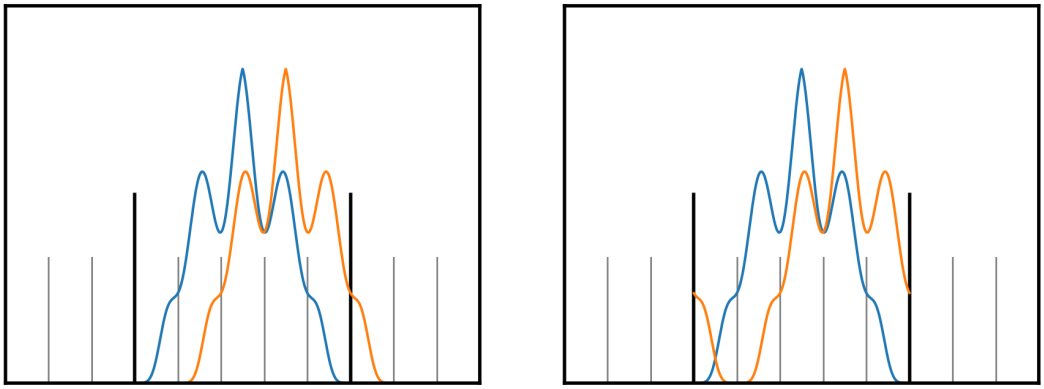

Figure 2.14: Illustrations of how the electron density for a Wannier function may look in one dimension. The thick black vertical lines signifies the edges of the BvK cell, while the thinner grey lines signifies the boundaries between the unit cell. The BvK boundary conditions are ignored in the translation of the MO in the illustration to the left, while it is retained in the translation in the illustration to the right.

The first possible solution is to translate the Wannier functions from the reference cell to other cells involved in integrals and simply ignore the BvK boundary conditions, as illustrated to the left in figure 2.2. We would then integrate over whole $\mathbf{R}^3$, and assume that the Wannier functions in the reference cell are zero outside the BvK cell.

The main problem with this solution is that the Wannier functions are only orthogonalized within the BvK cell as periodic functions (the situation illustrated to the right in figure figure 2.2). Without this property, the Wannier functions will not necessarily be orthogonal, leading to potentially erroneous pair energies, especially close to the edges of the BvK cell. The energy versus distance plot to the left in figure 2.16 shows an example of how the pair energies may behave when the BvK cell is chosen too small. In this case, the parameter *newk* in the Crystal program [21], [22] was set to 9. This parameter determines the number of k-points for which the Bloch functions used to construct the Wannier functions are computed. Increasing the *newk* parameter to 16 gives the result to the right in figure 2.16.

To try to resolve the orthogonality problem we may monitor the Wannier functions as the size of the BvK cell is increased. As the BvK cell becomes sufficiently large, we can expect the change in the Wannier functions with further increase in BvK cell size to be minimal. We may then assume that they have essentially converged to the form they would have in the full crystal, and the orthogonality problem would then disappear. A simple illustration of this is shown in figure 2.15, where the Wannier function changes significantly between the topmost figure and the middle figure with an increase in the size of the BvK cell. The

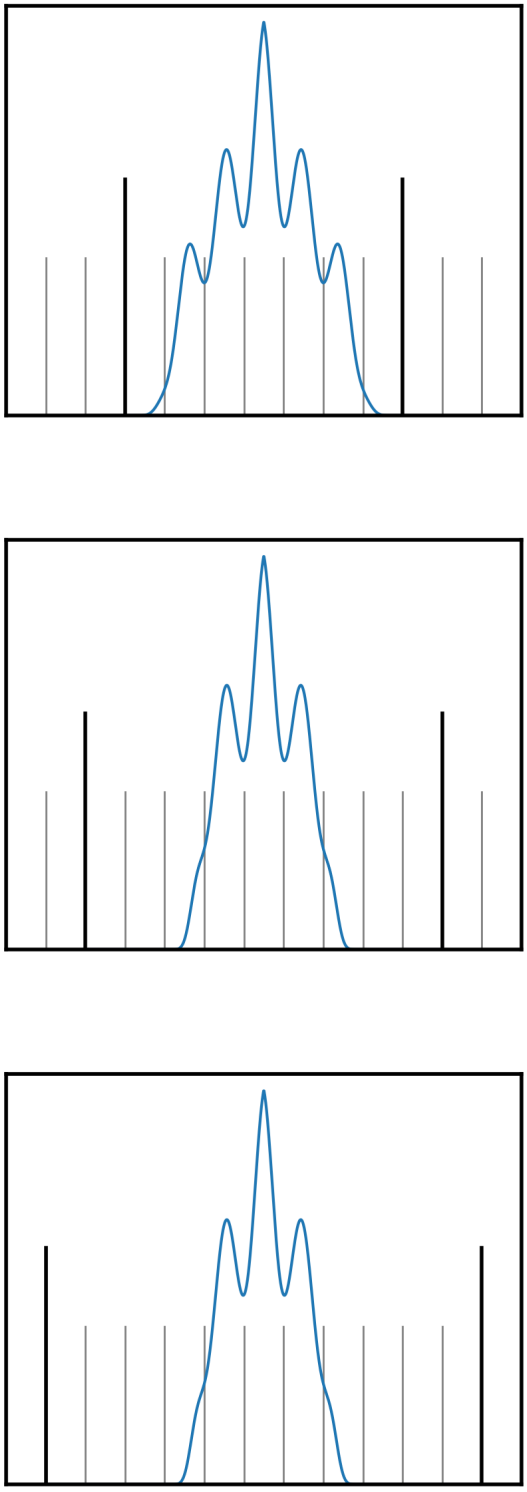

Figure 2.15: Illustrations of how the electron density for a Wannier function may change in one dimension as the size of the BvK cell is increased. The thick black vertical lines signifies the edges of the BvK cell, while the thinner grey lines signifies the boundaries between the unit cells.

change is minimal, however, between the middle and the bottommost figure with increased size of the BvK cell.

The second solution is to use Wannier functions correctly orthogonalized in the BvK supercell, and only calculate pairs within the BvK cell (or possibly in an even smaller supercell). Conceptually, this may sound dubious since we are effectively modelling a limited "circular" system as opposed to the full crystal. The idea, however, is that the total correlation energy should converge to the correct one as the size of the BvK cell is increased. This stems from the fact that we approach the strictly correct model for the crystal as the size of the BvK cell approaches infinity. A potential problem is that the BvK may have to be large in order to avoid wrong pair energies at the edges of the BvK cell. It may also be difficult to control the error in the correlation energy as a consequence of the limited amount of pairs. Specifically, we note that the pair cutoff algorithm presented in this thesis relies on the possibility of calculating pairs at large distances.

The two options just described corresponds to treating the matrix products $C^\dagger AC$ involved in the basis transformation of a matrix A as a block Toeplitz product, or block circulant product. The block Toeplitz product may be defined as

$$(\boldsymbol{AB})^{ij} = \sum_{k=-\infty}^{\infty} A^{k-i} B^{j-k} \tag{2.164}$$

where the superscript signifies a block index. In actual implementations the summation is not infinite since the Toeplitz matrices have a finite extents of non-zero elements, such that

$$A^{j-i>N} = A^{j-i<-N} = 0 \tag{2.165}$$

The block circulant product may be defined within the BvK supercell as

$$(\boldsymbol{AB}) = F^{-1}\{F\{A\} * F\{B\}\} \tag{2.166}$$

where the operator $*$ signifies the Hadamard product and F signifies the discrete Fourier transform.

2.8 Potential Energy Surfaces

Within the Born-Oppenheimer approximation, nuclei moves on a PES determined by the electronic structure and the electrostatic repulsion between the nuclei. The potential energy of the nuclei should vary continuously with the movement of the nuclei, which is illustrated for a diatomic molecule at the top of figure 2.17. In local correlation methods, several approximations are imposed.

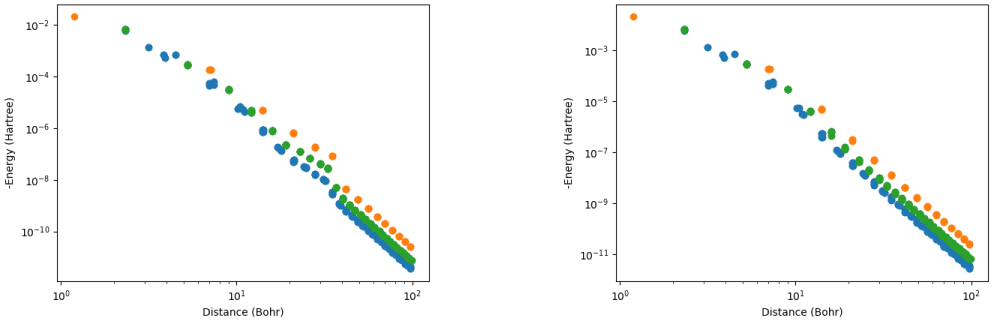

Figure 2.16: Pair correlation energy as function of pair distance for 1D ethylene with newk=9 (left) and newk=16 (right). The MP2 calculations were done using the original XDEC code with FOT $= 10^{-4}$ Hartree, extent tolerance $= 10^{-4}$ and a pair cutoff distance of 100 Bohr. Logarithmic scale is used on both axes.

The effects of these approximations may differ for different displacements of the nuclei, which may lead to steps on the energy surfaces [23]. This may be caused by for instance a sudden inclusion of more virtual orbitals in a fragment as the lattice parameter is reduced, or it may be the result of a pair cutoff. In the DEC algorithm the automatic fragmentation is an additional potential source of steps on the PES. The fragmentation may change for changes is parameters for various reasons, for example significant changes in bonding during phase transitions. The most significant perhaps, is small numerical differences in cases where bond orbitals between symmetry equivalent atoms. This has been observed to happen regularly in the bond orbitals in 2d ethylene in the original XDEC implementation, causing steps on the PES. Since the error in each fragment is determined by convergence, there is no guarantee that the error is the same for different fragmentations.

A simple illustration of how the non-smoothness may manifest on a PES is given in the middle and at the bottom of figure 2.17. In the illustration at the bottom of the figure, the extra terrain on the PES imposed by approximations are severe, and calculations of properties like vibrations and reaction barriers may be quite wrong. Local correlation methods naturally gives steps on the PES, but should be able to produce PES more reminiscent of the figure in the middle, and should also be able to control the error in the calculations, and thus the magnitude of the unevenness in the PES.

Figure 2.17 is used merely as an illustration. For a system of $N > 2$ atoms, the PES is a $6N - 6$ (or $6N - 5$ for linear systems) dimensional hypersurface. The problem, however, remains conceptually the same as illustrated in figure 2.17: The potential energy of the nuclei should vary continuously with the movement of the nuclei.

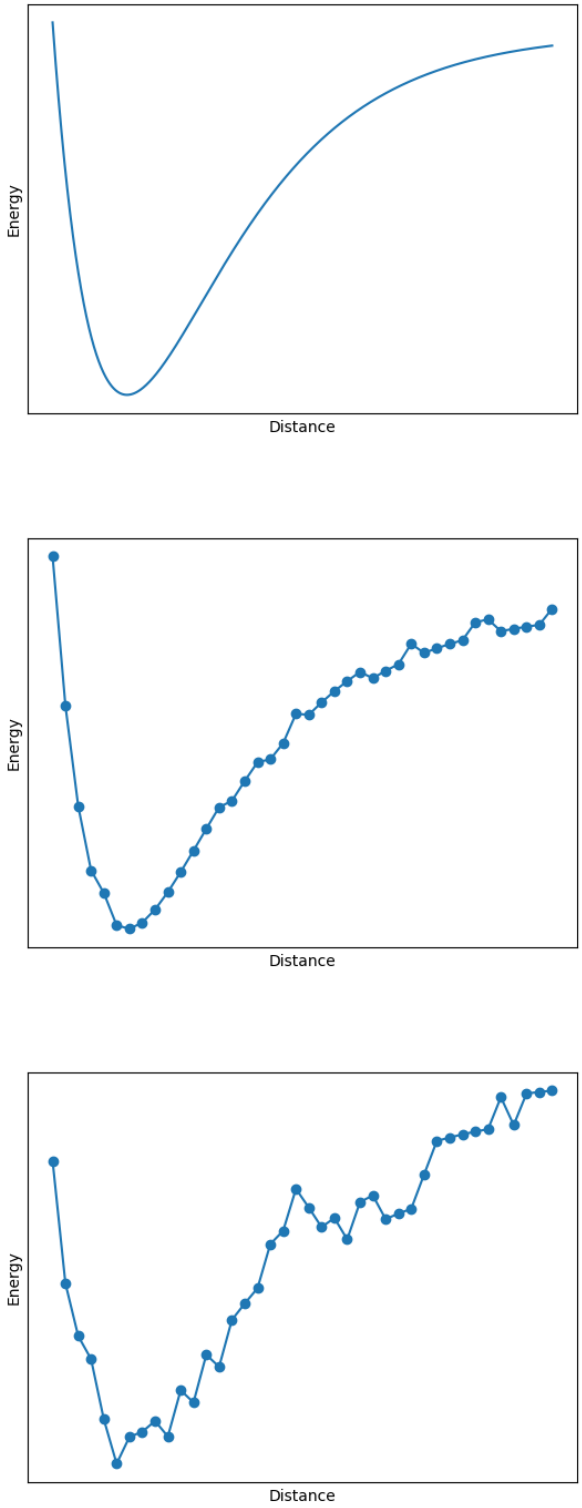

Figure 2.17: Illustration of the form of a potential energy surface for a diatomic molecule. Top: ideal PES. Middle: Some visible deviations from the ideal PES. Bottom: Large deviations from the ideal PES.

Chapter 3

Implementation

In this chapter, the implementation of the PAO solver and the pair algorithm is detailed.

3.1 MP2 PAO solver

To obtain a fixed-point iteration (FPI) scheme, we can start by extracting an amplitude from the sum in equation (2.152) and solve for that amplitude, which results in

$$
\begin{aligned}
t_{\boldsymbol{0}i,\boldsymbol{J}j}^{\boldsymbol{A}a,\boldsymbol{B}b} = \frac{1}{S_{aa}^{\boldsymbol{0}}(f_{ii}^{\boldsymbol{0}}+f_{jj}^{\boldsymbol{0}})S_{bb}^{\boldsymbol{0}} - f_{aa}^{\boldsymbol{0}}S_{bb}^{\boldsymbol{0}} - S_{aa}^{\boldsymbol{0}}f_{bb}^{\boldsymbol{0}}} \Bigg(& (\boldsymbol{0}i\boldsymbol{A}a|\boldsymbol{J}j\boldsymbol{B}b) \\
& - \sum_{\substack{\boldsymbol{C}c\boldsymbol{D}d\boldsymbol{K}k \\ \neq \boldsymbol{A}a\boldsymbol{B}b\boldsymbol{J}j}} S_{ac}^{\boldsymbol{C}-\boldsymbol{A}} f_{kj}^{\boldsymbol{J}-\boldsymbol{K}} t_{\boldsymbol{0}i,\boldsymbol{K}k}^{\boldsymbol{C}c,\boldsymbol{D}d} S_{db}^{\boldsymbol{B}-\boldsymbol{D}} \\
& - \sum_{\substack{\boldsymbol{C}c\boldsymbol{D}d\boldsymbol{K}k \\ \neq \boldsymbol{A}a\boldsymbol{B}b\boldsymbol{0}j}} S_{ac}^{\boldsymbol{C}-\boldsymbol{A}} f_{ik}^{\boldsymbol{K}} t_{\boldsymbol{0}k,\boldsymbol{J}-\boldsymbol{K}k}^{\boldsymbol{C}-\boldsymbol{K}c,\boldsymbol{D}-\boldsymbol{K}d} S_{db}^{\boldsymbol{B}-\boldsymbol{D}} \\
& + \sum_{\substack{\boldsymbol{C}c\boldsymbol{D}d \\ \neq \boldsymbol{A}a\boldsymbol{B}b}} f_{ac}^{\boldsymbol{C}-\boldsymbol{A}} t_{\boldsymbol{0}i,\boldsymbol{J}j}^{\boldsymbol{C}c,\boldsymbol{D}d} S_{db}^{\boldsymbol{B}-\boldsymbol{D}} + \sum_{\substack{\boldsymbol{C}c\boldsymbol{D}d \\ \neq \boldsymbol{A}a\boldsymbol{B}b}} S_{ac}^{\boldsymbol{C}-\boldsymbol{A}} t_{\boldsymbol{0}i,\boldsymbol{J}j}^{\boldsymbol{C}c,\boldsymbol{D}d} f_{db}^{\boldsymbol{B}-\boldsymbol{D}} \Bigg)
\end{aligned}
\tag{3.1}
$$

The solution is thus a fixed point of the function on the right-hand side. We may note here that the overlap matrix elements in the denominator have the value 1 if normalized PAOs are used. By adding the extracted amplitude back into the sum and subtract on the outside of the sum, we may write the equation on a more useful form as

$$
t_{\boldsymbol{0}i,\boldsymbol{J}j}^{\boldsymbol{A}a,\boldsymbol{B}b} = F_{\boldsymbol{0}i,\boldsymbol{J}j}^{\boldsymbol{A}a,\boldsymbol{B}b}(t) + t_{\boldsymbol{0}i,\boldsymbol{J}j}^{\boldsymbol{A}a,\boldsymbol{B}b} \tag{3.2}
$$

where the function $F_{\boldsymbol{0}i,\boldsymbol{J}j}^{\boldsymbol{A}a,\boldsymbol{B}b}(t)$ is defined as

$$
\begin{aligned}
F^{\boldsymbol{A}a,\boldsymbol{B}b}_{\boldsymbol{0}i,\boldsymbol{J}j}(t) =& \frac{1}{S^{\boldsymbol{0}}_{aa}(f^{\boldsymbol{0}}_{ii}+f^{\boldsymbol{0}}_{jj})S^{\boldsymbol{0}}_{bb} - f^{\boldsymbol{0}}_{aa}S^{\boldsymbol{0}}_{bb} - S^{\boldsymbol{0}}_{aa}f^{\boldsymbol{0}}_{bb}} \Bigg((\boldsymbol{0}i\boldsymbol{A}a|\boldsymbol{J}j\boldsymbol{B}b) \\
&- \sum_{\boldsymbol{C}c\boldsymbol{D}d\boldsymbol{K}k} S^{\boldsymbol{C}-\boldsymbol{A}}_{ac} f^{\boldsymbol{J}-\boldsymbol{K}}_{kj} \left(t^{\boldsymbol{C}c,\boldsymbol{D}d}_{\boldsymbol{0}i,\boldsymbol{K}k}\right) S^{\boldsymbol{B}-\boldsymbol{D}}_{db} \\
&- \sum_{\boldsymbol{C}c\boldsymbol{D}d\boldsymbol{K}k} S^{\boldsymbol{C}-\boldsymbol{A}}_{ac} f^{\boldsymbol{K}}_{ik} \left(t^{\boldsymbol{C}-\boldsymbol{K}c,\boldsymbol{D}-\boldsymbol{K}d}_{\boldsymbol{0}k,\boldsymbol{J}-\boldsymbol{K}k}\right) S^{\boldsymbol{B}-\boldsymbol{D}}_{db} \\
&+ \sum_{\boldsymbol{C}c\boldsymbol{D}d} f^{\boldsymbol{C}-\boldsymbol{A}}_{ac} \left(t^{\boldsymbol{C}c,\boldsymbol{D}d}_{\boldsymbol{0}i,\boldsymbol{J}j}\right) S^{\boldsymbol{B}-\boldsymbol{D}}_{db} + \sum_{\boldsymbol{C}c\boldsymbol{D}d} S^{\boldsymbol{C}-\boldsymbol{A}}_{ac} \left(t^{\boldsymbol{C}c,\boldsymbol{D}d}_{\boldsymbol{0}i,\boldsymbol{J}j}\right) f^{B-D}_{db} \Bigg)
\end{aligned} \tag{3.3}
$$

We may attempt to find the fixed point by the iterative scheme

$$
\left(t^{\boldsymbol{A}a,\boldsymbol{B}b}_{\boldsymbol{0}i,\boldsymbol{J}j}\right)_{n+1} = F^{\boldsymbol{A}a,\boldsymbol{B}b}_{\boldsymbol{0}i,\boldsymbol{J}j}(\boldsymbol{t}_n) + \left(t^{\boldsymbol{A}a,\boldsymbol{B}b}_{\boldsymbol{0}i,\boldsymbol{J}j}\right)_n \tag{3.4}
$$

where n signifies the iteration number. A convergence criterion the element of the residual with greatest magnitude (absolute value) can be used. Alternatively, the Frobenius norm of the residual may be used. The Frobenius norm is defined as

$$
||\boldsymbol{R}|| = \left(\sum_{0iJjAaBb} \left(R^{Aa,Bb}_{0i,Jj}\right)^2 \right)^{1/2} \tag{3.5}
$$

where the summation goes over all non-neglected amplitude indices. It should, however, in that case be normalized, since by the definition, its value will increase with the number of elements in the residual, and thereby tighten the convergence criterion for larger orbital spaces. From the definition, this can be done by multiplying a factor $1/\sqrt{N_t}$, where N_t is the number of non-neglected residual elements.

The solver can also be converged on the difference in energy between two steps, or the difference in residual norm or max absolute value. We have, however, experienced instances with slow convergence where these values are small even when the residual elements still have significant values.

3.1.1 Convergence and damping

We have experienced that the standard FPI scheme as formulated in equation (3.4) diverges. This may be fixed by introducing a positive damping factor $\alpha < 1$, such that the scheme becomes

$$
\left(t^{\boldsymbol{A}a,\boldsymbol{B}b}_{\boldsymbol{0}i,\boldsymbol{J}j}\right)_{n+1} = \alpha F^{\boldsymbol{A}a,\boldsymbol{B}b}_{\boldsymbol{0}i,\boldsymbol{J}j}(\boldsymbol{t}_n) + \left(t^{\boldsymbol{A}a,\boldsymbol{B}b}_{\boldsymbol{0}i,\boldsymbol{J}j}\right)_n \tag{3.6}
$$

Algorithm 1 Outline of the PAO solver scheme. The Einstein summation convention is used.

Obtain initial guess for amplitude tensor $\boldsymbol{t}$
Obtain virtual overlap matrix $\boldsymbol{S}$ and Fock matrix $\boldsymbol{f}$
Set up tensor $\boldsymbol{e}$ with elements $S^{\mathbf{0}}_{aa}(f^{\mathbf{0}}_{ii} + f^{\mathbf{0}}_{jj})S^{\mathbf{0}}_{bb} - f^{\mathbf{0}}_{aa}S^{\mathbf{0}}_{bb} - S^{\mathbf{0}}_{aa}$
Store tensors $\boldsymbol{\beta}'$,$\boldsymbol{\beta}''$ and $\boldsymbol{F}$ with same dimensions as $\boldsymbol{t}$
for i < max iterations **do**
    for C with virtual orbitals in AOS **do**
        for D with virtual orbitals in AOS **do**
            for J with occupied orbitals in AOS **do**
                $\boldsymbol{\beta}'^{C,D}_{0,J} \leftarrow \boldsymbol{t}^{C,D}_{0,Kk}\boldsymbol{f}^{J-K}_{k}$
                $\boldsymbol{\beta}''^{C,D}_{0,J} \leftarrow \boldsymbol{t}^{C-K,D-K}_{0k,J-K}\boldsymbol{f}^{K}_{k}$
            end for
        end for
    end for
    for A with virtual orbitals in AOS **do**
        for B with virtual orbitals in AOS **do**
            for J with occupied orbitals in AOS **do**
                $\boldsymbol{g} \leftarrow -(0A|JB)$
                $\boldsymbol{g} \mathrel{-}= \boldsymbol{f}^{C-A}_{c}\boldsymbol{t}^{Cc,Dd}_{0,J}\boldsymbol{s}^{B-D}_{d}$
                $\boldsymbol{g} \mathrel{-}= \boldsymbol{S}^{C-A}_{c}\boldsymbol{t}^{Cc,Dd}_{0,J}\boldsymbol{f}^{B-D}_{d}$
                $\boldsymbol{g} \mathrel{+}= \boldsymbol{S}^{C-A}_{c}\boldsymbol{\beta}'^{Cc,Dd}_{0,J}\boldsymbol{S}^{B-D}_{d}$
                $\boldsymbol{g} \mathrel{+}= \boldsymbol{S}^{C-A}_{c}\boldsymbol{\beta}''^{Cc,Dd}_{0,J}\boldsymbol{S}^{B-D}_{d}$
                $\boldsymbol{F}^{A,B}_{0,J} \leftarrow \boldsymbol{e}^{-1} * \boldsymbol{g}$
                Amplitudes outside amplitude extents are set to 0
            end for
        end for
    end for
    $\boldsymbol{t} \mathrel{-}= \alpha\boldsymbol{F}$
    $\boldsymbol{t}$ possibly updated by convergence acceleration
    if convergence criterion is satisfied **then**
        break
    end if
end for

Test runs have of shown that the scheme no longer diverges when an appropriate value of α is used. The convergence, however, is very slow, and seems to be too slow for some realistic systems.

3.1.2 DIIS

Direct inversion of the iterative subspace (DIIS) is a method introduced by Peter Pulay [24] to accelerate the convergence of SCF iterations. In DIIS, an improved solution tensor is sought in the subspace of the m previous iterations

$$\boldsymbol{t} = \sum_{i=1}^{m} c_i \boldsymbol{t}^i \tag{3.7}$$

where the sum always runs over the m previous iterations. For a given iteration i, an error tensor $\Delta\boldsymbol{t}^i = \boldsymbol{t}^{i+1} - \boldsymbol{t}^i$ is associated such that a total error tensor is given by

$$\Delta\boldsymbol{t} = \sum_{i=1}^{m} c_i \Delta\boldsymbol{t}^i \tag{3.8}$$

The coefficients c_i are determined by minimizing the norm of $\Delta\boldsymbol{t}$ with the condition that the sum of the coefficient is 1. Introducing this condition with Lagrange multipliers ultimately gives the following linear set of equations

$$\begin{pmatrix} B_{11} & B_{12} & \dots & B_{1m} & -1 \\ B_{21} & B_{22} & \dots & B_{2m} & -1 \\ \vdots & \vdots & \ddots & \vdots & \vdots \\ B_{m1} & B_{m2} & \dots & B_{mm} & -1 \\ -1 & -1 & \dots & -1 & 0 \end{pmatrix} \begin{pmatrix} c_1 \\ c_2 \\ \vdots \\ c_m \\ \lambda \end{pmatrix} = \begin{pmatrix} 0 \\ 0 \\ \vdots \\ 0 \\ -1 \end{pmatrix} \tag{3.9}$$

where $B_{ij} = \left\langle \Delta\boldsymbol{t}^i \middle| \Delta\boldsymbol{t}^j \right\rangle$. The coefficients may be obtained by diagonalizing the matrix B. We implemented DIIS in combination with the FPI scheme. A pseudo-code is given in algorithm 2. This algorithm is run at each iteration at the convergence acceleration step in algorithm 1.

3.1.3 Newton's method

Perturbation energies of order $2n$, where n is an integer, can be expressed as a minimization problem [20]

$$E^{(2n)} = \min_{\boldsymbol{t}} E_H^{(2n)}(\boldsymbol{t}) \tag{3.10}$$

where $E_H^{(2n)}$ is the Hylleraas functional. In the case of MP2 the Hylleraas functional can be formulated as [18]

Algorithm 2 Outline of the DIIS algorithm.

Obtain the maximal number of stored amplitudes N
Obtain iteration number i
Obtain amplitude tensor $\boldsymbol{t}^i$ and update tensor $\Delta\boldsymbol{t}^i$ from the FPI solver
if $i \geq N$ **then**
    $D \leftarrow D$
else
    $D \leftarrow i$
end if
Set up matrix $\boldsymbol{B}$ of dimension $D \times D$
$\boldsymbol{w} \leftarrow \boldsymbol{B}^{-1}$
$\boldsymbol{C} \leftarrow \boldsymbol{w}[:, D]$
Construct the amplitude tensor $\boldsymbol{t}^i_{DIIS}$
if $i \geq N$ **then**
    Delete $\boldsymbol{t}^{i-N}$ and $\Delta\boldsymbol{t}^{i-N}$
end if
Return $\boldsymbol{t}^i_{DIIS}$

$$E_H = \sum_{i \geq j} (2 - \delta_{ij}) \sum_{ab} \tilde{t}^{ab}_{ij} \left((ai|bj) + R^{ab}_{ij} \right) \tag{3.11}$$

where

$$\tilde{t}^{ab}_{ij} = 2t^{ab}_{ij} - t^{ba}_{ij} \tag{3.12}$$

The Hylleraas functional is a scalar that equals the correct MP2 energy when it is minimized, and is therefore convenient to use in Newton's method. The Newton's method scheme for the amplitudes may now be expressed as

$$t_{k+1} = t_k - \left[E^{''}_H(t_k) \right]^{-1} E^{'}_H(t_k) \tag{3.13}$$

where $E^{'}_H$ and $E^{''}_H$ are the gradient and Hessian of the Hylleraas functional. Autograd [25] was used for computing the Hessian matrix. We have implemented Newton's method for test systems with orbitals only in the reference cell.

3.2 Pair cutoffs

In this section, the various aspects involved in the automatic determination of pair cutoff is described.

3.2.1 General outline of the algorithm

In this section, we will assume that the fragment pairs have been sorted into groups such that the pairs in each group lays approximately on a straight line on an energy vs distance plot with logarithmic scales. The details of how this is done is described in section 3.2.4.

The cutoff is decided by smoothed cubic spline interpolation. We must therefore first decide on an interpolation range that is large enough so that we can assume any contributions outside of this range is negligible. Here, a maximum distance of 100 or 200 Bohr is used.

Then, for each group, the pair with smallest distance and longest distance in the interpolation range is computed. In addition an intermediate pair is computed at the smallest distance larger than some parameter *min_incr* from the smallest distance pair. Another intermediate pair is computed with the same condition relative to the first intermediate pair. We then have enough pairs somewhat spread out distance-wise to perform a cubic spline interpolation, and this procedure represent the minimum setup for initiating the pair algorithm. The procedures for computing intermediate pairs may be continued to increase the number of intermediate pairs and potentially improving the interpolation. Once the interpolation have been performed on each group separately, the energies of all non-calculated pairs in the interpolation range are estimated from the interpolation curves.

From this point on, the non-calculated pair that at any point has the highest estimated energy will be calculated. The pair calculations stop when the total estimated energy of the non-calculated pairs is smaller than parameter $\epsilon(\text{FOT}) = \lambda \times \text{FOT}$, where λ is a number, typically close to 1.

The cutoff algorithm may be summarised by the following steps:

1. For each group, compute close pairs, distant pairs and intermediate pairs. For the minimum setup, one pair is computed at closest distance, one at maximum distance of the interpolation range, and two intermediate pairs in between.
2. Estimate the energy of each pair in the interpolation range. Compute the estimated total pair energy E_{remain} of the non-calculated pairs.
3. If $E_{remain} > \lambda \times \text{FOT}$: Compute the pair with largest estimated energy. Else: Pair calculation is finished.

In the new implementation where we get the pair energies for the four pairs $\mathbf{0}P\boldsymbol{L}P$, $\mathbf{0}P\boldsymbol{L}Q$, $\mathbf{0}Q\boldsymbol{L}P$ and $\mathbf{0}Q\boldsymbol{L}Q$ simultaneously, the algorithm is altered such that the energy for each such set of four pairs is estimated. The set of four pairs that are estimated to have the greatest energy contribution is computed. Since there are overlaps between pairs with the same orbital indices between some of the sets, situations occur where some, but not all, pairs in one set is calculated. In this case, the pairs that have already been calculated is left out of the energy estimate.

3.2.2 The spline interpolation

For the smoothed spline interpolation, we use the UnivariateSpline in the interpolate sub-package of SciP [26]. The smoothing factor s [27] is set to 1000. This is essentially corresponds to a maximum smoothing in that implementation. The interpolation was done on the logarithmic distance versus energy datapoints. That is, the logarithm of the distances and logarithm of the negative of the pair energies.

3.2.3 Parallelization

In the case of a fixed cutoff distance, the pair calculations may be trivially parallelized with MPI. Given a run with N processes, the pair list may simply be divided into N equally large parts, each handed out to a process. The pair energies are simply collected and summed at the end. In this case, there are two main problems that may cause significant reduction in the speedup.

The first issue is related to the unevenness in computation time for different pairs, due mainly to varying number of occupied orbitals and the size of the excitations spaces. Notably, the number of virtual orbitals increases with the pair distance (up to some limit) due to the reduces overlap of the virtual spaces of each of the fragments involved. Therefore, the computation time increases with distance. If one process is given pairs consistently at lower distances than some other process, the first process will finish before the latter. In some cases, the time difference may be significant, and some sort of load balancing should be considered. In the present implementation, the pairs have simply been shuffled randomly before being handed out to the processes in order to even out the computation times for the processes.

The second issue involves the storing of integrals. Due to the intact translational symmetry, significant savings are made in the new XDEC algorithm by reusing integral calculations. Extra computations are done in the parallelized version since one process does not automatically know what integrals another process has already computed. Some of the same integrals may therefore be computed on the different processes.

When the automatic cutoff algorithm is used, the parallelization procedure is somewhat more complicated since the full list of pairs to calculate is not known beforehand. To deal with this, we split up the computation in two parts.

First, the list of initial pairs may be parallelized trivially. If the number of pairs does not match the number of processes, the number of pairs is increased until the number of pairs is an integer multiple of the number of processes.

In the second part, an estimate is made of which pairs to calculate in order to satisfy the criterion for remaining estimated energy. This list may then be parallelized in the same manner as described above. Again, the number of pairs in the list is always increased so that the number of pairs matches an integer multiple of N. If the remaining estimated energy condition is met, the calculation ends, possibly with a control calculation. Otherwise, a new set of pairs is handed out to the processes in the same way as described above.

3.2.4 Pair groups

The formation of pair groups happens in two steps. The first step is to group single fragments into sets of fragments, such that all fragments in a given set are considered equivalent. We may for example decide, by some means, that two or more distinct fragments may be treated as equivalent, and denote all these fragments as belonging to fragment type A. Another set of fragments that we decide are equivalent to each other, but distinctly different from those in category A, may be denoted by B, and so on. The second step is to form pair groups by all possible combinations of the fragment types. As an example, if we have two unique types of fragments A and B, we can form three pair groups by combining A with A, A with B and B with B. In general, if there are N unique fragments, there will be $N\left(N+1\right)/2$ pair groups.

This expression illustrates why it may be preferable not to treat every fragment as unique, but rather attempt to minimize the number of fragments treated as unique. In ethylene 1d, to take an example, there would be 21 groups, and this number would grow rapidly with increased number of atoms in each unit cell. This will lead to a correspondingly increased number of pair calculations for the purpose of doing interpolation. It would also cause a decrease in the sampling of pairs within each group since the pairs will be spread out among more groups.

We now move on to describing how we may decide whether or not two fragments may be treated as equivalent. When atomic fragments are used, a primitive method may be to group according to what element the atom in the fragment is. In ethylene, for example, the two carbons atoms would in this case have equivalent fragments, and the four hydrogen atoms would similarly have equivalent fragments. There are two problems with this model. The first issue is that two atoms of the same element may be quite different due to the environment. As an example, it is likely that a carbon atoms bonded to an oxygen atoms would behave quite differently from a carbon atom only bonded to hydrogen atoms and other carbon atoms. This problem may be solved by taking the environment into account when categorizing the fragments. The second issue is of an algorithmic nature, and was mentioned in section 2.7.3. If there is no enforcement of symmetry in the algorithm, fragments of two atoms that are symmetry equivalent may be non-equivalent in the calculation due to asymmetric assignment of orbitals. An example of this is shown in figure (2.12) where one of the carbon atoms has been assigned both of the C-C bond orbitals. One of the carbon atoms is therefore left with only what is essentially a 1s orbital, and therefore has correlation energy practically negligible compared the fragment on the other carbon atom.

Both problems are solved in the XDEC implementation by comparing the list of occupied orbitals. If the list of occupied orbitals of two fragments contains orbitals of the same spread within some tolerance, the two fragments are treated as equivalent. Otherwise, the two fragments are distinctly different. The two fragments of carbon in figure (2.12) are automatically treated as different since the program realizes that the set of occupied orbitals are different. This method does not consider the atoms that the fragments are associated with, and may therefore be used on other fragment types than atomic fragments.

The grouping method described above is shown to give sets of pairs, each of

which has less spread that the dataset as a whole. In cases with little variation in angles (1D systems) and quite spherical orbitals (core orbitals or in ionic bonding), the set of datapoints behave nicely with little spread. Cases with more than one dimensions and covalent bonds may give rise to dataset with more spreads internally in the groups, as seen in figure 2.12. This spread can be accounted for by writing the pair in the group as a function of both distance and the relative angles of the orbitals. Figure 2.11 shows the energy vs distance plot for the C5-C5 pair along with two possible angle sortings. As may be expected,

In the general case, however, the problem is significantly more complicated. To treat the general case, we may start by assigning an axis to each orbital to which the angle is measured relative to. Note that this most be done for each orbital, not each "equivalent" orbital, since they may be oriented differently, as exemplified by the orbitals on the hydrogen atoms in ethylene. The axis may be chosen as being along the direction of largest spreads, but a simpler heuristic approach may be to use the associated bond axis. The major complication is that we now have three important axes: the two fragment axes and the axis between the fragments in the pair, and there are several angles that may be important.

The method described above is a somewhat heuristic method where the categorization of fragments are done before any calculation. It is also possible with more dynamic grouping where the fragments are grouped on the fly according to initial energy calculations. Since the static grouping have worked well on the systems tested so far, we have not pursued this method further.

3.2.5 Defining the fragment position

As previously explained, in the DEC algorithm, orbitals are assigned to atoms based on some physical justification. When the pair energies are calculated, a pair distance must be assigned, either to be used to determine which pairs to calculated based on a cutoff distance, or in interpolations. To do this, a position is assigned to each fragment, and the position is used to calculate the pair distances. In the original XDEC implementation, the positions of the atomic nuclei were used. It is, however, the positions of the Wannier functions that are relevant in the energy calculations, not the nuclear positions. The distances obtained are therefore not necessarily ideal to use in the interpolations, and a more satisfying definition of the position should be related to the Wannier centers.

Since the pair energy is strongly related to the spread of the occupied orbitals, better definitions of the position should somehow put more weight on the positions of those orbitals with largest spread. For systems where each atomic fragment has one occupied orbital with significantly larger spread than the others, simply defining the atomic fragment position as the Wannier center of the orbital with largest spread is a good choice. Figure 3.1 shows pair energy as function of pair distance for a 1D ethylene system, where the positions are defined by the nuclei (left figure) and the occupied Wannier function with largest spread (right figure). The figure shows clearly the datapoints are much more predictable when the fragment position is defined by the Wannier position.

The situation is less straightforward when there are two or more occupied or-

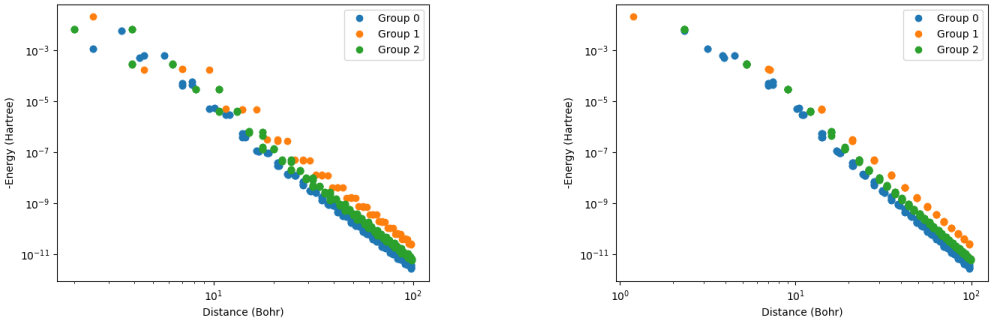

Figure 3.1: Pair correlation energy versus pair distance for 1D ethylene where the atomic position are used as fragment position in the leftmost plot, and the Wannier center of the occupied orbital with largest spread is used as fragment position in the rightmost plot.

bitals in the same fragment with similar spread. If they have the same spread, the simplest solution is to use the centroid of the Wannier centers as fragment position. That is, given a set of k occupied Wannier functions i of similar spread, the fragment position would be defined as

$$\boldsymbol{R}_{frag} = \frac{\sum_i \langle i | \hat{\boldsymbol{r}} | i \rangle}{k} \tag{3.14}$$

The behavior of the pair energy as function of distance must then be expected to be more complicated since there are several significant distances at play. Furthermore, there may be cases where two or more orbitals have quite similar, but not equal, spreads. In that case, the Wannier centers must somehow be weighed when determining an ideal position. An example could be the center of mass inspired expression

$$\boldsymbol{R}_{frag} = \frac{\sum_i \sigma_i \langle i | \hat{\boldsymbol{r}} | i \rangle}{\sum_i \sigma_i} \tag{3.15}$$

where the mass have been replaced with the orbital spread. This seems give more well behaved dataset for more complicated fragments. In the current implementation, the centroid of the Wannier functions is used if to or more orbitals is less than a tolerance σ_{tol} smaller that the orbitals with largest spread. In all other cases, a single Wannier center is used in the definition. A pragmatic alternative may be to refuse to create fragments with several non-core occupied orbitals.

3.2.6 Extrapolated pairs

Spline interpolation curves have a tendency of bending close to the edges of the interpolation interval. This makes estimates for the remaining energy somewhat

unstable, and dependent on the distance at which the distant pairs are chosen. This problem can be solved by calculating extra pairs at distances far larges than the interpolation interval goes. This would, however, take extra calculation time for pairs that does not actually contribute to the energy calculation. An alternative approach, which is used here, is to place out artificial pairs at large distances. The values of these may be chosen by some extrapolation method. Here, linear regression is used on the logarithmic data points. Alternatively, a CR^{-6} extrapolation from the distant pair may be used. This method is in a sense coarse and may be imprecise, but tests have shown that the result is not very sensitive to exactly where the extrapolated pairs are chosen.

Chapter 4

Results and discussion

Tests of the convergence of the MP2 solver for PAOs and the performance of PAOs relative to virtual Wannier functions is shown in section 4.1. In section 4.2, tests of the stability of the cutoff algorithm, including an analysis of angle sorting, is presented. Finally, in section 4.3, the cutoff algorithm is applied in the generation of a PES for the 3D LiH system.

The test systems described in section 2.7.2 is used in this chapter. In addition, a 2D LiH system and a 3D He system is used. For helium, neon and the ethylene systems, 6-31G basis sets [28] obtained from Basis Set Exchange [29], [30]. The helium system uses the same basis set as neon. In LiH, the hydrogen atom has a valence triple-zeta with polarization [31], while Li has a 6-1G [32] basis set. The lattice structures and coordinates for the atoms in the test systems are given in appendix B.

4.1 Non-orthogonal virtual orbitals

4.1.1 Convergence of PAO solver

As a validation of the implementation, we begin by looking at a simple 3D He system with orbitals only in the reference cell. Figure 4.1 shows the maximum absolute value of the residual as a function of the number of iterations for the reference cell of the helium system using plain FPIs, FPIs with DIIS convergence acceleration and Newton's method. A damping factor of 0.1 was used for the FPIs. Closer scrutiny shows that the Newton solver converges the equations to within machine precision (of order 10^{-16}) in two iterations with a fragment energy of -0.02311742 Hartree. This validates that solutions can be found for the amplitude equations in the present implementation.

After 100 iterations in the plain FPI solver, the residual has a maximum absolute value of 0.00138, while the inclusion of DIIS improves the value to 1.95106e-05. Correspondingly, the plain solver gives an energy that deviates from that of the Newton solver in the forth decimal place (-0.02304416 Hartree) while the result with DIIS deviates in the sixth decimal place (-0.02311602 Hartree). This shows that DIIS gives a significant convergence acceleration relative to the plain FPI

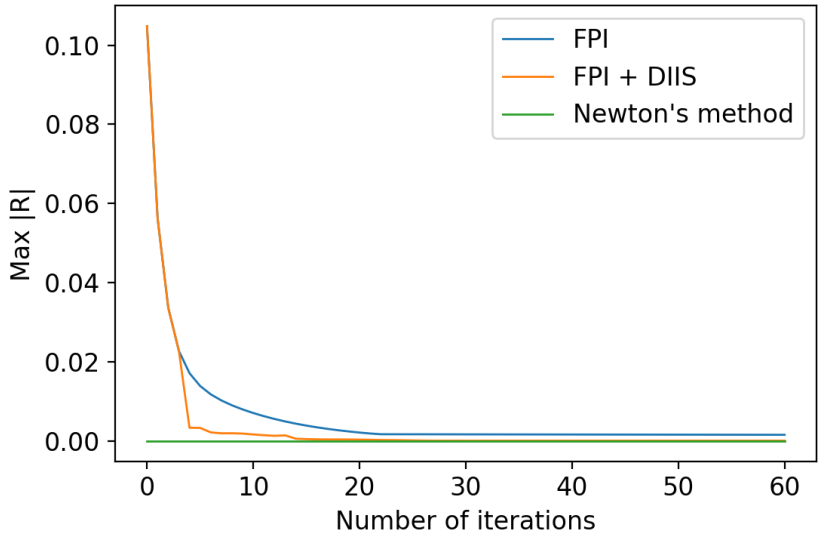

Figure 4.1: Max value of residual as function of number of iterations for the plain FPI solver, FPI with DIIS convergence acceleration and Newton's method for the reference cell of a 3D helium crystal. The new XDEC code was used and the virtual space was represented by PAOs.

solver, and suggests that the result of the DIIS solver in this case is good enough for use in calculations with FOT at least 10^{-5} Hartree.

Even though the Newton solver converges fast and is convenient in the sense that the Hessian of the Hylleraas functional is a constant, it is ruled out as a possible general solver in anything but relatively small fragments due to the rapid growth in the number of amplitudes. Using the Newton solver requires the storage and inversion of a Hessian matrix of dimensions N^2, where N is the number of amplitudes. We therefore use FPIs with DIIS for the rest of the calculations.

Figure 4.2 shows the maximum absolute value and the Frobenius norm of the residual of the FPI solver without DIIS, and with DIIS with 4 and 8 stored amplitudes. The test was run on a C fragment in 1D ethylene with one core orbital and one C-C bond orbital. We see that the Frobenius norm converges much more systematic than the absolute value, and we therefore suggest it as the preferable convergence criterion.

As for the number of amplitudes to store in the DIIS scheme, we see that 4 amplitudes actually performs better than 8 amplitudes unless very many iterations are performed. This seems to be related to a slow-down in the convergence for few iterations when the full matrix has yet to be constructed. After 100 iterations the solver with 8 amplitudes has converged as well as the one with 4 amplitudes, but this is undesirably many iterations in most systems. We therefore use 4 amplitudes as a standard in the DIIS algorithm.

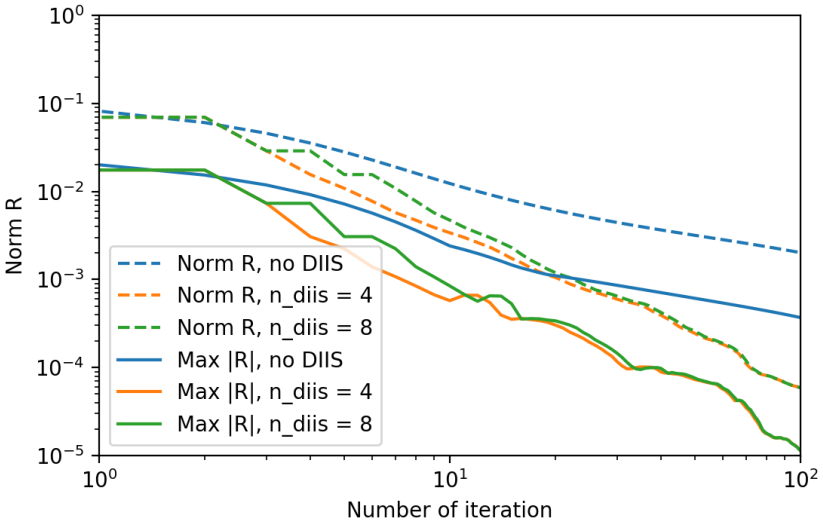

Figure 4.2: Frobenius norm and max absolute value of residual as function of number of iterations for the fixed-point iteration solver with various number (8, 16 and 32) of stored amplitudes in the DIIS scheme. The system was ethylene 1d, with a C-fragment consisting of one core-orbital and one C-C bond orbital. The number of orbitals were 17 virtual and 6 occupied. Both axes has logarithmic scales. The new XDEC code was used and the virtual space was represented by PAOs.

4.1.2 Representation of virtual orbital spaces

Figures 4.3, 4.4 and 4.5 shows the fragment energy as function of the number of virtual orbitals in 1D ethylene, 2D LiH and 3D neon. For 3D neon all occupied orbitals in the reference cell were included in the fragment, while the H-fragment was used in the LiH system and a C-fragment with one core orbital and one bond orbital was used in 1D ethylene. We see that for 1D ethylene, the convergence of the fragment energy is quite similar for PAOs and virtual Wannier functions (virtual Wannier functions are denoted LVOs for orthonormal *localized virtual orbitals*). For the orbital located on the H-atom in 2D LiH, there is a region up to about 15 virtual orbitals where the energy is closer to the converged fragment energy when using PAOs, but the difference is only in the fifth decimal place. In 3D neon, however, the fragment energy is converged with very few PAOs, and 27 LVOs are needed to achieve the energy level obtained with only 8 PAOs. A large reduction in the number of virtual basis functions can there be achieved with FOT = 10^{-4} Hartree.

In addition, hen using LVOs in 3D neon, there is an energy plateau about 2×10^{-4} Hartree higher than the final converged baseline. This is a potential cause of non-smoothness on PESs, and in this system, that problem would seemingly be solved with PAOs.

Based on these observations, there does not seem to be a general benefit of using PAOs instead of virtual Wannier functions in the XDEC implementation, although the improvement was significant in 3D neon. This result is somewhat contrary to that of Hansen et al. [6], as they suggested based on tests on diamond, LiH and HCN that the PAOs performed better than LVOs. However, there are some potential causes for this discrepancy. Firstly, the discrepancy may be due to differences in the way the energy is calculated, as the Cryscor implementation generated orbital specific virtuals (OSVs) and subsequently orthogonalized the set of orbitals. In addition, the systems and basis sets are not the same.

4.2 Cutoff determination

4.2.1 Number of interpolation pairs

In the cutoff algorithm, the interpolation curve, and therefore the number of pairs calculated, will vary somewhat based on the choice of distant pairs. The reason for this may be either that the maximum range of the interpolation is too short, significant differences in the distant pair energies due to angle dependency, or it may simply be due to small changes in the pair calculations, for instance making the interpolation curve bend somewhat differently. The issue with small "random" changes in the interpolation curve due to differences in the selected intermediate pairs is an important factor in the stability of the algorithm, and this is tested in the next section.

To eliminate the problem of the size of the interpolation range, we could simply choose a very large cutoff distance for the interpolation range. A potential problem that may arise is that, especially in 3D systems, the number pairs quickly grows very large. As an example, in 3D LiH with interpolation cutoff at

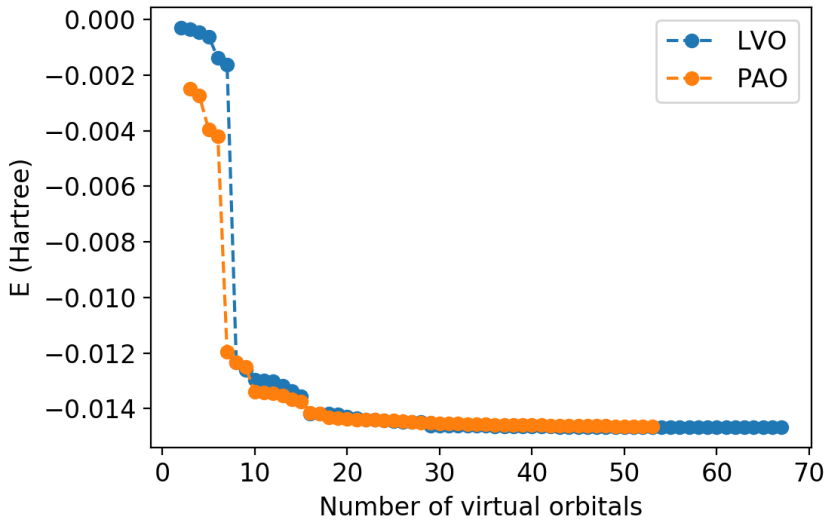

Figure 4.3: Fragment energy versus the number of virtual orbitals for a C-fragment with one core orbital and one bond orbital in 1D ethylene.

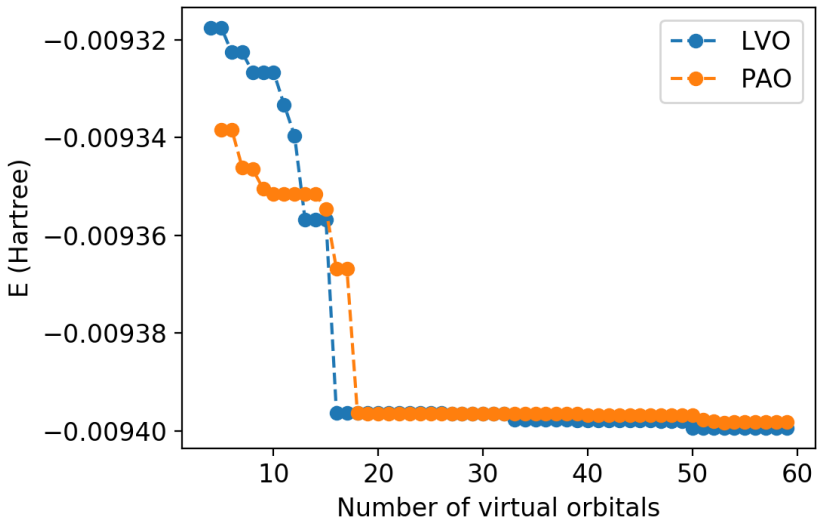

Figure 4.4: Fragment energy versus the number of virtual orbitals for the H-fragment in 2D LiH.

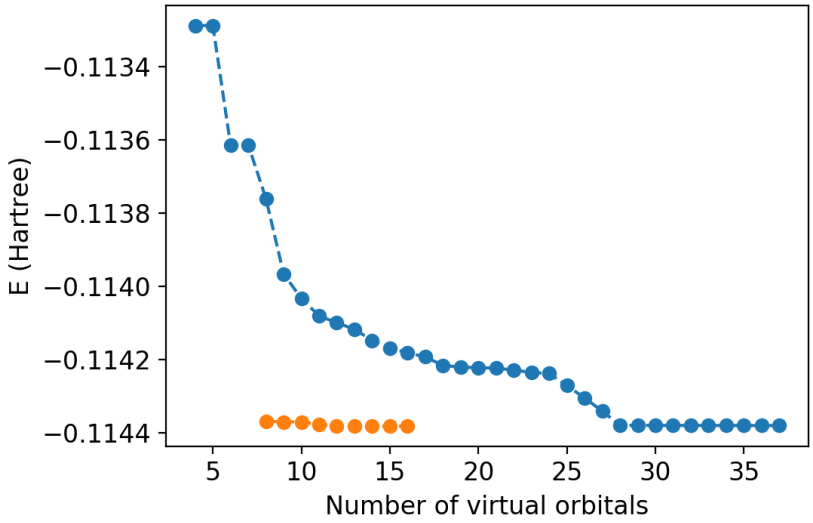

Figure 4.5: Fragment energy versus the number of virtual orbitals in 3D neon. All the occupied orbitals in the reference cell was included in the fragment.

200 Bohr, the pair list contains 575752 pairs. This number obviously grows fast with further increase in interpolation cutoff distance. These have to be stored and used in the interpolation.

The least number of pairs necessary in the interpolation range may be estimated by fixing the distant pairs, and changing only the interpolation range. Table 4.1 shows results from runs on LiH with FOT $= 10^{-3}$ Hartree and with varying interpolation cutoff, but with the distant pairs fixed at ∼200 Bohr. With a cutoff factor of 1.0, the number of pairs calculated is the same for an interpolation cutoff of 30 and 200 Bohr. With an cutoff factor of 0.1, the number of pairs increase by 6 when the interpolation cutoff is is increased from 30 to 50. Another pair is computed when the interpolation cutoff is further increased to 100 Bohr. We assume that this case may be used as an estimate for a calculation with FOT $= 10^{-4}$ Hartree and cutoff factor of 1.0.

The issue of pair contributions at very long range are typically most severe for 3D systems due to the rapid increase in the sheer number of pairs. We may therefore conclude that we should be safe in including pairs up to 100 Bohr when interpolating on 1D and 2D systems with FOT no smaller than 10^{-4} Hartree.

4.2.2 Stability

Table 4.2 shows the correlation energy in 2D ethylene with fixed pair cutoff distance at 100 Bohr and FOT $= 10^{-3}$. Table 4.3 shows the corresponding energy and errors computed using the cutoff algorithm with 2 and 5 intermediate pairs, and with 7 different values of min_incr. The deviation from the results in table 4.2 is given as the error. The 2D ethylene systems are chosen since they

Table 4.1: Number of computed pairs and estimated remaining energy with cutoff factor 1.0 and 0.1 and various interpolation intervals in LiH. All computations were done with distant pairs at ∼200 Bohr, and the interpolation cutoff defines the maximum pair distances included in the energy estimation. FOT was set to 10^{-3} Hartree.

Cutoff factor	**Interpolation cutoff (Bohr)**	**Number of computed pairs**
1.0	30	22
	50	22
	100	22
	150	22
	200	22
0.1	30	100
	50	106
	100	107
	150	107
	200	107

Table 4.2: Correlation energy and the number of calculated pairs in stacked and flat 2D ethylene with a cutoff distance at 100 Bohr. The calculations were done with the original XDEC implementation with an extent tolerance = 10^{-3}.

System	**Energy (Hartree)**	**Number of pairs**
Stacked 2D ethylene	-0.167065	7986
Flat 2D ethylene	-0.167292	8074

Table 4.3: The minimum and maximum errors from runs with the cutoff algorithm and various number (2 and 5) and placements of intermediate pairs. For each result, 7 runs were performed with 7 different values for min_incr distributed uniformly in the range [4,10] for 2 intermediate pairs and [2,6] for 5 intermediate pairs. The calculations were done with the original XDEC implementation with an extent tolerance = 10^{-3}.

System	**Number of intermediate pairs**	**Lambda**	**Min error (Hartree)**	**Max error (Hartree)**
Flat 2D ethylene	2	1.0	8.78e-4	1.08e-3
		0.1	8.67e-5	1.18e-4
	5	1.0	9.15e-4	9.76e-4
		0.1	8.91e-5	9.79e-5
Stacked 2D ethylene	2	1.0	7.99e-4	2.20e-3
		0.1	7.24e-5	8.52e-5
	5	1.0	7.94e-4	1.48e-3
		0.1	7.03e-5	7.79e-5

Table 4.4: Estimated pair non-calculated pair energy for C5-C5 pairs in flat 2D ethylene with no angles sorting (A1), two angle groups (A2) and 9 angle groups (A3). The calculated pairs was in all cases the initial pairs for A3 with $min\_incr = 7$ Bohr. The reference is computed with a fixed cutoff at 100 Bohr.

System	**Estimated pair energy (Hartree)**	**Relative error (%)**
Reference	-2.2812e-6	
A1	-1.8674e-6	18.1
A2	-2.0176e-6	11.6
A3	-2.3005e-6	-0.85

contain pair energies with significant angle dependency, and the stability with respect to the choice of intermediate pairs are expected to be significantly more problematic in these systems than for instance in 3D LiH.

We see that with only two intermediate pairs and $\lambda = 1$, the results is quite dependent on the intermediate pairs. This is especially true in stacked 2D ethylene, where difference between the smallest and greatest error is larger than the FOT. Increasing the number of intermediate pairs to 5 significantly stabilizes the results. We note, however, that if no additional sampling conditions are imposed on the intermediate pairs, there is no guarantee that not all intermediate pairs will be significantly off the ideal interpolation curve.

For $\lambda = 0.1$, which we regard as an estimate for the FOT $= 10^{-4}$ case, the results are significantly more stable, also relative to the target error of 10^{-4}. This is not surprising since the greater sampling will undermine the potential bias in the selection of intermediate pairs.

We finally note that variations in the spline estimates may be significantly more problematic in 3D systems, as relatively small variations may cause significant differences in the number of pair calculations. To aim for an algorithm that is not dependent on large sampling or chance, it may be useful to consider ways of taking into account the angle dependencies.

4.2.3 An analysis of angle considerations

Table 4.4 shows the relative error between the estimated non-computed pair energy and the actual non-computed pair energy (up to a cutoff of 100 Bohr) when the pairs are sorted into one, two and nine angle groups for the C5-C5 pairs in flat 2D ethylene as illustrated in figure 2.11. The case with no angle sorting, two angle groups and nine angle groups will be referred to as A1, A2 and A3 respectively. The actual energies are not so important since they are too small to have major impact, but the results are somewhat scalable in the sense that the relative error would be the same if all pair energies were multiplied the same number. This may therefore give an indication on the applicability of angle sortings or other ways of accounting for angles in systems where highly angle dependent pairs have a greater contribution to the pair energy, as for instance in diamond. Generally, an increased pair energy could be the result of a greater number of pairs, that the pairs start out at smaller distances or simply

a larger pair energy from each pair. We note, however, that the pairs in such systems may not be as well behaved as in this case.

The pairs used in all calculations are the initial pairs generated for the A3 case with the primitive pair setup (the pair with smallest distance, two intermediate pairs with min_incr = 7 and one distant pair at approximately 200 Bohr). Even though this is an artificial setup for the A1 and A2 systems, it should give a good sampling of pairs angle-wise.

As seen from table 4.4, the angle sorting gives a large reduction in the relative error of the estimated pair energies, from 18 % without angle sorting, to less than 1 % with 9 angle groups. There is also an improvement when going from no angle grouping to two separate angle groups. If similar results can be obtained generally for systems with large angle dependencies in the pair energies, taking into account the angle dependencies may be a fruitful path forward.

Although the pair energies in this case can be improved by angle sorting, the general case introduces significant additional issues. Firstly, the additional angle degrees of freedom can result in a large number of pair calculations necessary to start the algorithm. Already on the A3 case, at least 36 pairs is needed to begin the interpolation on the C5-C5 pairs alone. Introduction of an extra dimension in the system and extra rotational degrees of freedom could significantly increase this number. Secondly, the procedure must be automated. This includes an automatic determination of whether angles are important for any pair group, and an automatic determination of how it is convenient to slice up the angle degrees of freedom.

Given the correlation between the directional orbital spread and the pair energy at a given distance as suggested previously, we suggest that the spread values may be used in the process of determining whether angle considerations are important. In the case where angle sorting is not used, spreads can alternatively be used to counteract biases in calculations of intermediate and distant pairs by ensuring pair computations at angles corresponding to different orbitals spreads.

Another approach to the angle problem is to treat distance and angles on a more equal footing. In the angle problem discussed here for flat 2D ethylene, the energy moves on a surface with distance and the angle as coordinates as shown in figure 4.6. In the more general system where more angles must be taken into account, energy will similarly move on a higher dimensional hyper-surface of angle coordinates and one distance coordinate. From this perspective, multivariate interpolation may be interesting to consider.

4.3 Potential energy surfaces

In this section, we will first look at a case of non-smooth PES in 1D ethylene due to premature convergence of the virtual orbital space. Thereafter, we look at the case of fixed cutoff distance in 3D LiH before applying the cutoff algorithm to the generation of a PES for 3D LiH.

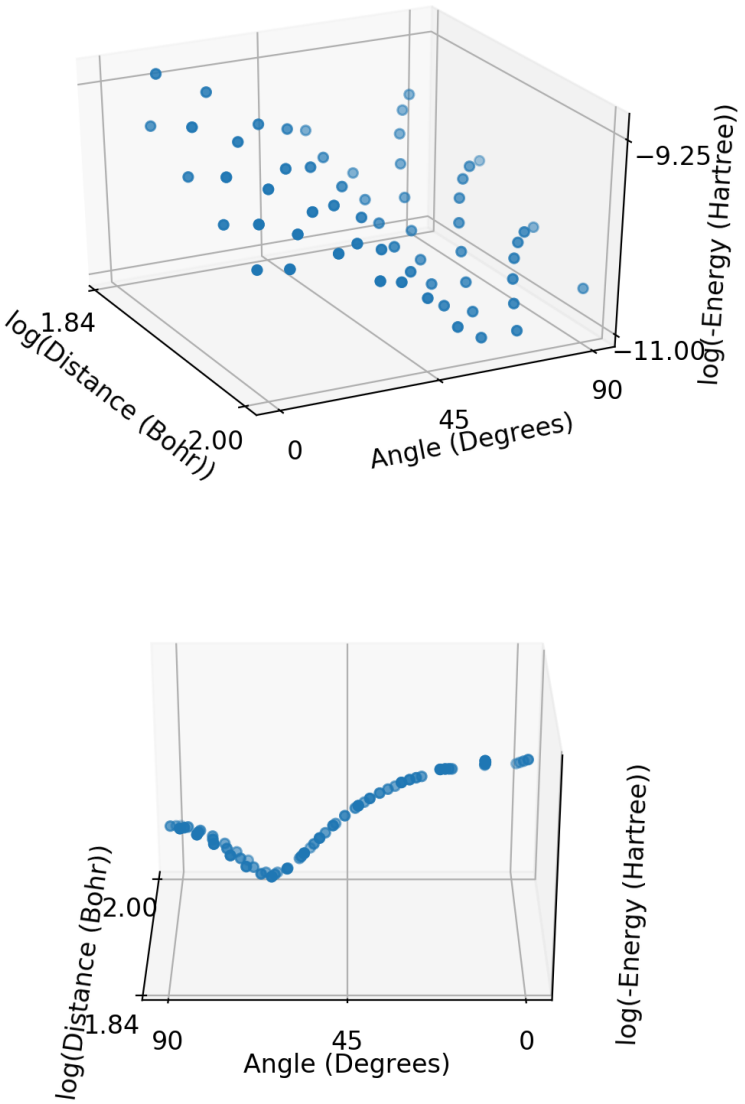

Figure 4.6: Logarithm of the negative pair energy as function of the logarithm of the pair distance and angle in flat 2D ethylene. The distance range is 70-100 Bohr, and the plot is shown from two different angles for clarity. In the topmost figure, a general view is given of the datapoints, while the bottommost figure highlights the angle dependency.

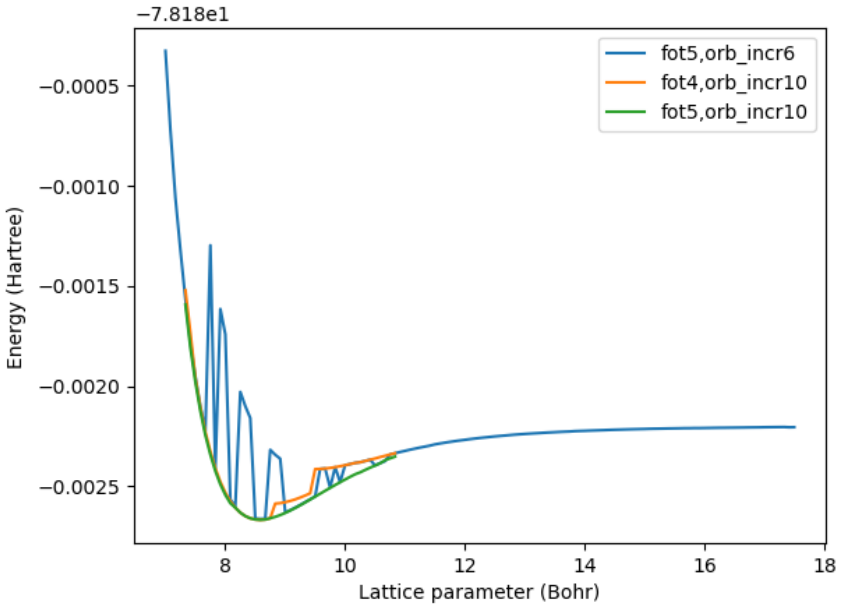

Figure 4.7: PES for ethylene 1D as function of the lattice parameter and a fixed size for the ethylene molecules. 6 and 10 additional orbitals were included in each iteration of the fragment optimization. The calculation were done in the new XDEC code with all the occupied orbitals included in one fragment, and pair energies were calculated for the two nearest unit cells.

4.3.1 Premature convergence of fragment spaces

Figure 4.7 shows how premature convergence of fragments may give rise to large steps on a PES in the 1D ethylene system. In this run, all occupied orbitals were included in one fragment and pairs for the two closest unit cells were computed. Including only 6 orbitals for each step in the fragment optimization gives rise to significant jumps in the energy. The cause of this is premature convergence due to the non-systematic convergence of the fragment energy as the number of virtual Wannier functions is increased by a distance-based measure. Including 10 orbitals at each step overcomes the plateaus on the convergence curve, and we see steps on the PES of magnitudes that are in accordance with the FOT. However, we note that this does not serve as a guarantee against premature convergence, as cases with longer plateaus has been experienced. It is therefore an important future research area to find methods of eliminating the effects of the non-systematic convergence.

4.3.2 Fixed pair cutoff

Figure 4.8 shows a one dimensional PES for 3D LiH surface where the cell parameter is varied. The run was done with a fixed cutoff distance of 9 Bohr, FOT = 10^{-3} Hartree and a maximum error in orbital extents of 10^{-3}. The orbital spaces for the fragments does not change along the PES, and the differences

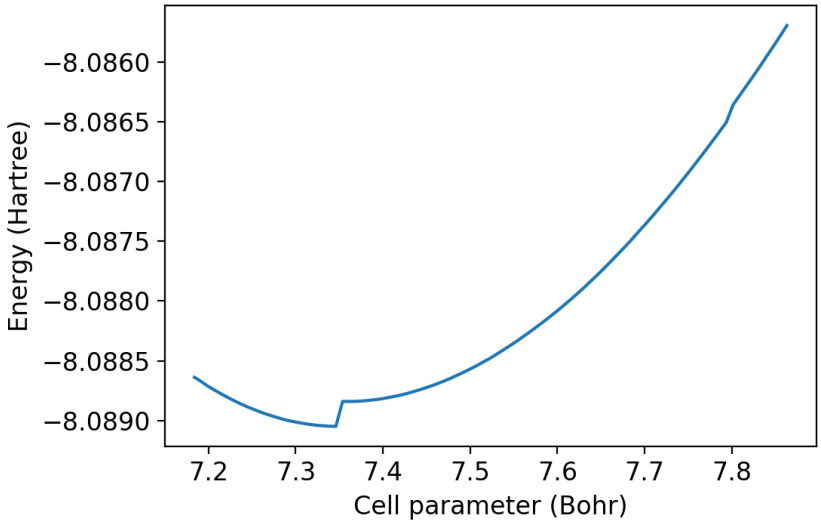

Figure 4.8: 1D PES for 3D LiH where the lattice parameter is varied and a fixed pair cutoff distance at 9 Bohr was used. The calculations were done with the original XDEC implementation with FOT = 10^{-3} and with an extent tolerance = 10^{-3}.

in orbital extents does not cause visible steps.

The surface has a step located close to the minimum that is caused by the sudden inclusion of 12 symmetry equivalent H-H pairs. The magnitude of the step is roughly 2×10^{-4}. It is noteworthy that the step is an order of magnitude larger the largest single pair contribution at that distance due to the number of pairs at the same distance.

As long as a fixed pair cutoff distance is used and not the same number of pairs are computed for all runs, the pair contribution will cause steps. The step is of an order smaller than those previously shown for differences in fragment convergence, but for very short cutoff distances this may change. There may also be systems where the pair steps may be more significant.

We finally mention that although a cutoff of 9 Bohr may seem small, it is not entirely unreasonable. As an example, Wang et al. [4] investigated cutoffs of occupied indices in the range from 4 to 6 Å in the CiM implementation, even though they suggested using a cutoff at 5.5 Å (about 10.4 Bohr).

4.3.3 Automatic pair cutoff

3D LiH Figure 4.10 shows a snapshot of a PES for 3D LiH where the cell parameter is varied and the automatic cutoff algorithm is used. The setup was otherwise the same as for the run with fixed cutoff distance in section 4.3.2. The run was done with the minimal setup of the pair algorithm, and cutoff factor λ of 1.0, 0.5 and 0.1 was used. The PES with fixed cutoff at 9 Bohr is included

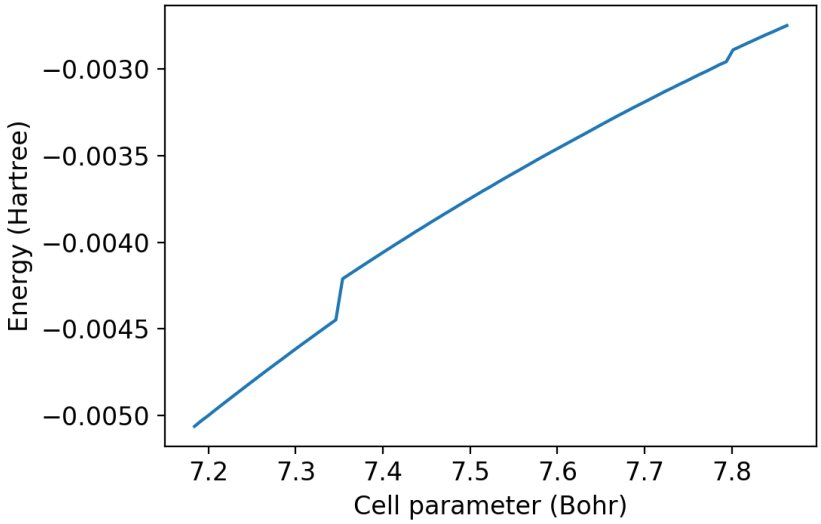

Figure 4.9: Pair energy as function of the lattice parameter in 3D LiH and a fixed pair cutoff distance at 9 Bohr. The calculations were done with the original XDEC implementation with FOT = 10^{-3} and with an extent tolerance = 10^{-3}.

for comparison. We see that several steps occur on the PES with $\lambda = 1.0$, and the largest occurs at about 7.4 Bohr and are of a magnitude of about 2×10^{-4} Hartree, which is the same as with the 9 Bohr cutoff. The numbers of pairs calculated at this step, however, jumped from 20 to 21, while it jumped from 56 to 80 in the fixed cutoff case.

With $\lambda = 0.5$ the largest steps are somewhat smaller, but still of similar magnitudes since a jump of up to three pairs appears at one step. Even though the largest step is somewhat smaller than with $\lambda = 1.0$, the steps are of comparable magnitude.

For $\lambda = 0.1$ the steps are not visible on the plot, even though small steps still occur due to changes in the number of pairs. Although smaller steps is expected due to the smaller value of λ, there is another significant factor in the improved smoothness, namely that the magnitude of each pair contribution have decreased faster than the decrease in the value of λ. This may be illustrated with an example. There occurs a step on the $\lambda = 0.5$ curve at approximately 7.97 Bohr. At this point, the pair energy of the final computed pair was -1.4×10^{-4} Hartree for $\lambda = 0.5$. For $\lambda = 0.1$, however, this value was only -2.0×10^{-6}.

We can analyse this by roughly dividing the cutoff distances in 3D systems like LiH into two regions: one region at small distances where the pair energy contributions mainly stems from a few pairs, and one region at larger distances where the number of pairs is the dominating contribution to the pair energy. The reason for the large improvement in going from $\lambda = 0.5$ to $\lambda = 0.1$ is that we have reached the second region.

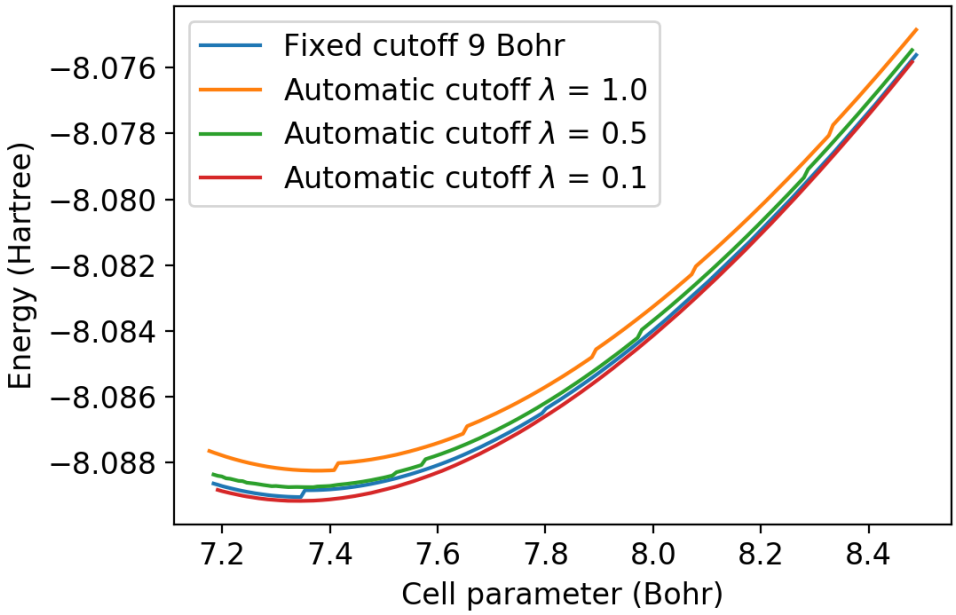

Figure 4.10: 1D PES for 3D LiH where the lattice parameter is varied. The cutoff algorithm was used with 2 intermediate pairs, min_incr = 10 and a interpolation cutoff at 100 Bohr. A calculation with a fixed cutoff at 9 Bohr was included for comparison. The calculations were done with the original XDEC implementation with FOT = 10^{-3} and with an extent tolerance = 10^{-3}.

The automatic cutoff algorithm offer no guarantee for a smooth PES unless some specific smoothing conditions is enforced. The main objective of the use of automatic cutoff should therefore be that the steps is of an order determined by a FOT, along with a potential saving in pair computations. There are at least two sources of steps in this case. The first is the magnitude of the single pair energies. The second, and perhaps most problematic, is potential variations in the spline curve as the intermediate and distant pairs changes along the PES.

Chapter 5

Summary and outlook

5.1 Non-orthogonal virtual orbitals

We have implemented a MP2 solver for non-canonical and non-orthogonal virtual orbitals. The plain FPI solver diverged, and the introduction of a damping factor led to a solver with slow convergence. The convergence of the equations were significantly improved with the implementation of DIIS convergence acceleration.

We have further applied the solver in a test of the performance of PAOs relative to that of virtual Wannier functions. The tests showed a great improvement of the PAOs in 3D neon compared to virtual Wannier functions, but the same improvement was not seen in 1D ethylene and 2D LiH.

It is not clear to the author why the results differed so much between the various systems, and from a theoretical perspective, it would be of great interest with an explanation of why the PAOs perform so much better in some instances, and not in others. From a computational perspective, it would be of interest to be able to classify those systems where PAOs perform better than Wannier functions and vice versa, or if possibly other representations of the virtual space is preferable.

Generally, a minimization of the number of virtual orbitals necessary to span the important part of the virtual space is of great computational interest. Since the correlation energy seems to come from only a few orbitals, and the repeated computation of fragment energy with increasing orbital spaces is relatively cheap in the new XDEC implementation, we suggest that the orbital spaces may be increased by one orbital at a time such that orbitals contributing less than a given tolerance to the fragment energy can be thrown out. This may have the potential to decrease the computational cost of pair calculations significantly.

5.2 Pair cutoff

For handling pair calculations, we have presented an algorithm for automatically determining which pairs to calculate in local CC and MP theory. The pairs are

automatically sorted into groups based on the orbital spreads of the occupied orbitals in each fragment. Spline interpolations are performed on each group and a pair energy estimate is assigned to all pair within the interpolation region. The pair energy estimates are used both to decide which pair to calculate at any point, and to decide on a pair calculation cutoff. The method attempts to resemble a vertical cutoff based on pair energy contributions instead of a purely distance-based cutoff.

We have illustrated that the pair energy within each group depends on both the pair distance and angles between the orbitals in the fragments involved. Only the distance dependency have been implemented, but we have presented a preliminary analysis of the angle problem that suggested a potential practical use for angle considerations.

Furthermore, we suggested that the orbital spread measured along various axes can be used as a quantitative, although not necessarily precise, measurement for explaining the angle dependencies of the pair energies. It could be of interest to see if this can be used in the pair algorithm, for instance in improving the sampling of pairs computed in each group. We also propose that the directionality of the orbitals spreads may be used the determine whether or not the angle dependency is significant enough that it has to be taken into account.

As further investigations, it would be of interest to investigate how the angle sortings could be of practical use, for instance utilizing multivariate interpolation. A persistent problem in this relation will be the number of degrees of freedom in relative rotations of the fragments compared to the number of pairs that is calculated.

As a more general remark, a larger sample of test systems is needed to establish the generality of the cutoff algorithm. This could establish whether certain setups in the algorithm, also those that are not directly related to the angle dependencies of pair energies, must be adjusted. As an example, this could be the notion that orbital spreads of the occupied orbitals is sufficient in the automatic generation of pair groups.

We finally note that the cutoff algorithm should have some sort of mechanism that detects potential failures, for instance due to large angle dependencies or bad grouping of fragments. Such a method may for example be based on extra pair computations after the cutoff has been reached, or on deviations between pairs and the interpolation curve. No final implementation of such a mechanism have been made so far.

5.3 Potential energy surfaces

As a more practical application, we have shown on a 3D LiH system how the automatic cutoff algorithm may be used to produce PES with a smoothness determined from the FOT.

As the 3D LiH systems represents a relatively simple system from a cutoff perspective in the sense that the bonding is ionic and lacks distinct directionality, further studies on the smoothness of PESs in systems with covalent bonds, as for example in diamond, is of interest

We also illustrated on a 1D ethylene system how premature convergence of the virtual orbital spaces may cause steps on PESs. The premature convergence is caused by the non-systematic convergence of fragment energy as additional virtual orbitals are included by distance. A method for minimizing the number of virtual basis functions is therefore not just important for improved performance, but can also undermine the occurrence of steps on PESs.

Bibliography

[1]P. A. M. Dirac, "Quantum mechanics of many-electron systems", Proceedings of the Royal Society of London. Series A, Containing Papers of a Mathematical and Physical Character (1905-1934) **123**, 714–733 (1929).

[2]P. Pulay, "Localizability of dynamic electron correlation", Chemical Physics Letters **100**, 151–154 (1983).

[3]C. Pisani, L. Maschio, S. Casassa, M. Halo, M. Schütz, and D. Usvyat, "Periodic local mp2 method for the study of electronic correlation in crystals: theory and preliminary applications", Journal of Computational Chemistry **29**, 2113–2124 (2008).

[4]Y. Wang, Z. Ni, W. Li, and S. Li, "Cluster-in-molecule local correlation approach for periodic systems.", Journal of chemical theory and computation **15**, 2933–2943 (2019).

[5]E. Rebolini, G. Baardsen, A. S. Hansen, K. R. Leikanger, and T. B. Pedersen, "Divide-expand-consolidate second-order møller-plesset theory with periodic boundary conditions.", Journal of chemical theory and computation **14**, 2427–2438 (2018).

[6]A. S. Hansen, G. Baardsen, E. Rebolini, L. Maschio, and T. B. Pedersen, "Representation of the virtual space in extended systems – a correlation energy convergence study", Molecular Physics (2020).

[7]S. Weinberg, *Lectures on quantum mechanics*, Cambridge, 2015.

[8]E. U. Condon, "The theory of complex spectra", Physical Review **36**, 1121–1133 (1930).

[9]A. Szabo, *Modern quantum chemistry : introduction to advanced electronic structure theory*, New York, 1982.

[10]I.-M. Høyvik and P. Jørgensen, "Characterization and generation of local occupied and virtual hartree–fock orbitals", Chemical Reviews **116**, 3306–3327 (2016).

[11]J. Pipek and P. G. Mezey, "A fast intrinsic localization procedure applicable for ab initio and semiempirical linear combination of atomic orbital wave functions", The Journal of Chemical Physics **90**, 4916–4926 (1989).

[12]N. Marzari and D. Vanderbilt, "Maximally localized generalized wannier functions for composite energy bands", Physical Review B **56**, 12847–12865 (1997).

[13]N. Marzari, A. Mostofi, J. Yates, I. Souza, and D. Vanderbilt, "Maximally localized wannier functions: theory and applications", Reviews Of Modern Physics **84** (2012).

[14]M. Ziółkowski, B. Jansík, T. Kjaergaard, and P. Jørgensen, "Linear scaling coupled cluster method with correlation energy based error control.", The Journal of chemical physics **133**, 014107–014107 (2010).

[15]R. D. Adamson, J. P. Dombroski, and P. M. Gill, "Chemistry without coulomb tails", Chemical Physics Letters **254**, 329–336 (1996).
[16]S. Li, J. Ma, and Y. Jiang, "Linear scaling local correlation approach for solving the coupled cluster equations of large systems", Journal of Computational Chemistry **23**, 237–244 (2002).
[17]C. Pisani, L. Maschio, S. Casassa, M. Halo, M. Schütz, and D. Usvyat, "Periodic local mp2 method for the study of electronic correlation in crystals: theory and preliminary applications", Journal of Computational Chemistry **29**, 2113–2124 (2008).
[18]M. Dornbach and H.-J. Werner, "Analytical energy gradients for local second-order møller-plesset perturbation theory using intrinsic bond orbitals", Molecular Physics: Dieter Cremer Memorial Issue **117**, 1252–1263 (2019).
[19]G. Hetzer, P. Pulay, and H.-J. Werner, "Multipole approximation of distant pair energies in local mp2 calculations", Chemical Physics Letters **290**, 143–149 (1998).
[20]T. U. Helgaker, *Molecular electronic-structure theory*, Chichester, 2000.
[21]R. Dovesi, R. Orlando, A. Erba, C. M. Zicovich-Wilson, B. Civalleri, S. Casassa, L. Maschio, M. Ferrabone, M. De La Pierre, P. D' Arco, Y. Noël, M. Causà, M. Rérat, and B. Kirtman, "Crystal14: a program for the ab initio investigation of crystalline solids", International Journal of Quantum Chemistry **114**, 1287–1317 (2014).
[22]R. Dovesi, V. R. Saunders, C. Roetti, R. Orlando, C. M. Zicovich-Wilson, F. Pascale, B. Civalleri, K. Doll, N. M. Harrison, I. J. Bush, P. D'Arco, M. Llunell, M. Causà, and Y. Noël, "Crystal14 user's manual, university of torino", (2014).
[23]N. J. Russ and T. D. Crawford, "Potential energy surface discontinuities in local correlation methods", The Journal of Chemical Physics **121**, 691–696 (2004).
[24]P. Pulay, "Convergence acceleration of iterative sequences. the case of scf iteration", Chemical Physics Letters **73**, 393–398 (1980).
[25]D. Maclaurin, D. Duvenaud, M. Johnson, and J. Townsend, *Autograd*, `https://github.com/HIPS/autograd`, (accessed: 11.06.2020).
[26]P. Virtanen, R. Gommers, T. Oliphant, M. Haberland, T. Reddy, D. Cournapeau, E. Burovski, P. Peterson, W. Weckesser, J. Bright, S. v. D. Walt, M. Brett, J. Wilson, K. Millman, N. Mayorov, A. Nelson, E. Jones, R. Kern, E. Larson, and C. Carey, "Scipy 1.0: fundamental algorithms for scientific computing in python", Nature Methods **17**, 261–272 (2020).
[27]P. Dierckx, "An algorithm for smoothing, differentiation and integration of experimental data using spline functions", Journal of Computational and Applied Mathematics **1**, 165–184 (1975).
[28]W. J. Hehre, R. Ditchfield, and J. A. Pople, "Self-consistent molecular orbital methods. xii. further extensions of gaussian-type basis sets for use in molecular orbital studies of organic molecules", The Journal of Chemical Physics **56**, 2257–2261 (1972).
[29]D. Feller, "The role of databases in support of computational chemistry calculations", Journal of Computational Chemistry **17**, 1571–1586 (1996).
[30]K. L. Schuchardt, B. T. Didier, T. Elsethagen, L. Sun, V. Gurumoorthi, J. Chase, J. Li, and T. L. Windus, "Basis set exchange: a community database for computational sciences", Journal of Chemical Information and Modeling **47**, 1045–1052 (2007).

[31]M. F. Peintinger, D. V. Oliveira, and T. Bredow, "Consistent gaussian basis sets of triple-zeta valence with polarization quality for solid-state calculations", Journal of Computational Chemistry **34**, 451–459 (2013).
[32]B. Civalleri, A. M. Ferrari, M. Llunell, R. Orlando, M. Mérawa, and P. Ugliengo, "Cation selectivity in alkali-exchanged chabazite: an ab initio periodic study", Chemistry of Materials **15**, 3996–4004 (2003).

Appendix A

Commutators and anti-commutators

The anti-commutation relations for creation and annihilation operators in an orbital basis are

$$\{a^\dagger_{p\sigma}, a^\dagger_{q\tau}\} = 0 \tag{A.1}$$
$$\{a_{p\sigma}, a_{q\tau}\} = 0 \tag{A.2}$$
$$\{a^\dagger_{p\sigma}, a_{q\tau}\} = \delta_{pq}\delta_{\sigma\tau} \tag{A.3}$$

We also list the three somewhat primitive, but highly useful rules

$$[A, B_1B_2] = [A, B_1]B_2 + B_1[A, B_2] \tag{A.4}$$
$$[A, B_1B_2] = \{A, B_1\}B_2 - B_1\{A, B_2\} \tag{A.5}$$
$$\{A, B_1B_2\} = [A, B_1]B_2 + B_1\{A, B_2\} = \{A, B_1\}B_2 - B_1[A, B_2] \tag{A.6}$$

These relations may easily be verified by simply expanding the right-hand side. Lets compute the commutators of the singlet excitation operator $E_{pq} = a^\dagger_{p\alpha}a_{q\alpha} + a^\dagger_{p\beta}a_{q\beta}$ and the creation operator

$$\begin{aligned}
[E_{pq}, a^\dagger_{r\gamma}] &= [a^\dagger_{p\alpha}a_{q\alpha}, a^\dagger_{r\gamma}] + [a^\dagger_{p\beta}a_{q\beta}, a^\dagger_{r\gamma}] \\
&= a^\dagger_{p\alpha}\{a_{q\alpha}, a^\dagger_{r\gamma}\} - \{a^\dagger_{p\alpha}, a^\dagger_{r\gamma}\}a_{q\alpha} + a^\dagger_{p\beta}\{a_{q\beta}, a^\dagger_{r\gamma}\} - \{a^\dagger_{p\beta}, a^\dagger_{r\gamma}\}a_{q\beta} \\
&= \delta_{qr}\left(a^\dagger_{p\alpha}\delta_{\alpha\gamma} + a^\dagger_{p\beta}\delta_{\beta\gamma}\right) \\
&= a_{p\gamma}\delta_{qr}
\end{aligned} \tag{A.7}$$

The commutator between E_{pq} and an annihilation operator may be computed in the same manner, an the result is

$$[E_{pq}, a_{r\gamma}] = -a_{q\gamma}\delta_{pr} \tag{A.8}$$

Using these results, the commutator between two singlet excitation operators may be calculated as follows

$$\begin{aligned}
[E_{pq}, E_{rs}] &= [E_{pq}, a^\dagger_{r\alpha}a_{s\alpha} + a^\dagger_{r\beta}a_{s\beta}] \\
&= [E_{pq}, a^\dagger_{r\alpha}a_{s\alpha}] + [E_{pq}, a^\dagger_{r\beta}a_{s\beta}] \\
&= [E_{pq}, a^\dagger_{r\alpha}]a_{s\alpha} + a^\dagger_{r\alpha}[E_{pq}, a_{s\alpha}] + [E_{pq}, a^\dagger_{r\beta}]a_{s\beta} + a^\dagger_{r\beta}[E_{pq}, a_{s\beta}] \\
&= \delta_{qr}a_{p\alpha}a_{s\alpha} - \delta_{ps}a^\dagger_{r\alpha}a_{q\alpha} + \delta_{qr}a_{p\beta}a_{s\beta} - \delta_{ps}a^\dagger_{r\beta}a_{q\beta} \\
&= \delta_{qr}(a_{p\alpha}a_{s\alpha} + a_{p\beta}a_{s\beta}) - \delta_{ps}(a^\dagger_{r\beta}a_{q\beta} + a^\dagger_{r\beta}a_{q\beta}) \\
&= \delta_{qr}E_{ps} - \delta_{ps}E_{rq}
\end{aligned} \tag{A.9}$$

The two-electron singlet operator may be defined as

$$e_{pqrs} = E_{pq}E_{rs} - \delta_{qr}E_{ps} \tag{A.10}$$

Using the result from equation (A.9), the commutator between the singlet excitation operator and the two-electron singlet excitation operator can be evaluated as follows

$$\begin{aligned}
[E_{tu}, e_{pqrs}] &= [E_{tu}, E_{pq}E_{rs}] - \delta_{qr}[E_{tu}, E_{ps}] \\
&= [E_{tu}, E_{pq}]E_{rs} + E_{pq}[E_{tu}, E_{rs}] - \delta_{qr}[E_{tu}, E_{ps}] \\
&= \delta_{pu}E_{tq}E_{rs} - \delta_{tq}E_{pu}E_{rs} + \delta_{ru}E_{pq}E_{ts} \\
&- \delta_{ts}E_{pq}E_{ru} - \delta_{qr}\delta_{pu}E_{ts} + \delta_{qr}\delta_{ts}E_{pu} \\
&= \delta_{pu}(e_{tqrs} + \delta_{qr}E_{ts}) - \delta_{tq}(e_{purs} + \delta_{ur}E_{ps}) + \delta_{ru}(e_{pqts} + \delta_{qt}E_{ps}) \\
&\quad - \delta_{ts}(e_{pqru} + \delta_{qr}E_{pu}) - \delta_{qr}\delta_{pu}E_{ts} + \delta_{qr}\delta_{ts}E_{pu} \\
&= \delta_{pu}e_{tqrs} - \delta_{tq}e_{purs} + \delta_{ru}e_{pqts} - \delta_{ts}e_{pqru}
\end{aligned} \tag{A.11}$$

Using these results, we may calculate the commutator between the singlet excitation operator and some electronic Hamiltonian on the form

$$\hat{H} = \sum_{pq} h_{pq}E_{pq} + \frac{1}{2}\sum_{pqrs} g_{pqrs}e_{pqrs} + h_{nuc} \tag{A.12}$$

We first note that the commutator with h_{nuc} is always zero. The commutator may then be calculated as

$$
\begin{aligned}
[\hat{H}, E_{ai}] &= \sum_{pq} h_{pq}[E_{pq}, E_{ai}] + \frac{1}{2}\sum_{pqrs} g_{pqrs}[e_{pqrs}, E_{ai}] \\
&= \sum_{pq} h_{pq}(\delta_{aq}E_{pi} - \delta_{pi}E_{aq}) \\
&\quad + \frac{1}{2}\sum_{pqrs} g_{pqrs}(-\delta_{pi}e_{aqrs} + \delta_{aq}e_{pirs} - \delta_{ri}e_{pqas} + \delta_{as}e_{pqri}) \\
&= \sum_{p}(h_{pa}E_{pi} - h_{ip}E_{ap}) \\
&\quad + \frac{1}{2}\sum_{pqr}(-g_{ipqr}e_{apqr} + g_{paqr}e_{piqr} - g_{pqir}e_{pqar} + g_{pqra}e_{pqri})
\end{aligned}
\tag{A.13}
$$

The nested commutator $\left[\left[\hat{H}, E_{ai}\right], E_{bj}\right]$, can now be computed by inserting the results of equation (A.13). When computing the expectation value $\langle\Phi_0|\left[\left[\hat{H}, E_{ai}\right], E_{bj}\right]|\Phi_0\rangle$ however, many of the terms vanishes. The two first terms, for example, vanishes due to Kronecker deltas between occupied and virtual indices and excitation of the Salter determinant with the resulting orthogonality.

For the remaining commutator expectation values, all but one cancel either due to Kronecker delta between occupied and virtual indices, excitations that is impossible to de-excite, or cancellation of the contributions from the two terms in equation (A.10). The only non-vanishing contribution is

$$
\frac{1}{2}\sum_{pqr} g_{paqr}\langle\Phi_0|[e_{piqr}, E_{bj}]|\Phi_0\rangle \tag{A.14}
$$

This can be evaluated with the result from equation (A.11), and only the last term from that equation can be non-zero. This gives the equation

$$
\langle\Phi_0|\left[\left[\hat{H}, E_{ai}\right], E_{bj}\right]|\Phi_0\rangle = \frac{1}{2}\sum_{pq} g_{paqb}\langle\Phi_0|e_{piqj}|\Phi_0\rangle \tag{A.15}
$$

Here, the only non-zero contributions are if $p = i$ and $q = j$ or if $p = j$ and $q = i$. The final result can then be computed as

$$\begin{aligned}
\langle\Phi_0|\left[\left[\hat{H}, E_{ai}\right], E_{bj}\right]|\Phi_0\rangle &= \frac{1}{2}\langle\Phi_0| g_{iajb}e_{iijj} - g_{jaib}e_{jiiij}|\Phi_0\rangle \\
&= \frac{1}{2}\langle\Phi_0| g_{iajb}E_{ia}E_{jb} - g_{jaib}E_{jj}|\Phi_0\rangle|\Phi_0\rangle \\
&= \frac{1}{2}\langle\Phi_0| (g_{iajb}a^\dagger_{i\alpha}a_{i\alpha} + a^\dagger_{i\beta}a_{i\beta})(a^\dagger_{j\alpha}a_{j\alpha} + a^\dagger_{j\beta}a_{j\beta}) \\
&\quad - g_{jaib}(a^\dagger_{j\alpha}a_{j\alpha} + a^\dagger_{j\beta}a_{j\beta})|\Phi_0\rangle \\
&= 2g_{iajb} - g_{jaib}
\end{aligned} \tag{A.16}$$

Appendix B

Coordinates for test systems

The distances are given in ångström. Fractional coordinates are used along axes with periodicity.

1D ethylene

Lattice parameter: 3.704240458100000
H 0.000000000000000 0.000000000000000 0.000000000000000
H -0.357142857142857 0.000000000000000 0.000000000000000
H -0.357142857142857 0.000000000000000 1.833069849551200
H 0.000000000000000 0.000000000000000 1.833069849551200
C 0.142857142857143 0.000000000000000 0.916534924775600
C 0.500000000000000 0.000000000000000 0.916534924775600

Stacked 2D ethylene

Lattice parameters: 3.704240458100000 5.291772083000001
Angle between lattice vectors: 90.000000000000000
H 0.000000000000000 0.000000000000000 0.000000000000000
H -0.357142857142857 0.000000000000000 0.000000000000000
H -0.357142857142857 0.000000000000000 1.833069849551200
H 0.000000000000000 0.000000000000000 1.833069849551200
C 0.142857142857143 0.000000000000000 0.916534924775600
C 0.500000000000000 0.000000000000000 0.916534924775600

Flat 2D ethylene

Lattice parameters: 3.704240458100000 5.291772083000001
Angle between lattice vectors: 90.000000000000000
H 0.000000000000000 0.000000000000000 0.000000000000000
H -0.357142857142857 0.000000000000000 0.000000000000000
H -0.357142857142857 0.34639999999999993 0.000000000000000
H 0.000000000000000 0.34639999999999993 0.000000000000000
C 0.142857142857143 0.17319999999999997 0.000000000000000
C 0.500000000000000 0.17319999999999997 0.000000000000000

2D LiH

Lattice parameters: 4.0834 3.80
Angle between lattice vectors: 60
H 0.500000000000000 0.500000000000000 0.000000000000000
Li 0.000000000000000 0.000000000000000 0.000000000000000

3D LiH

Lattice parameter: 4.0834
Primitive lattice parameter: 2.88740
Angle between primitive lattice vectors: 60
Space group: 225
H 0.500000000000000 0.500000000000000 0.500000000000000
Li 0.000000000000000 0.000000000000000 0.000000000000000

3D helium

Lattice parameters: 2.487132879010000 2.540050599840000 2.592968320670000
Angle between lattice vectors: 90
He 0.000000000000000 0.000000000000000 0.000000000000000

3D neon

Lattice parameters: 2.487132879010000 2.540050599840000 2.592968320670000
Angle between lattice parameters: 90
Ne 0.000000000000000 0.000000000000000 0.000000000000000